POLYTECHNIQUE MONTRÉAL
affiliée à l'Université de Montréal

Column Generation-Based Techniques for Intensity-Modulated Radiation Therapy (IMRT) and Volumetric Modulated Arc Therapy (VMAT) Treatment Planning

MEHDI MAHNAM
Département de mathématiques et de génie industriel

Thèse présentée en vue de l'obtention du diplôme de *Philosophiæ Doctor*
Génie industriel

Août 2019

POLYTECHNIQUE MONTRÉAL
affiliée à l'Université de Montréal

Cette thèse intitulée :

Column Generation-Based Techniques for Intensity-Modulated Radiation Therapy (IMRT) and Volumetric Modulated Arc Therapy (VMAT) Treatment Planning

présentée par **Mehdi MAHNAM**
en vue de l'obtention du diplôme de *Philosophiæ Doctor*
a été dûment acceptée par le jury d'examen constitué de :

Francois SOUMIS, président
Michel GENDREAU, membre et directeur de recherche
Louis-Martin ROUSSEAU, membre et codirecteur de recherche
Nadia LAHRICHI, membre et codirectrice de recherche
Issmail EL HALLAOUI, membre
Matthias EHRGOTT, membre externe

DEDICATION

To my wife, Mojgan, and
To my father and mother
for their love, endless support and encouragement.

ACKNOWLEDGEMENTS

I wholeheartedly appreciate my supervisor, Prof. Michel Gendreau and my co-advisors Prof. Louis-Martin Rousseau and Prof. Nadia Lahrichi for their excellent guidance, immense knowledge, continuous support, and commitment in a team-work, which had a great impact on my work.

Besides my advisors, I would like to thank Prof. Edwin Romeijn for hosting me as a visiting student at Georgia Institute of Technology. It was really a unique opportunity to collaborate with him and be a part of his research group.

In addition, I would like to thank Prof. Fancois Soumis, Prof. Issmail El Hallaoui and Prof. Matthias Ehrgott for accepting to serve on my thesis committee. I really appreciate their attention and feedbacks.

Moreover, I would like to thank Prof. David Craft for providing the data sets, and Dr. Martin Hinse and Dr. Marc-Andre Renaud for their helpful comments.

Furthermore, I acknowledge the Vanier Canada Graduata Scholarship program for providing financial scholarships during three years of my PhD study and also the Fonds de recherche du Québec - Nature et technologies (FRQNT) that supported my visit at Institute of Technology.

I also would like to extend my gratitude to all my friends in CIRRELT for their endless help and support.

RÉSUMÉ

Les statistiques ont estimé à environ 14,1 millions le nombre de cas de cancer en 2018 dans le monde, et qui devrait passer à 24 millions d'ici 2035. La radiothérapie est l'une des premières méthodes de traitement du cancer, qu'environ 50% des patients reçoivent au cours de leur maladie. Cette méthode endommage le matériel génétique des cellules cancéreuses, détruisant ainsi leur capacité de reproduction. Cependant, les cellules normales sont également affectées par le rayonnement ; par conséquent, le traitement doit être effectué de manière à maximiser la dose de rayonnement aux tumeurs, tout en minimisant les effets néfastes des radiations sur les tissus sains. Les techniques d'optimisation sont utilisées afin de déterminer la dose et la position du rayonnement à administrer au corps du patient.

Ce projet aborde la radiothérapie externe à travers la radiothérapie par modulation d'intensité (IMRT), ainsi qu'une nouvelle forme appelée modulation d'intensité volumétrique par thérapie par arcs (VMAT). En IMRT, un nombre fini de directions sont déterminées pour le rayonnement du faisceau, tandis qu'en VMAT l'accélérateur linéaire tourne autour du corps du patient alors que le faisceau est allumé. Cette technologie permet de modifier dynamiquement la forme du faisceau et le débit de dose pendant le traitement. Le problème de planification du traitement consiste à choisir une séquence de distribution des formes de faisceaux, à optimiser le dé bit de dose du faisceau et à déterminer la vitesse de rotation du portique, si nécessaire.

Cette recherche tire profit de la méthode de génération de colonnes, en tant que méthode d'optimisation efficace en particulier pour les problèmes à grande échelle. Cette technique permet d'améliorer le temps de traitement et les objectifs cliniques non linéaires et non convexes, dans la planification de traitement en VMAT. Un nouveau modèle multi-objectif de génération de colonnes pour l'IMRT est également développé.

Dans le premier essai, nous développons un nouvel algorithme de génération de colonnes qui optimise le compromis entre le temps et la qualité du traitement délivré pour la planification de traitement en VMAT. Pour ce faire, une génération simultanée de colonnes et de rangées est développée, afin de relier les colonnes, contenant la configuration des ouvertures de faisceaux, aux rangées du modèle, représentant la restriction de temps de traitement. De plus, nous proposons une technique de regroupement par grappe modifiée, afin d'agréger des éléments de volume similaires du corps du patient, et de réduire efficacement le nombre de contraintes dans le modèle. Les résultats de calcul montrent qu'il est possible d'obtenir un traitement de haute qualité sur quatre processeurs en parallèle.

Dans le deuxième essai, nous développons une approche de planification automatique intégrant les critères de l'histogramme dose-volume (DVH). Les DVH sont la représentation de dose la plus courante pour l'évaluation de la qualité de traitement en technologie VMAT. Nous profitons de la procédure itérative de génération de colonnes pour ajuster les paramètres du modèle lors de la génération d'ouverture, et répondre aux critères DVH non linéaires, sans tenir compte des contraintes dures dans le modèle. Les résultats sur les cas cliniques montrent que notre méthodologie a été significativement améliorée, pour obtenir des plans cliniquement acceptables sans intervention humaine par rapport à une simple optimisation VMAT. De plus, la comparaison avec un système de planification de traitement commercial existant montre que la qualité des plans obtenus à partir de la méthode proposée, en particulier pour les tissus sains, est largement meilleure alors que le temps de calcul est moindre.

Dans le troisième essai, nous abordons la planification de traitement en IMRT, qui est formulée comme un problème d'optimisation convexe à grande échelle, avec un espace de faisabilité simplex. Nous intégrons d'abord une nouvelle approche de solution basée sur la méthode Frank-Wolfe, appelée Blended Conditional Gradients, dans la génération de colonnes, pour améliorer les performances de calcul de la méthode. Nous proposons ensuite une technique de génération de colonnes multi-objectif, pour obtenir directement des ouvertures qui se rapprochent d'un ensemble efficace de plans de traitement non dominés. A cette fin, nous trouvons les limites inférieure et supérieure du front de Pareto, et générons une colonne avec un vecteur de poids des objectifs pré-assigné ou nouveau, réduisant la distance maximale de deux bornes. Nous prouvons que cet algorithme converge vers le front de Pareto. Les résultats de recherche d'un bon compromis de traitement entre la destruction des volumes cibles et la protection des structures saines dans un espace objectif bidimensionnel, montrent l'efficacité de l'algorithme dans l'approche du front de Pareto, avec des plans de traitement livrables en 3 minutes environ, et évitant un grand nombre de colonnes. Cette méthode s'applique également à d'autres classes de problèmes d'optimisation convexe, faisant appel à la fois à une génération de colonnes et à une optimisation multi-objectifs.

ABSTRACT

The statistics have estimated about 18.1 million cancer cases in 2018 around the world, which is expected to increase to 24 million by 2035. Radiation therapy is one of the most important cancer treatment methods, which about 50% of patients receive during their illness. This method works by damaging the genetic material within cancerous cells and destroying their ability to reproduce. However, normal cells are also affected by radiation; therefore, the treatment should be performed in such a way that it maximizes the dose of radiation to tumors, while simultaneously minimizing the adverse effects of radiations to healthy tissues. The optimization techniques are useful to determine where and how much radiation should be delivered to patient's body.

In this project, we address the intensity-modulated radiation therapy (IMRT) as a widely-used external radiotherapy method and also a novel form called volumetric modulated arc therapy (VMAT). In IMRT, a finite number of directions are determined for the beam radiation, while in VMAT, the linear accelerator rotates around the patient's body while the beam is on. These technologies give us the ability of changing the beam shape and the dose rate dynamically during the treatment. The treatment planning problem consists of selecting a delivery sequence of beam shapes, optimizing the dose rate of the beam, and determining the rotation speed of the gantry, if required.

In this research, we take advantages of the column generation technique, as a leading optimization method specifically for large-scale problems, to improve the treatment time and non-linear non-convex clinical objectives in VMAT treatment planning, and also develop a new multi-objective column generation framework for IMRT.

In the first essay, we develop a novel column generation algorithm optimizing the trade-off between delivery time and treatment quality for VMAT treatment planning. To this end, simultaneous column-and-row generation is developed to relate the configuration of beam apertures in columns to the treatment time restriction in the rows of the model. Moreover, we propose a modified clustering technique to aggregate similar volume elements of the patient's body and efficiently reduce the number of constraints in the model. The computational results show that a high-quality treatment is achievable using a four-thread CPU.

In the second essay, we develop an automatic planning approach integrating dose-volume histogram (DVH) criteria, the most common method of treatment evaluation in practice, for VMAT treatment planning. We take advantage of the iterative procedure of column generation to adjust the model parameters during aperture generation and meet nonlinear

DVH criteria without considering hard constraints in the model. The results on clinical cases show that our methodology had significant improvement to obtain clinically acceptable plans without human intervention in comparison to simple VMAT optimization. In addition, the comparison to an existing commercial treatment planning system shows the quality of the obtained plans from the proposed method, especially for the healthy tissues, is significantly better while the computational time is less.

In the third essay, we address the IMRT treatment planning, which is formulated as a large scale convex optimization problem with simplex feasibility space. We first integrate a novel Frank-Wolfe-based solution approach, so-called Blended Conditional Gradients, into the column generation to improve the computational performance for the method. We then propose a multi-objective column generation technique to directly obtain apertures that approximate an efficient non-dominated set of treatment plans. To this end, we find lower and upper bounds for the Pareto front and generate a column with a pre-assigned or new weight-vector of the objectives, reducing the maximum distance of two bounds. We prove this algorithm converges to the Pareto front. The results in a two-dimensional objective space to find the trade-off plans between the treat of target volumes and sparing the healthy structures show the efficiency of the algorithm to approximate the Pareto front with deliverable treatment plans in about 3 minutes, avoiding a large number of columns. This method is also applicable for other classes of convex optimization problems requiring both column generation and multi-objective optimization.

TABLE OF CONTENTS

LIST OF TABLES

LIST OF FIGURES

LIST OF SYMBOLS AND ACRONYMS

BAO	Beam Angle Optimization
BCG	Blended Conditional Gradients
CG	Column Generation
CICL	Centre Intégré de Cancérologie de Laval
CT	Computed Tomography
CTV	Clinical Target Volume
CUDA	Compute Unified Device Architecture
DAO	Direct Aperture Optimization
DLTO	Direct Leaf Trajectory Optimization
DM	Decision Maker
DVC	Dose-Volume Constraint
DVH	Dose-Volume-Histogram
ESN	Extreme Supported Non-dominated
EUD	Equivalent Uniform Dose
FMO	Fluence Map Optimization
FW	Frank-Wolfe
GPU	Graphic Processing Unit
GTV	Gross Tumour Volume
IMAT	Intensity Modulated Arc Therapy
IMRT	Intensity Modulated Radiation Therapy
Linac	Linear Accelerator
LPF	Lower Pareto Front
LS	Leaf Sequencing
MCO	Multi-Criteria Optimization
MINLP	Mixed Integer Non-Linear Programming
MIP	Mixed Integer Programming
MLC	MultiLeaf Collimator
MOLP	Multi-Objective Linear Programming
MRI	Magnetic Resonance Imaging
MU	Monitor Unit
NDP	Non-Dominated Point
NTCP	Normal-Tissue Complication Probability
OAR	Organ at Risk

PCG	Pareto-based Column Generation
PF	Pareto Frontier
PSP	Pricing Sub-Problem
PTV	Planning Target Volume
RMP	Restricted Master Problem
SA	Simulated Annealing
SND	Supported Non-Dominated
TCP	Tumor Control Probability
TPS	Treatment Planning System
UND	Upper Non-Dominated
UPF	Upper Pareto Front
USN	Unsupported Non-dominated
VMAT	Volumetric Modulated Arc Therapy

LIST OF APPENDICES

CHAPTER 1 INTRODUCTION

The statistics have estimated about 18.1 million cancer cases in 2018 around the world, which is expected to increase to 24 million by 2035 [130]. In Canada, it has been estimated about 206,200 new cases of cancer in 2018, which will cause the death of approximately 80,800 people. Canadian Cancer Society has also predicted that 40% of Canadians will develop cancer in their lifetime, and about 25% will die of this disease [121].

Radiation therapy is an effective technique against cancer, from which approximately 50 percent of all cancer patients can benefit. This method works by damaging the genetic material within cancerous cells and destroying their ability to reproduce [10]. However, normal cells will be damaged as well as cancer cells in this process. Therefore, the treatment should be performed in such a way that it maximizes the dose of radiation to tumors, while minimizing the adverse effects of radiations to healthy tissues, simultaneously [52].

The source of radiation may be external, referred to as *external* radiotherapy, by producing photon *beams* outside the body or internal by placing the source inside the patient, called *brachytherapy*. In this project, we focus on the external radiotherapy, which is more common. In this type of treatment, the radiation beams are delivered by a linear accelerator (*linac*) mounted on a *gantry* from several directions to the patient. Figure 1.1 shows these pieces of equipment in external radiation therapy. This device is capable of rotating so that beams can be delivered from around the patient. The combination of gantry and couch rotation can facilitate the delivery of radiation beams from different feasible directions.

1.1 Treatment process

After a patient is diagnosed with cancer and the physician includes radiation therapy as part of the treatment, the patient takes the following steps in the treatment-flow [60]:

- Step 1 (CT Scan): A Computed Tomography (CT) scan of the patient is performed, which gives a 3D density map of the internal geometry of the patient.
- Step 2 (Image Segmentation): Different organs in the CT scan are identified, either by automated software or by manual contouring of the CT images.
- Step 3 (Beam Dose Calculation): Given a set of candidate beams of different locations, the dose delivered to the patient is estimated for each direction.
- Step 4 (Beam Optimization): Given the patient geometry, candidate beams, and a physician prescribed desired dose distribution, an optimal set of beam directions and

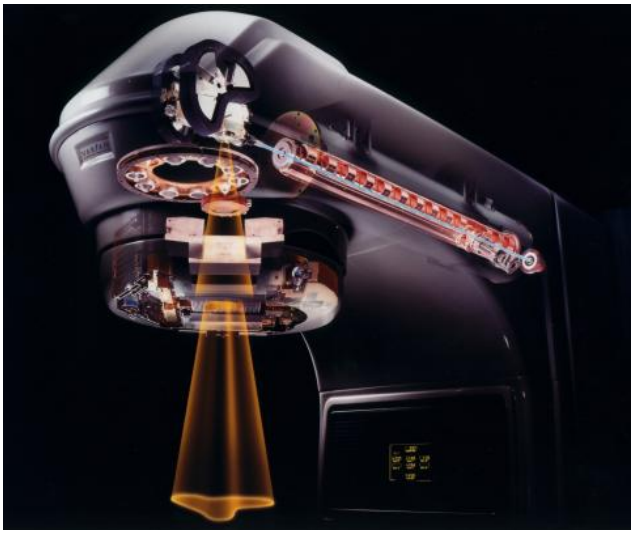

Figure 1.1 Linear accelerator [1]

intensities is computed.

- Step 5 (Plan Evaluation): Once the dose distribution has been computed, a radiologist and physician evaluate the plan in details and approve.

The output of this process is a *treatment plan* consisting the optimal beam directions, beam shapes, and their corresponding intensity, to make a trade-off between the treatment of the tumor in conflict with sparing the healthy tissues. This treatment plan can be delivered over several sessions, known as fractions. In practice, this process, still in a large degree, is accomplished through a trial-and-error process that is guided by a physician [62]. Optimization techniques can be useful to implement this process automatically, and make it more precise and efficient.

1.2 Radiation therapy techniques

There are several external radiotherapy modalities, of which the oncologist recommends the most effective method to the patient bounded by what is available at the clinic.

- Three-dimensional conformal radiation therapy (3D-CRT): This technique uses sophisticated scans to create detailed three-dimensional representations of the tumor and surrounding tissues. Then, several blocks would be employed to shape the radiation beams. This method cannot conform well to an arbitrary three-dimensional shape unless the target has a relatively simple shape or large number of beams are used [127].

- Intensity Modulated Radiation Therapy (IMRT): This technique is a specialized form of 3D-CRT, which has more flexibility to fit the tumor by breaking up the beam into many small beamlets, and adjust the intensity of each beamlet individually [51].
- Volumetric Modulated Arc Therapy (VMAT): Contrary to IMRT that employs only a few fixed directions, VMAT is a form of radiotherapy which incorporates rotation of the beam around the patient's body while the beam is on. Moreover, the dose rate, beam shape, and gantry speed are dynamically adjustable during the rotation. Therefore, the conformity is greater in this method, while takes less treatment time [25].
- Stereotactic Radiotherapy: The beam in this technique is precise, achieved through rigid immobilization, e.g., with a head frame as is used in the treatment of brain tumors [84].
- Proton Beam Therapy: This method is a form of radiation treatment that uses protons rather than X-rays to treat certain cancers. This type of radiation deposits less energy before and after the tumor and allows to reduce the dose to nearby healthy tissues [74].
- Neutron Beam Therapy: This method is a specialized form of high-energy radiation therapy, typically useful for certain radioresistant tumors, i.e., the irradiation is unable or difficult to reduce the tumor volume [85].

In this research, we focus on the treatment planning in IMRT and VMAT, which are widely applicable for different cancer patients and their technology in principle is similar. In both methods, the radiation beam is decomposed into a rectangular grid of *beamlets*, and a piece of equipment called *Multi-Leaf Collimator* (MLC) is used to adjust the intensity of each beamlet. This equipment is made up of two opposite banks of metal leaves, leading and trailing, which can be shifted towards each other, automatically. Then, a beamlet is open if it is not blocked by either the leading or trailing leaf, and the relative motion of the leaves controls the intensity. A sample of MLC is shown in Figure 1.2.

1.3 Intensity Modulated Radiation Therapy (IMRT)

IMRT is the most commonly used type of external radiotherapy. This method achieves the geometric shape of the tumor and its optimal dose intensity by delivering through sequential different beam shapes, called *apertures*, each with uniform intensity level. In IMRT, a fixed number of directions are used to deliver radiation through multiple apertures. Along with shaping the MLC apertures and adjusting the corresponding intensities, we can limit the dose reaching the healthy tissues.

Figure 1.2 A sample of MultiLeaf Collimator (MLC) [126].

To evaluate the dose absorbed by the patient, we divide the body into small cubic volume elements called *voxel*. The number of voxels is typically in order of $O(10^5)$. The dose received by voxel v from beamlet i at unit intensity is estimated in each beam direction by dosimetry methods, denoted D_{iv}. $D = [D_{iv}]$ is called the dose-influence matrix. The planning process is usually divided into three following problems [52]

1. Beam Angle Optimization (BAO): In this problem, a finite number of directions, or beam angles, which makes up set $\mathcal{B}$, are selected, from which the treatment will be delivered. This number is typically between 5 to 9 beams, based on the cancer type. If candidate directions are only obtained from the rotation of the gantry, it is called *coplanar*, otherwise if other parameters such as coach angles were also involved, it would be *non-coplanar*.

2. Fluence Map Optimization (FMO): In this problem, we optimize the intensity, or fluence, of each beamlet i from each direction $b \in \mathcal{B}$. Let x denote the beamlet intensity, the basic FMO model with objective function F is as follows:

$$\min \quad F(z) \tag{1.1a}$$

$$z_v = \sum_{b\in\mathcal{B}} \sum_{i\in\mathcal{I}} D_{iv}^b \, x_i^b \qquad \forall v \in \mathcal{V} \tag{1.1b}$$

$$x_i^b \geq 0 \qquad \forall i \in \mathcal{I}, b \in \mathcal{B} \tag{1.1c}$$

   There are a variety of linear and non-linear models developed for this problem, which are reviewed in Section 2.1.2.

3. Leaf Sequencing (LS): IMRT cannot directly deliver the fluence map, since the radia-

tion source can only deliver a uniform intensity at any time. We can decompose the fluence map into a finite number of MLC apertures and optimize their corresponding uniform intensity. This problem is known as Leaf Sequencing (LS) problem, matrix decomposition or realization.

This hierarchical approach may have a major effect on the quality of treatment plans [47]. Moreover, the number of apertures required in this method is often relatively large which causes long treatment time. To solve this problem, FMO and LS problems are integrated, as *Direct Aperture Optimization* (DAO), to directly form the aperture shapes and optimize their intensity [108]. Let A^k indicate the shape of aperture k, y_k be the intensity of the aperture k, and $D(A^k)$ denote the vector of dose deposition coefficients corresponding to aperture $k \in K$, i.e., $D(A^k) = \sum_{i \in A^k} D_i^k$. The basic DAO treatment planning model looks as follows:

$$\min\ F(z) \tag{1.2a}$$

$$z_v = \sum_{k \in K} D_v(A_k)\, y_k \qquad \forall v \in \mathcal{V} \tag{1.2b}$$

$$y_k \geq 0 \qquad \forall k \in K. \tag{1.2c}$$

However, this integration results in a large-scale optimization problem with enormous number of decision variables.

We will review the mathematical models and algorithms proposed for FMO and LS problems and specifically the column-generation based algorithms for DAO, in details, in Section 2.1.

1.4 Volumetric Modulated Arc Therapy (VMAT)

Recently, the arc therapy has emerged and gained widespread clinical interest as a technique to address the limitations of fixed-field treatments. In this method, the radiation can be delivered from up to 360° of beam angles, with dynamic dose rate and gantry speed [98]. In this problem, the full arc around the patient is divided into *arc segments*, and the fluence maps and MLC leaf trajectories are optimized for each arc. The treatment time by VMAT is about half of plans implemented by IMRT [25]. However, VMAT is much more complex due to the dynamic nature of the gantry motion, dose rate constraints, and MLC leaf constraints. A sample of these machines is shown in Figure 1.3.

To model this problem, there are two approaches: The first approach forms *partial arcs* covering the work-area around the patient, and determines the trajectory of MLC leaves during the arc. Another approach is to consider a finite number of points around the patient, so-called *control points* or *sectors* and optimize the aperture shape and intensity associated

with each point. We briefly review these models for VMAT treatment planning in Section 2.2.

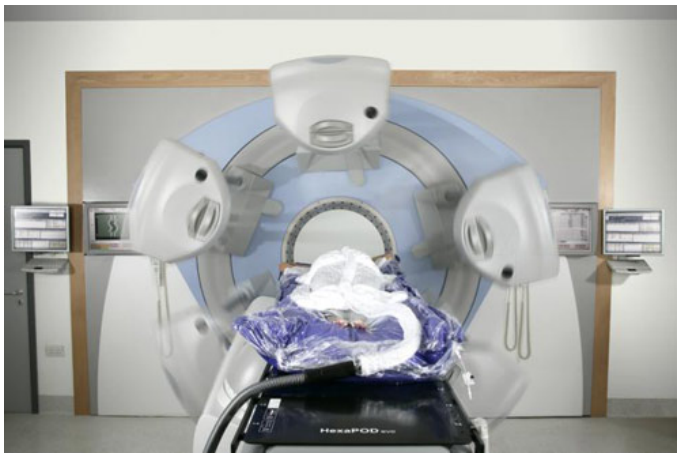

Figure 1.3 A VMAT machine [2].

1.5 Column generation

IMRT and VMAT treatment planning are large scale problems due to the large number of voxels and candidate apertures. To have an idea of the number of apertures in VMAT, suppose a small rectangular (5×10) beam and 100 control points. There are 7.1×10^{251} possible apertures. In real cases, the number of beamlets and sectors is usually much larger.

Column generation (CG) is a leading optimization technique to solve large-scale problems with decomposable structure specially when there are a large number of variables [43]. This approach has successfully been used in many applications such as Vehicle Routing Problem (VRP) [56], airline crew pairing [44], and cutting-stock problems [125] as exact or heuristic methods.

In this technique, instead of generating all the feasible columns in advance, we decompose the model into two subproblems: (1) the restricted master problem (RMP), which contains a subset of the columns, and (2) the pricing sub-problem (PSP), in which promising new columns are generated, expecting to improve the RMP objective function. This iterative procedure continues until there is no more promising column to improve the solution.

We use this method for IMRT and VMAT treatment planning problems to consider new features and also extend this technique to the multi-objective framework.

1.6 Clinical evaluation criteria

Several measures have been proposed to evaluate the quality of treatment plans. One of the most commonly used methods in practice is Dose-Volume-Histogram (DVH). These histograms relate the radiation dose to tissue volume, describing the fraction of the structure, in percentage, which receives a certain dose or above. For example, $V_{20} = 30\%$ means "no more than 30% of the structure exceeds a radiation dose of 20 Gy". Gy is the unit of absorbed dose and one Gy is equal to one Joule (J) of energy deposited in one kilogram (kg) of matter. A sample of DVH diagram is shown in Figure 1.4.

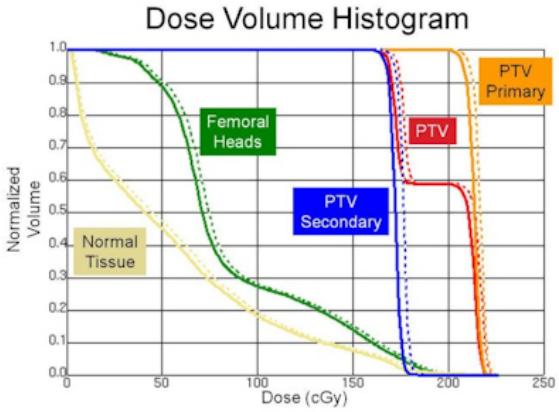

Figure 1.4 A sample of Dose-Volume-Histogram (DVH).

1.7 General contributions

In this dissertation, we focus on developing column generation-based algorithms to improve the quality of treatment plans and also delivery times in IMRT and VMAT.

In the first article presented in Chapter 4, we propose a matheuristic algorithm for the VMAT treatment planning problem, optimizing the trade-off between the treatment time and treatment quality. In this model, the multi-leaf collimator leaf positions, dose rates, and the gantry speed are determined, simultaneously. To this end, column-and-row generation is developed to relate the MLC apertures configuration in columns to time restriction in the rows.

In the second article presented in Chapter 5, we develop an automatic planning approach integrating dose-volume histogram (DVH) criteria in direct aperture optimization for VMAT, during the course of column generation. We take the advantage of iterative procedure in this method to modify the weight vector of the penalty function based on the DVH criteria and

decrease the use of trial-and-error in the search for clinically acceptable plans.

In the third article presented in Chapter 6, we first improve the computational performance of the column generation method developed for DAO in IMRT, using a new efficient first-order solution method to solve the convex restricted master model. We then propose a multi-objective column generation technique to directly obtain columns that efficiently approximates a non-dominated set of solutions. In this algorithm, a column is generated to improve the entire Pareto front rather than a single-objective. This method is implemented for direct aperture optimization (DAO) to find the trade-off plans between the treatment of target volumes and sparing the healthy structures.

CHAPTER 2 LITERATURE REVIEW

In this chapter, we review the prior researches in the same area of this dissertation. The literature on mathematical models of the IMRT and VMAT treatment planning are briefly surveyed in Sections 2.1 and 2.2, respectively. Moreover, we specifically survey the literature on modelling the DVH criteria in Section 2.3 and also multi-objective optimization in IMRT in Section 2.4.

2.1 Intensity Modulated Radiation Therapy (IMRT)

The first optimization model applied in radiation therapy treatments was a linear model by Bahr et al. [13]. After, there has been an increasing attention to applications of OR methods in medical physics [62]. IMRT was introduced in the 1990s, in which each treatment beam has its intensity distribution, individually [28]. As categorized in Chapter 1, the traditional treatment planning is divided into three problems, which can be solved sequentially: Beam Angle Optimization (BAO), Fluence Map Optimization (FMO), and Leaf Sequencing (LS). We briefly review these problems in this chapter. For more detailed information, we refer the reader to the comprehensive reviews by Shepard et al. [117], Holder and Salter [62], and Ehrgott et al. [52].

2.1.1 Beam Angle Optimization (BAO)

The purpose of beam angle optimization problem is to select the best set of directions from all available beam orientations that satisfy the treatment goals [8, 76]. The main difficulty of this problem is evaluating each set of directions based on the quality of dose distribution, while it will be optimized in the second stage. Therefore, the beam's-eye-view, the geometric characteristics of candidate directions, and the estimation of FMO objectives are useful measure employed to assess the candidate solutions. Several exact, heuristic, and metaheuristic algorithms have been developed for this problem [7, 8, 50, 73]. In this study, we assume the directions are given and fixed, and our focus is on aperture generation and optimization.

2.1.2 Fluence Map Optimization (FMO)

In the second step, we optimize the *intensity* (or *fluence*) of beamlets for the fixed beam directions. The main goal is to deliver a specific level of radiation dose, so-called *prescription dose*, to the targets, while sparing critical structures by ensuring that the level of dose received

by the normal structures does not exceed a *tolerance dose*. This problem has received lots of attention in terms of medical aspects, as well as optimization techniques [51].

FMO objectives: In the literature, various mathematical optimization models and algorithms have been proposed for the FMO problem, with respect to different objective functions and constraints. Inspired by Ehrgott et al. [52], we classify these mathematical models into three categories as follow:

In the first category, the objectives of linear programming models are taken into account minimizing the average/min/max deviation from lower or upper bounds. The main constraints are: (1) non-negativity constraints for the beam intensities, and (2) lower/upper bounds on the dose to the target and critical organs. The proposed linear models may be infeasible in practice. Thus, Holder [61] has proposed a new linear programming model with elastic constraints, in which the constraints are allowed to be violated and penalized in the objective function.

$$w_C \parallel T_C - Z_C \parallel_\infty + w_N \parallel Z_N - T_N \parallel_\infty \tag{2.1}$$

where T_C and T_N are the threshold of the target and normal structures; and Z_C and Z_N are the total dose to the target and normal structures.

In the second category, we minimize the *weighted least squares*, penalizing the weighted sum of average squared deviation from the prescribed dose for each structure as follows [20, 120, 138].

$$w_C \parallel T_C - Z_C \parallel_2^2 + w_N \parallel Z_N - T_N \parallel_2^2 \tag{2.2}$$

This function is convex and the most prevalent objective in the literature [7, 8, 106, 109].

In the third category, nonlinear radio-biological models have been developed. In these criteria, biological effects produced by the underlying dose distributions are optimized, e.g., equivalent uniform dose (EUD), estimated probabilities of tumor control (TCP) and normal-tissue complications (NTCP) [93, 95, 132, 136].

FMO techniques: Many exact, heuristic, and metaheuristic algorithms have been developed for FMO, and we review some popular and recent studies briefly. Webb [131] proposed a Simulated Annealing (SA) algorithm for this problem and different variants of this algorithm were developed by Mageras and Mohan [81]. Genetic algorithm is also implemented in this problem to find quick and promising solutions by Langer et al. [71] and Cotrutz and Xing [30]. However, these algorithms are very slow in reaching the optimum in comparison to gradient based methods [120]. Alber and Reemtsen [6] proposed a Lagrangian barrier-penalty

algorithm to optimize a biological model including EUD and partial volume constraints and employed tumor control probability as the objective. Aleman et al. [9] presented a convex FMO formulation using the objective function proposed by Romeijn et al. [106] and implemented an interior point algorithm that yields an optimal treatment plan in seconds. Moreover, Men et al. [87] implemented the fluence optimization on graphics processing units (GPU). In this paper, a penalty-based quadratic optimization model, using a gradient projection method with Armijo's line search rule, was adopted. They achieved speedup factors of 20–40, without losing accuracy using GPU computing.

2.1.3 Leaf Sequencing (LS)

The outcome of the FMO problem is a fluence map for each beam direction. In order to deliver this ideal map, we find a positive linear combination of apertures formed by MLC, where the coefficient of each aperture represents the intensity or time the aperture is irradiated to the patient. The number of apertures obtained from this decomposition algorithm and sum of all aperture intensities, so-called *beam-on time*, are two measures of this problem.

It has been proved that minimizing the number of necessary apertures in LS is NP-hard in the strong sense, i.e., the exact solution cannot be obtained in a polynomial computational time using current computing methods [12]. Therefore, a large number of heuristics have been developed [54]. Kalinowski [64] has proposed a heuristic, which first minimizes the beam-on time and then among available decompositions finds the one with minimal number of apertures. Moreover, there are different technical constraints in MLC to form the aperture, such as leaf collision, leaf perturbation, and interdigitation.

2.1.4 Direct Aperture Optimization (DAO)

The sequential approach of the traditional IMRT treatment planning may lead to a potential loss in the treatment quality, dose discrepancy, and a long treatment time. Due to these reasons, the Direct Aperture Optimization (DAO) problem has been developed, which integrates FMO and LS problems and directly optimizes the shape and intensity of MLC apertures.

However, the integrated model is large, with enormous number of candidate apertures. Column generation has successfully been used as exact or heuristic methods for large-scale problems with decomposable structure. The heuristic versions of CG have also been applied for IMRT and VMAT treatment planning.

Preciado-Walters et al. [102] formulated this problem as a mixed integer linear program maximizing minimum tumor dose and considering dose-volume constraints. A coupled pair

of column generation is proposed, in which the first one is designed to produce intensity maps, and the second one to enforce the dose-volume restrictions. In each iteration, the aperture which makes the largest improvement to the objective function will be added to the treatment plan until the plan quality is acceptable. Results have shown that the method could find near-optimal solutions for FMO with DVH constraints, but took a few hours. Romeijn et al. [108] proposed a column generation-based algorithm to produce aperture shapes in this problem and could present outstanding results. To demonstrate dose-volume constraints, a convex approximation developed by Romeijn et al. [106] using Conditional Value-at-Risk (CVaR) was utilized. For the pricing subproblem, they have developed an integer programming model, which was reduced to the network flow problem. Moreover, three MLC constraints including consecutiveness, interdigitation, and connectedness of leaves are considered in the pricing subproblem. Men et al. [86] extended this work by allowing the incorporation of more convex treatment plan criteria, and also the effects of transmission of radiation through the leaves of MLC. In addition to three MLC constraints formulated by Romeijn et al. [108], they considered the MLC systems which work only with the rectangular shape. The results on ten head-and-neck cancer cases show that incorporating the transmission effects could spare all saliva glands, effectively. In the same line of research, Men et al. [88] implemented their column generation-based algorithm for DAO by GPU. The results in 10 prostate and head-and-neck cases show that the computational time has significantly decreased from about 2 minutes to 0.7 – 3.8 seconds.

2.2 Volumetric Modulated Arc Therapy (VMAT)

An initial version of VMAT, Intensity Modulated Arc Therapy (IMAT), was proposed by Yu [134] as a rotational alternative to the IMRT delivery technique. As mentioned earlier in Section 1.4, to model the dynamic gantry motion, we divide the work area around the patient into a finite number of equi-spaced points, so-called *control points*, each point is a snapshot of the gantry and MLC during the continuous delivery. Also, instead of fixed beam directions, we can consider *arcs* to identify the MLC leaf trajectories. Earl et al. [47] proposed a simulated annealing heuristic for IMAT to determine the position of MLC leaves during each arc, whereas the number and range of arcs were fixed. Unfortunately, IMAT was not successful in practice because of its time inefficiency.

In 2008, Otto [96] presented a simple heuristic which sequentially adds the control-points and uses simulated annealing in each iteration to determine the aperture shapes and intensities.

Thereafter, two main approaches have been developed: (1) *two-stage* and (2) *direct aperture*. In the former, at the first stage, a huge FMO is solved to find the optimal intensity for

each beamlet in each control-point and obtain an *ideal* fluence map. At the second stage, this map is converted into a sequence of deliverable arcs such that the dose distribution is similar to the ideal fluence map [39]. The deliverable arc-sequencing is typically based on *unidirectional* leaf motion in which, the leaf pairs move unidirectionally from one side of the field to the other. Craft et al. [39] proposed an algorithm to determine the arcs in the second stage, so-called VMERGE, by merging the neighbouring fluence maps, iteratively, based on a similarity score to decrease the delivery time. Wala et al. [129] made this method more flexible and efficient by generating partial-arc plans via an iterative heuristic called PMERGE, and eliminating the unneeded arc segments without significantly compromising dose quality. Salari et al. [113] replaced the merging heuristic with an exact discrete bi-criteria optimization based on a network flow model. The objectives were minimizing the treatment time and minimizing the deviation from the ideal dose. They employed a customized box algorithm to characterize the Pareto frontier. Also, Papp and Unkelbach [99] proposed an arc-based model to deliver the ideal fluence map and directly optimize the unidirectional leaf trajectories. They proposed a linear model by approximating the dose deposition coefficient at each arc and solve it sequentially to find a good approximation for direct leaf trajectory problem in VMAT. Similarly, the number of arcs, the size of arcs, and dose rate are assumed to be constant.

The required computation in the two-stage approach is drastically time-consuming. The direct-aperture approach extends DAO to VMAT, i.e., it generates the apertures for the control-points and optimizes their corresponding intensities, simultaneously. Men et al. [89] proposed a column generation-based heuristic which sequentially adds aperture shapes at 177 control points while ensuring that each new aperture is compatible with the previous ones. They implemented the CUDA to take advantage of the parallel processing power of GPU. Peng et al. [100] improved this approach by considering the dynamicity of gantry speed and bounds on the dose rate after fixing the apertures. Using CUDA programming, the treatment plans by this algorithm could be produced in around one minute. Moreover, Peng et al. [101] studied VMAT with constant gantry speed and dose rate (VMATc), beneficial in developing countries without access to specialized treatment equipment to vary the parameters continuously.

Unkelbach et al. [123] provide a comprehensive review of optimization techniques for VMAT treatment planning.

Recent studies have extended VMAT optimization tools to take the treatment times and clinical criteria into account. Akartunalı et al. [5] proposed a mixed-integer programming model for VMAT treatment planning problem and developed new valid inequalities. The

model still was large, complex, and difficult to solve. They also developed two Lagrangian relaxation (LR) heuristics, a centring-based heuristic, and a guided variable neighborhood search (GVNS); the last approach was the most efficient. Balvert and Craft [14] investigated the trade-off between delivery time and fluence map optimization in VMAT. They optimized the leaf trajectories and dose rates for a given delivery time and obtained the complete trade-off curve for delivery time and plan quality. Recently, Dursun et al. [46] formulated a mixed integer programming model for the VMAT treatment planning and proposed an exact branch-and-price algorithm. To reduce the complexity of the model for the exact method, they minimize the beam-on time, as a linear objective. The pricing sub-problem is decomposable by rows of the MLC and modelled using graph theory; the shortest path problem is employed to solve it.

2.3 DVH criteria

One of the main technical challenges of the treatment planning is to find the optimal model parameters for generating an acceptable plan within a reasonable time. The dose–volume histogram is the most common method to evaluate the quality of obtained plan. In practice, the treatment planning technicians solve the problem several times for each patient, taking into account various parameters, e.g., the weights for target volumes and healthy organs, to find a clinically acceptable DVH. This manual procedure is time-consuming, especially for complex cases.

Langer [70] was the first study that considered dose-volume constraints (DVCs) by solving large number of successive linear programming models. The nonlinear form of DVCs can be considered as penalty in the objective function [27, 120] or within model constraints [29]. When DVCs are directly incorporated into the objective functions of least-squares models, the objective function becomes non-convex and non-differentiable [138].

Two approaches have been developed to handle DVH criteria. The first adds dose–volume constraints directly to the mathematical model, and the second automatically adjusts the penalty parameters in the objective function to reduce the violation of the predetermined thresholds.

In the first method, the non-convex nature of the DVCs leads to a nonlinear model [41]. We can linearize these types of constraints by introducing binary variables, but this results in a large mixed integer problem (MIP) [72, 102]. Despite many improvements to the MIP formulation [58], it is has been shown that the FMO problem with DVCs is non-convex and NP-hard [122]. Romeijn et al. [106] proposed a linear approximation of the DVCs based on the Conditional Value-at-Risk (CVaR) for FMO. Then, Romeijn et al. [108] developed

a column generation based algorithm for DAO and used the CVaR-based constraints in the model. However, this approach drastically increases the number of constraints in the model.

The second method automatically adjusts the model parameters in the objective function to meet the predetermined DVH criteria [22, 23, 128]. Wu and Mohan [133] employed a gradient optimization method for the FMO model and considered a simple algorithm adjusting voxel weights in the objective function based on dose-volume histogram. Li et al. [75] improved the previous work by a two-step approach for FMO problem: In the first step, the organ weights of the quadratic objective function are roughly adjusted; and in the second step, the voxel weighting factors are adjusted based on the DVH curves. In the same line of research, Zarepisheh et al. [137] have proposed an algorithm that automatically adjusts the FMO parameters to minimize the distance between the DVHs for the entire plan and the reference DVHs. They iteratively navigate the Pareto front and project the plan corresponding to the reference DVHs onto that surface. Recently, fuzzy inference systems also have been used for the FMO problem [45].

2.4 Multi-criteria optimization in radiation therapy

To find a trade-off between contradictory normal and tumor structures in radiotherapy treatment planning, several multi-criteria optimization (MCO) techniques have been developed. These methods look for solutions that cannot improve any single objective without deteriorating at least one other. We can can classify these techniques into several categories regarding the type of preference of the decision maker (DM). In Lexicographic techniques, the decision maker prioritize the objectives based on their importance a priori [22, 23, 78, 124]. In interactive methods, the decision maker guides the exploration during an iterative procedure [139]. In Pareto frontier (PF) optimization, we explore for a set of solutions, so-called non-dominated points, in which we cannot improve any objective without deteriorating at least one other objective [31, 34, 36, 37]. For a general review of MCO approaches in IMRT, we refer the reader to two comprehensive reviews by Küfer et al. [69] and Craft [33]. For the rest of the chapter, we limit ourselves to Pareto frontier optimization with convex objectives.

In PF optimization, the set of all non-dominated points is called Pareto front or Pareto frontier or Pareto surface, and there are a variety of methods to approximate this set. These approaches can be classified into inner approximation methods [114], outer approximation methods [16], and sandwich methods [66, 119]. In inner approximation, the lower boundary facets of the convex hull of the Pareto points contained in the set are used, while outer approximations find supporting tangential hyperplanes of the Pareto frontier and take their intersection to approximate the Pareto set. Sandwich methods combine these two techniques

and we can have an upper bound on the approximation error. For more details on this topic, we refer the reader to a comprehensive review by Ruzika and Wiecek [110].

In IMRT, Küfer et al. [67] have formulated the first multi-objective model for FMO problem. Craft et al. [38] have introduced the Sandwich method for higher dimensional IMRT problem. Later, they have shown that the number of required Pareto optimal solutions to represent Pareto frontier of up to five dimensions is linearly dependent to the number of objectives [32]. Moreover, Craft and Richter [35] proposed a Pareto front navigation algorithm for the stop and shoot IMRT problem based on deliverable plans, while the number of segments are restricted. In this work, the plans are already segmented to maximum 50 segments using Raystation 2.0 and two methods 2D-cut and ND navigation methods are developed to navigate by combining a limited number of plans. Shao and Ehrgott [116] also proposed a Sandwich algorithm for the multiobjective linear programming problem in FMO. In the same line of research, Ehrgott et al. [53] extended their algorithm to approximate the convex multi-objective nonlinear programming problems. Rennen et al. [104] enhanced the higher dimensional Sandwich algorithms by introducing the concept of dummy points to the inner approximation and a new error measure. Bokrantz [17] proposed a sandwich algorithm for approximating Pareto fronts of MOO problems based on enumerating the vertices of an outer approximation of the Pareto frontier in IMRT and the details are described by Bokrantz and Forsgren [18].

In most of these methods, the multi-criteria optimization has been formulated for the FMO problem. This model is easy to solve for multiple times, approximating the Pareto frontier. However, it is not deliverable in practice and another algorithm is required to produce a deliverable plan as close as desired to the obtained FMO plan.

Although the column generation technique has been widely used specially for DAO, few studies have addressed its implementation in MCO. Salari and Romeijn [111] incorporated the beam-on time into the treatment planning using direct aperture optimization in IMRT. They proposed an iterative solution approach which sequentially finds the optimal treatment plan for different segments of the beam-on time to obtain the set of Pareto-efficient frontier. In another study, Salari and Unkelbach [112] proposed a multi-criteria column-generation for IMRT treatment planning. The idea to extend the standard CG to multi-criteria approach was to consider multiple weighted-sum restricted master models based on fixed weight vector scenarios, e.g., three in the case. For the multi-criteria pricing problem, they formulated a mixed-integer programming (MIP) model and three heuristics to obtain the aperture yielding the largest improvement in the entire Pareto front. The computational results have validated that their method obtained a balanced approximation of the Pareto front over a

wide range of clinically relevant plans. However, the penalty weight scenarios are fixed during the column generation process and they can not guarantee that the non-dominated set is well-approximated. Recently, Lin et al. [77] developed a MOLP formulation for direct aperture optimization in IMRT treatment planning, so-called revised normal boundary intersection, and used the column generation algorithm to solve the linear models in its sub-problems.

CHAPTER 3 GENERAL ORGANIZATION OF THE DOCUMENT

The literature review on VMAT treatment planning techniques in Section 2.2 shows that the delivery time is assumed fixed, in most of the studies, at different levels of the treatment planning and minimized in the post-optimization phase. This fixing procedure in independent phases may cause a potential loss in the treatment time. Considering these shortcomings, in Chapter 4, we propose an efficient algorithm that simultaneously optimizes the aperture shapes and their corresponding intensity, and total delivery time in VMAT treatment planning. This method incorporates the advantages of both arc-based and control-point-based approaches.

The literature review on DVH criteria in Section 2.3 reveals that most studies have focused on FMO and there is no work in the literature addressing DVH criteria in DAO. This feature is especially useful in VMAT with respect to the large scale of the mathematical models in this problem. In Chapter 5, we take advantage of iterative procedure of column generation for aperture generation and intensity optimization to automatically handle dose-volume criteria by adjusting the priority of the structures and voxels in VMAT treatment planning. Thus, both the dosimetric-derived non-convexity of DVH criteria, and the hardware-derived constraints, i.e., the MLC apertures, are taken into account, simultaneously.

Our literature review in Section 2.4 showed that few studies, in general, have addressed the column generation-based multi-criteria optimization. To address this gap in the literature, in Chapter 6, we develop an algorithm to find an approximation of a non-dominated set of solutions during the course of column generation, avoiding a large number of columns. This extension to column generation, so-called Pareto-based column generation (PCG), is formulated for multi-criteria DAO treatment planning. Moreover, for the efficiency of the algorithm, we improved the column generation algorithm proposed for DAO by integrating a new first-order optimization technique in the master model. In this method, we generate strong columns without solving the master model to optimality in each iteration.

In Chapter 7, we provide a general discussion on the proposed methods as a whole. Finally, in Chapter 8, we summarize the contributions of the dissertation, explain the limitations of the proposed approaches, and offer future research directions.

CHAPTER 4 ARTICLE 1: SIMULTANEOUS DELIVERY TIME AND APERTURE SHAPE OPTIMIZATION FOR THE VOLUMETRIC-MODULATED ARC THERAPY (VMAT) TREATMENT PLANNING PROBLEM

Mehdi Mahnam

Department of Mathematics and Industrial Engineering, Polytechnique Montréal
Interuniversity Research Center on Enterprise Networks, Logistics and Transportation (CIRRELT),
Montreal, Canada

Michel Gendreau

Department of Mathematics and Industrial Engineering, Polytechnique Montréal
Interuniversity Research Center on Enterprise Networks, Logistics and Transportation (CIRRELT),
Montréal, Canada

Nadia Lahrichi

Department of Mathematics and Industrial Engineering, Polytechnique Montréal
Interuniversity Research Center on Enterprise Networks, Logistics and Transportation (CIRRELT),
Montréal, Canada

Louis-Martin Rousseau

Department of Mathematics and Industrial Engineering, Polytechnique Montréal
Interuniversity Research Center on Enterprise Networks, Logistics and Transportation (CIRRELT),
Montréal, Canada

Abstract. In this paper, we propose a novel heuristic algorithm for the volumetric-modulated arc therapy (VMAT) treatment planning problem, optimizing the trade-off between delivery time and treatment quality. We present a new mixed integer programming model in which the multi-leaf collimator leaf positions, gantry speed, and dose rate are determined simultaneously. Our heuristic is based on column generation; the aperture configuration is modeled in the columns and the dose distribution and time restriction in the rows. To reduce the number of voxels and increase the efficiency of the master model, we aggregate similar voxels using a clustering technique. The efficiency of the algorithm and the treatment quality are evaluated on a benchmark clinical prostate cancer case. The computational results show that a high-quality treatment is achievable using a four-thread CPU. Finally, we analyze the effects of the various parameters and two leaf-motion strategies.

Keywords. Radiation therapy treatment planning, VMAT, column generation, heuristic.

History. This article is published in *Physics in Medicine and Biology*, Vol. 62, No. 14, pp. 5589–5611, (2017).12

4.1 Introduction

Volumetric-modulated arc therapy (VMAT) is a novel form of external radiotherapy which incorporates rotation of the beam around the patient's body, while the beam is on. In this technology, the beam shape, rotation speed, and dose rate change continuously [96]. This minimizes the adverse effects of radiation to normal tissues and matches the radiation to the profile of the tumor. In general, the main advantages are a better dose distribution around the patient, lower radiation to normal tissues, faster treatment, and decreased patient discomfort [135].

Similar to intensity modulated radiation therapy (IMRT), the beams are formed by a multi-leaf collimator (MLC). This equipment has a finite number of leaf pairs, each consisting of a leading and a trailing leaf. The treatment planning problem in VMAT involves selecting sequences of MLC shapes and determining the optimal dose rate and gantry rotation speed around the patient [105].

An initial version of VMAT, intensity modulated arc therapy (IMAT), was proposed by Yu [134] as a rotational alternative to the IMRT delivery technique in radiotherapy. Unfortunately, IMAT was not widely adopted because of its time inefficiency. Otto [96] proposed a simple heuristic as the first study for VMAT treatment planning problem. Several optimization approaches have subsequently been developed for this large-scale problem; a comprehensive review is provided by Unkelbach et al. [123].

The methods proposed to model MLC restrictions in VMAT treatment planning can be classified into two groups: (1) arc-based and (2) control-point-based. In the arc-based approach, leaf motions during an arc are determined using a traditional two-stage method. In the first stage, fluence map optimization (FMO), the profile of beams for all the sectors are determined. A deliverable arc-sequencing, typically based on unidirectional leaf motion, is then designed such that the dose distribution is similar to the ideal fluence map [26, 39]. Wala et al. [129] improved this method by generating efficient partial-arc plans via an iterative heuristic called PMERGE. Salari et al. [113] replaced the merging heuristic with an exact discrete bi-criteria optimization. In the same line of research, Papp and Unkelbach [99] proposed an arc-based model to deliver the ideal fluence map and directly optimize the unidirectional leaf trajectories. Although the treatment plan resulting from the arc-based approach is reliable, the required computation is very time-consuming.

The control-point-based approach considers a finite number of points around the patient, the so-called control points or sectors, and each is associated with an aperture. The apertures are designed taking into account the MLC constraints, and the model optimizes the cor-

responding intensity. For this approach, heuristics based on column generation (CG) have been developed. These algorithms sequentially generate new aperture shapes in the pricing sub-problem (PSP) and add them to the master model, thus ensuring that each new aperture is compatible with the previous ones [89, 100]. Moreover, to take advantages of GPU computing, effective parallel processing algorithm have been implemented. The goal of this approach is to develop online adaptive radiotherapy techniques that can handle the inter-fraction variation of the patient's geometry.

Recently, Peng et al. [101] extended the control-point-based approach to the case with constant gantry speed and dose rate (VMATc) using a heuristic framework. VMATc is beneficial in developing countries without access to specialized treatment equipment which allows the parameters to vary continuously. Akartunalı et al. [5] proposed a unified mixed-integer programming model for VMAT, tomotherapy, and CyberKnife. Although the formulation was improved by considering polyhedral analysis and valid inequalities, this model is large, complex, and difficult to solve. The authors developed two Lagrangian relaxation (LR) heuristics, a centring-based heuristic, and a guided variable neighborhood search; the last approach was the most efficient. Nguyen et al. [92] developed a nongreedy approach using an L_2-norm fidelity term in the objective and a level set function to optimize the fluence intensity and aperture shapes simultaneously. Balvert and Craft [14] investigated the trade-off between delivery time and fluence map matching. They optimized the leaf trajectories and dose rates for a given delivery time and obtained the complete trade-off curve for delivery time and plan quality by solving the model heuristically with a sequence of delivery times.

Most models in the literature fix the key parameters—delivery time and dose rate—at different levels of the treatment planning. In this paper, we propose an efficient algorithm that simultaneously optimizes the aperture shapes, delivery time, and dose rate. The method incorporates the advantages of both arc-based and control-point-based approaches. We formulate a new mixed integer programming model. We form successive generations of apertures using graph algorithms for the sequencing and a gradient-based model with column-and-row generation to optimize the intensities. To increase the computational efficiency and also the treatment quality, we avoid solving the large FMO optimization model, and evaluate the treatment plans directly using voxels rather than fluence maps. Our model could easily be generalized to take into account multiple gantry rotations. However, in this paper we focus on treatment plans with a single gantry rotation to determine high-quality plans with a minimum delivery time. In summary, this paper makes the following contributions to VMAT treatment planning problem:

1. The new formulation simultaneously optimizes the gantry speed, dose rate, and leaf trajectories.

2. We optimize the total delivery time and the treatment quality. The gantry speed and consequently the delivery time at each sector around the patient are considered dynamic.

3. The algorithm is based on simultaneous column-and-row generation to relate the MLC apertures and the delivery time. Moreover, the feasibility of the movement constraints is taken into account in the PSP rather than the master problem, which increases the efficiency of the algorithm.

4. To decrease the computational time, we propose a new model of down-sampling based on the geometry of the voxels in the patient's body and clustering algorithms from data mining. This method aggregates similar voxels while considering the effect of all the voxels in the objective function of the model.

The remainder of the paper is organized as follows. Section 2 introduces the basic notation and the VMAT formulation in our framework. In Section 3, we propose our CG-based heuristic including the master model, PSP, greedy heuristic, and post-optimization. Section 4 presents computational experiments and results for a prostate case. Finally, Section 5 provides concluding remarks and discusses future research.

4.2 VMAT treatment planning formulation

To model the problem, we discretize each structure s of the patient into small cubic volume elements called *voxels*, $\mathcal{V}_s$, and denoted $\mathcal{V}_T$ and $\mathcal{V}_N$ for tumorous and normal tissues. Each beam is decomposed into a rectangular grid of *beamlets*, I. A beamlet is on if it is not blocked by either the leading or trailing leaf, and the relative motion of the leaves controls the intensity. The estimated dose received by voxel j from beamlet i at unit intensity is denoted D_{ij}, in Gy/MU. $D = [D_{ij}]$ is called the dose-influence matrix. We assume that the dose absorbed by a given voxel can be determined by adding the dose from each of the individual beamlets comprising the aperture. The dose received at voxel j from all the beamlets of aperture A is denoted $D_j(A)$.

In VMAT treatment planning, the continuous dose delivery is discretized over a finite number of *sectors*, H, by changing the angle of the beam, with typically 180 2°-spaced beam angles. This discretization is necessary because estimating the dose-influence matrix in each sector, D^h_{ij}, by dosimetry techniques is time-consuming. Moreover, each sector is associated with an aperture A regarding the position of the MLC trailing (left) and leading (right) leaves, the dose rate ρ (in MU/s), and the gantry speed ν_g (in deg/s). We assume that the aperture,

dose rate, gantry speed, and dose-influence matrices are constant for adjacent sectors. This approximation is good-enough when the angular distance between the two sectors is small. In addition, the gantry speed is the inverse of the sector time, and we use these terms interchangeably.

In this paper, the 360 degrees around the patient are covered by the set of arcs K, and each arc k of length δ^k contains a finite number of equi-spaced sectors, H^k, from h_s^k to h_f^k. Moreover, A_h^k denotes the aperture corresponding to sector h in arc k. To model the feasible treatment plans, we restrict the machine characteristics as follows:

- MLC constraints: The leading and trailing leaves are taken into account in the MLC ranges in the leaf motion constraints, and no overlap is allowed. Moreover, compatibility between adjacent MLC apertures, Δ_A, is required based on the maximum MLC leaf speed, ν_l^U.
- Gantry speed constraints: We impose lower and upper bounds ν_g^L and ν_g^U on the gantry speed to guarantee that the machine is in motion and within the feasible range.
- Dose rate constraints: We assume that the dose rate is bounded above by R, and a zero dose rate is allowed to avoid useless apertures.
- Adjacency constraints: We require compatibility of adjacent sectors in terms of the dose rate and the sector time in addition to the aperture shape, Δ_A. Thus, we restrict the rate of change of the dose rate, Δ_ρ, and the sector time, Δ_t.

The model for the VMAT problem is as follows, where $y^k = 1$ if and only if arc k is selected in the solution:

$$\mathbf{GP}: \min_{y,\rho,t} \quad F(\boldsymbol{z}) + w\,T \tag{4.1a}$$

s.t.

$$z_j = \quad \sum_{k\in K}\sum_{h\in H_k} D_{jh}(A_h^k)\, y^k\, \rho_h\, t_h \qquad \forall j \in \mathcal{V} \tag{4.1b}$$

$$\sum_{k\in K} a_h^k\, y^k = 1 \qquad \forall h \in H \tag{4.1c}$$

$$\mid \rho_{h+1} - \rho_h \mid \leq \Delta_\rho \qquad \forall h = 1, 2, \cdots, |H| - 1 \tag{4.1d}$$

$$0 \leq \rho_h \leq R \qquad \forall h \in H \tag{4.1e}$$

$$\sum_{k\in K} \tau_{h,h+1}^k\, y^k \leq t_h \qquad \forall h \in H \tag{4.1f}$$

$$\mid t_{h+1} - t_h \mid \leq \Delta_t \qquad \forall h = 1, 2, \cdots, |H| - 1 \tag{4.1g}$$

$$\underline{T} \leq t_h \leq \overline{T} \qquad \forall h \in H \tag{4.1h}$$

$$\sum_{h\in H} t_h \leq T \tag{4.1i}$$

$$y^k \in \{0, 1\} \qquad \forall k \in K \tag{4.1j}$$

Here vector $\boldsymbol{z}$ is the dose absorbed by the voxels, and $F(\mathbf{z})$ is a voxel-based convex function. T is the total delivery time, which is penalized by a small value of w. The objective is to maximize the treatment quality and minimize the delivery time. The dose absorbed by voxel j, z_j, is computed in Equation (4.1b) based on the sectors covered by arc k, H_k; the dose-influence matrix D; the aperture shape A_h^k; the arc selection variable y^k; and the sector time t_h. Also, a_h^k indicates the coverage of sector h by arc k, and thus Constraint (4.1c) ensures that each sector h is covered exactly by one arc. Constraints (4.1d, 4.1e) enforce lower and upper bounds on the dose rate and limit the change in the rate between adjacent sectors to at most Δ_ρ. Constraints (4.1f) ensure that the time spent at each sector t_h is sufficient to allow the leaf movements to reach the aperture shape positions in the next sector, A_{h+1}^k, given the maximum leaf speed ν_l^U. Constraint (4.1g) limits the rate of change in the sector time between adjacent sectors to at most Δ_t. Finally, Constraint (4.1h) enforces the lower and upper bounds on the delivery time, and Constraint (4.1i) determines the total delivery time T.

Because of the non-linearity in Equation (4.1b) and the binary variable y, this is a large-scale mixed integer nonlinear programming (MINLP) model. It is difficult to solve the proposed MINLP model, especially in real-world cases even by commercial software. In the next section, we propose an efficient heuristic to produce high-quality treatment plans.

4.3 Proposed method

Column generation (CG) is a leading optimization technique to solve large-scale problems with decomposable structure specially when there are a large number of variables [43]. This approach has successfully been used in many applications such as Vehicle Routing Problem (VRP) [56], airline crew pairing [44], and cutting-stock problems [125] as exact or heuristic methods. This method has also been applied in classic radiotherapy treatment planning problems, e.g. Intensity Modulated Radiation Therapy (IMRT) [108], and new technologies, e.g., Volumetric Modulated Arc Therapy (VMAT) [100].

In the column generation (CG) technique, instead of generating all the feasible columns in advance, we decompose the model into two subproblems: (1) the restricted master problem (RMP), which contains a subset of the columns, and (2) the PSP, in which promising new columns are generated, expecting to improve the RMP objective function. In our model, each column k is an arc from sector h_s^k to h_f^k, made up of the apertures of the leading and trailing leaves in a sequence of sectors. Without loss of generality and to simplify the method, we assume that the number of arcs and their lengths are fixed. The procedure starts with a subset of initial arcs completely surrounding the patient. We then repeatedly solve the following two subproblems until no new improving column is available:

- RMP: Given a large set of arcs ($K' \subseteq K$), we select the best subset that covers all the sectors, optimizing the intensities, gantry speed, and dose distribution z^*. We transfer the dual values of the voxels to the PSP.
- PSP: Given the dual values from RMP, we identify promising arcs using graph theory and add them to the pool of generated arcs (K').

To see the benefits of CG in VMAT, consider a rectangular (n_r, n_c) beam, with n_r rows and n_c columns, and h sectors. The total number of aperture shapes is about $((n_r/2)(n_c+1)(n_c+2))^h$ while the optimal solution has only h apertures. In an instance with a $(5, 10)$ beam and 100 sectors, there are 7.1×10^{251} possible apertures. In real cases, the number of beamlets and sectors is usually much larger. Therefore, CG generates good apertures while avoiding those that are unhelpful, similar, or infeasible. Furthermore, CG is a linearization method that converts the nonlinear GP model into two linear models.

4.3.1 Master Model

The master model optimizes the dose rate and gantry speed during the LINAC rotation around the patient given the generated arcs. The total number of potential arcs K is large,

so a subset $K' \subset K$ is considered in the RMP. This model is solved several times during the CG procedure, so the algorithm must be efficient. To decrease the computational time, we have developed a convex model with a convex cost function, linearized the solution space, and reduced the number of constraints by aggregating similar voxels.

Cost function

Several objective functions have been proposed in radiotherapy treatment planning, including quadratic objectives, nonlinear radio-biological objectives, e.g., TCP and NTCP, and the equivalent uniform dose (EUD) [52]. We use the following *quadratic voxel-based least square penalty function* to measure the treatment quality:

$$F(\boldsymbol{z}) = \sum\nolimits_{s\in S} \sum\nolimits_{j\in\mathcal{V}_s} \underline{w}_s \, [\underline{d}_j - z_j]_+^2 + \overline{w}_s \, [z_j - \overline{d}_j]_+^2, \tag{4.2}$$

where $[\bullet]_+$ denotes $max\{0, \bullet\}$ and $\underline{d}_j$ and $\overline{d}_j$ are prespecified lower and upper dose thresholds for voxel j. Moreover, $\underline{w}_s$ and $\overline{w}_s$ are the weights for the underdose and overdose in structure s, respectively. This objective is well known because of its convexity and the quality of the resulting treatment plans [99, 100, 108]. Its disadvantage is the large number of constraints required to linearize the $[\bullet]_+$ operator for the relevant voxels.

Linearization

In model (GP), the dose received by each voxel j depends on the dose rate and the time in the sectors, which is the so-called sector-dependent approach. This approach is nonlinear, and we make two simplifying assumptions to linearize the model. First, we replace the product of the decision variables ρ and t in Constraint (4.1b) by a new variable called the *fluence rate*, defined to be $\gamma = \rho\, t$. We can determine the optimal dose rate for each sector by simultaneously optimizing the fluence rate and the sector time. Second, the nonlinear term $\gamma_h \, y^k$ gives the fluence rate of sector h in arc k if selected. To avoid this product, we assume a constant fluence rate through the arc, γ^k, as in the arc-dependent approach. Constraint (4.1b) is thus replaced by Equation (4.3), where the dose absorbed by voxel j depends only on the fluence rate of arc k, γ^k, and aperture k, A^k:

$$z_j = \sum\nolimits_{k\in K} D_{jh}(A_h^k)\, \gamma^k \qquad\qquad \forall j \in V_s \tag{4.3}$$

The linear feasible space of the arc fluence rate, γ^k, with regard to the arc variable, y^k, the

sector time t_h, the maximum dose rate R, and the linearizing relaxations [3] is as follows:

$$\gamma^k \leq R\, t_h \qquad \forall k \in K, \forall h \in H^k \tag{4.4}$$

$$0 \leq \gamma^k \leq y^k\, R\, \overline{T} \qquad \forall k \in K \tag{4.5}$$

$$\gamma^k \geq 0 \qquad \forall k \in K \tag{4.6}$$

To make the model more efficient, we replace Constraints (4.4) by

$$\sum_{k \in K} a_h^k\, \gamma^k \leq R\, t_h \qquad \forall h \in H \tag{4.7}$$

Although the fluence rate is fixed for any given arc, it can change between arcs. Moreover, the gantry speed, ν_g^h, can change from one sector to another. Finally, when we have found the final arcs, we use a post-optimization model to determine the sector-based fluence rates (see Section 4.3.4). In addition, restricting the leap of fluence rate between adjacent sectors is taken into account in the post-optimization model.

The proposed master model is a mixed integer programming model with binary arc variables, y^k. At the beginning of the algorithm, we relax the binary variables in the relaxed restricted master problem (RRMP):

$$\textbf{RRMP}: \min_{y,\gamma,t} \quad F(\mathbf{z}) + w\, T \tag{4.8a}$$

s.t.

$$z_j = \textstyle\sum_{k \in K'} D_{jh}(A_h^k)\, \gamma^k \qquad \forall\, j \in V_s \tag{4.8b}$$

$$\textstyle\sum_{k \in K'} a_h^k\, y^k \leq 1 \qquad \forall\, h \in H \tag{4.8c}$$

$$\textstyle\sum_{k \in K'} \tau_{h,h+1}^k\, y^k \leq t_h \qquad \forall\, h \in H \tag{4.8d}$$

$$\textstyle\sum_{h \in H} t_h \leq T \tag{4.8e}$$

$$\textstyle\sum_{k \in K'} a_h^k\, \gamma^k \leq R\, t_h \qquad \forall\, h \in H \tag{4.8f}$$

$$\gamma^k \leq y^k\, R\, \overline{T} \qquad \forall\, k \in K' \tag{4.8g}$$

$$\underline{T} \leq t_h \leq \overline{T} \qquad \forall\, h \in H \tag{4.8h}$$

$$y^k, \gamma^k \geq 0, \qquad \forall\, k \in K' \tag{4.8i}$$

In this relaxation, the upper bound $y^k \leq 1$ is dropped because it is induced by (4.8c). In addition to the quadratic objective function, the *column-dependent rows* in Constraints (4.8g)

and the large number of Constraints (4.8b) are the two main challenges of this model. We discuss the first challenge in Section 4.3.1 and develop an objective function for the PSP based on an equivalent relaxation. To overcome the second challenge, we develop a down-sampling algorithm inspired by clustering methods to aggregate similar voxels (Section 4.3.1).

Column-dependent rows

In standard CG, the effect of a new column is computed by minimizing its *reduced cost* in the objective function of the PSP [43]:

$$\min_{k \in K \setminus K'} z^* = c_k - \pi^T a_k, \tag{4.9}$$

where c and a are the objective and constraint coefficients, and π is the vector of the dual values of the corresponding constraints in the master model. If $z^* < 0$, introducing the new column into the solution of the master problem would decrease the objective. However, in our model, there are two columns y^k and γ^k for each arc k, determining the selection value and fluence rate, respectively. These columns are linked by Constraint (4.8g), and the linking constraints are not in the RRMP a priori; thus, the reduced costs of the columns may be computed incorrectly in the PSP because no dual information for the missing constraints is available.

General approaches for *simultaneous column-and-row generation* have been developed [91]. However, our model has the following simplifying properties:

Property 1. For each arc, columns y and γ are linked through a single linking constraint.
Property 2. γ cannot take a positive value unless y is positive.
Property 3. Adding new linking constraints does not violate primal feasibility.

In this case, analyzing the reduced costs of columns y and γ separately would lead to incorrect results. In particular, column y, considered independently of γ, cannot have a negative reduced cost because it does not affect the dose distribution $\mathbf{z}$. Moreover, suppose that for a given arc, the reduced cost of γ is negative while the reduced cost of y is positive. Although column γ is eligible to enter the basis, it is forced to be zero and the resulting iteration will be degenerate because of Property (2). To avoid this, we must generate the two columns simultaneously together with the corresponding linking constraint (4.8g).

In Appendix A, we present a new model, RRMP$'$, based on only column γ. It is shown that any optimal solution of RRMP can be transformed into an equivalent optimal solution in RRMP$'$. Then, models RRMP and RRMP$'$ are equivalent, and we can derive the objective

function of the PSP from RRMP′ in Section 4.3.2. To determine the best combination of arcs in the integer model, we generate column y and the linking constraint (4.8g) based on column γ and add them to the model.

Voxel aggregation

As mentioned earlier, the master model is time-consuming because of the large number of voxels. In the literature, random down-sampling is often implemented to simplify the problem. In a new technique, Küfer et al. [68] and Scherrer et al. [115] clustered the voxels via heuristics based on hierarchy construction in IMRT optimization; they developed an acceptable approximation that could be solved ten times faster.

In this paper, we propose an efficient method inspired by the K-means algorithm, a well-known technique to classify data by fixing a certain number of clusters a priori [80]. We treat the voxels as points that must be clustered into $|C|$ groups. To define the set of observations, we consider full open radiation (open beamlets in all sectors, i.e., $\sum_{h\in H} D_h$). The effect of beamlets on each voxel is a vector in R^n with n beamlets. We first randomly assign the voxels to the clusters and define the centroid of each cluster to be the mean of the observations. The original K-means method computes the distance of each voxel from the centroid of all the clusters and assigns it to the nearest one. We instead calculate the distance of the voxel from its *neighboring* clusters; this is because we expect a high degree of similarity among neighbors. We also take into account the average Euclidean distance of the voxels from the corresponding centroid as a measure of the quality of the clustering. This objective is nonincreasing, and the process continues until there is no significant improvement.

This method uses the geometric information about the voxels and the fact that neighboring voxels usually have similar dosimetry profiles. The weight of each cluster in the objective is proportional to the number of embedded voxels, so all the voxels are taken into account despite the down-sampling. Algorithm 1 gives the pseudocode for the aggregation method. We perform the aggregation at the beginning of the CG, and the sets of aggregated voxels are then fixed until the post-optimization.

4.3.2 Pricing subproblem

In the PSP, we use a graph approach to determine the arrangement of the leading and trailing leaves in the δ sectors from h_s to h_f. This approach was inspired by Boland et al. [19] and Romeijn et al. [108], who proposed a network model to produce the aperture shapes in IMRT, and also by Luan et al. [79], who extended it to IMAT. In our model, each node represents a pair of MLC leaves in a sector, and the arcs represent feasible movements in the graph.

Algorithm 1 Voxel Aggregation

Input: Dose-influence matrices in all sectors D^h, number of clusters $|C|$
Output: List of voxels in each cluster $c*$
Calculate D^F with full radiation: $D^F = \sum_{h \in H} D^h$
Randomly assign voxels to clusters
while stop criteria not satisfied **do**
    for voxel $j = 1$ to $|V|$ **do**
        $\overline{d}_{j,\overline{c}_j}$ = distance from voxel j to its current cluster $\overline{c}_j$
        for neighboring voxel $j' = 1$ to $|N_j|$ **do**
            $d_{j,\overline{c}_{j'}} = \| D_j^F - D_{\overline{c}_{j'}}^F \|_2^2$
            if $d_{j,\overline{c}_{j'}} < d_{j,\overline{c}^*}$ **then**
                $\overline{c}_j^* = \overline{c}_{j'}$
            end if
        end for
        if $\overline{c}_j^* \neq \overline{c}_j$ **then**
            Move voxel j to cluster c_j^*
        end if
    end for
end while
stop

Graph algorithm

Let graph $G = (V, E)$ be a layered acyclic digraph where V is the set of nodes and E the set of arcs. Each node in the h^{th} layer (denoted by L_h) defines a feasible arrangement of MLC leaves in each row of sector h. The arrangement of trailing and leading leaves (t, l) in row m and sector h is denoted by $(h, t, l)_m$. Figure 4.1 shows example positions for a pair of leaves. Moreover, E contains the multi-layer arcs (u, v) where if $u \in L_h$ then $v \in L_{h+1}$. Our goal is to cover all the sectors in an arc, even possibly with closed apertures if required. We define two dummy nodes D and D': the start node D is linked to the first layer, and the nodes of the last layer are linked to D'. Smaller partial arcs could easily be generated by linking D and D' to all the layers.

Our network takes into account the MLC constraints by eliminating infeasible nodes and arcs. As the first constraint, the range of leaf movements must be within certain limits, $\Delta^{min} \leq l - t \leq \Delta^{max}$. This constraint avoids collisions of leaves with $\Delta^{min} > 0$ and also ensures that the maximum tip difference is in the specified range Δ^{max}. We remove infeasible nodes outside of these bounds. Moreover, leaf movements should be compatible between adjacent sectors, i.e., leaf movements between adjacent sectors are restricted based

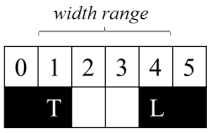

Figure 4.1 Leaf position with $(t, l) = (1, 4)$. The trailing (left) leaf is located in beamlet 1, and the leading (right) leaf is located in beamlet 4. The beamlets between these two are open and the others are blocked. Columns 0 and 5 are dummy blocked beamlets demonstrating the range of the leaf movement.

on the maximum leaf speed, ν_l^U. We remove the infeasible arcs from the graph to guarantee the compatibility of adjacent sectors in the PSP. To consider the effect of the adjacency constraints, we transfer the minimum required time for the leaf movement at each sector h of arc k to the master model with the parameter τ_h^k. Figure 4.2 shows an instance of the pricing graph with three layers and maximum leaf movement $\Delta_l = 1$. An advantage of the graph approach is that increasing the number of technical constraints decreases the size of the graph.

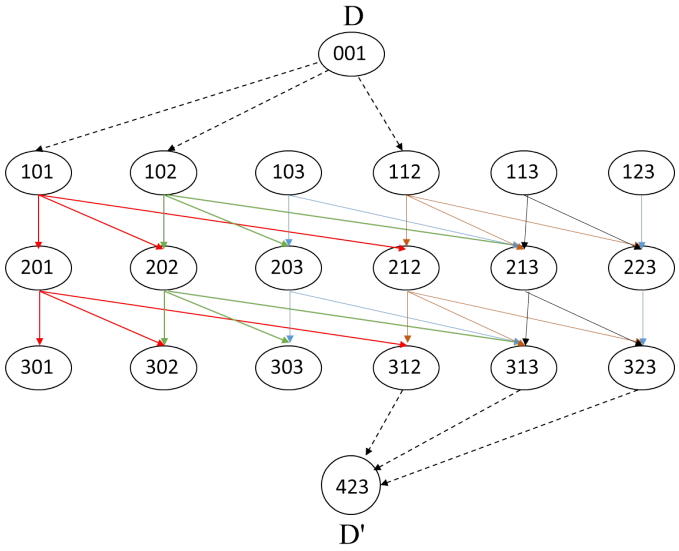

Figure 4.2 A pricing graph with three layers. We assume that the leaf movement is unidirectional from left to right and the maximum leaf movement is $\Delta_l = 1$ beamlet. Δ_l depends on the leaf and gantry speed parameters. For instance, if $\nu_l^U = 3$ cm/s, $\nu_g = 6°$/s, $\delta = 2°$, and the beamlet width $w_b = 1$ cm, Δ_l is 1. This value affects the arc feasibility during the building of the graph. For example, movement from node (101) to (213) is infeasible, and the corresponding arc is removed.

Pricing objective function

As explained in Section 4.3.1 and A, the PSP is based on the reduced cost of RRMP′:

$$\min_{k\in K\setminus K'}\{\sum_{h\in H}\sum_{j\in\mathcal{V}} D^k_{jh}(A^k)\,\hat{\pi}_j - \sum_{h\in H}(\tau^k_{h,h+1}\,\hat{\varphi}^h + a^k_h\,\hat{\sigma}_h)\}, \tag{4.10}$$

where $\hat{\pi}_j$, $\hat{\varphi}_h \leq 0$, and $\hat{\sigma}_h \leq 0$ are the dual values of Equations (A.5), (A.6), and (A.7) in RRMP′, respectively. Therefore, it suffices to solve the PSP with the objective function (4.10) and to add columns to the master model if the objective value is negative. To transfer this objective into the graph, we define the weight of each node $(h,t,l)_m$ as follows:

$$\sum_{j\in\mathcal{V}} D^{(t,l)_m}_{jh}(A^{(t,l)_m})\,\hat{\pi}_j - \hat{\sigma}_h. \tag{4.11}$$

The weight of each arc connecting node $(h,t,l)_m$ in sector h to $(h+1,t',l')_m$ in sector $h+1$ is computed as follows:

$$-\tau_{(h,t,l)_m,(h+1,t',l')_m}\,\hat{\varphi}^h, \tag{4.12}$$

where $\tau_{(h,t,l)_m,(h+1,t',l')_m}$ is the minimum time for vertex $(h,t,l)_m$ in sector h to reach $(h+1,t',l')_m$. Obviously, if a node is on the shortest path, $a^k_h = 1$ and the corresponding cost according to its sector and leaf position is taken into account; otherwise, the cost is not considered and $a^k_h = 0$.

Implementation details

The pricing subproblem, determining the best leaf pattern for a given range of sectors is solved by a polynomial-time shortest-path algorithm [4]. According to the directed acyclic graph G in this problem, we use the topological sorting technique, which runs in $O(|V|+|E|)$ time. Although the run time is negligible, the time to refeed the graph weights regarding the large number of voxels is considerable. We solve the PSPs in parallel for new arcs to reduce the computational time. To this end, a large graph with 180 layers (sectors) is defined and a slave PSP for each new arc k is implemented. For instance, if the length of the arcs is four, the PSPs are PSP_1 (1–4), PSP_2 (5–8), $\cdots$, PSP_{45} (177–180).

The independent arcs around the patient and the shared memory of the problem allow us to implement pricing in parallel using open multi-processing (openMP). This approach is easy to implement and flexible [65]. It starts with a single thread (the master thread) that creates sets of parallel worker threads (forks) in the parallel region. The threads are executed in parallel, and they synchronize and join the master thread at the end of the parallelization.

In our work, the graph is shared among all the threads, and the threads simultaneously generate disjoint arcs in different parts of the graph.

4.3.3 Greedy Heuristic

The optimal solution for the arc selection variable y^k in the RRMP is usually fractional. The next step is 1) a branch-and-price search on the set of columns generated or 2) the use of a simple heuristic to round and fix the best columns. The first approach is too time-consuming, so we use a greedy heuristic to provide a feasible solution. At each CG iteration, we fix the lower bound of the y^k variable with the largest fractional part to 1. This method is fast but greedy. To accelerate the process, if there are other arcs with high fractional values, e.g., $y^k > 0.85$, we fix them also to 1 and skip the pricing problem for arcs that contain some or all of the corresponding sectors. Algorithm 2 gives the pseudocode for the greedy column-and-row generation heuristic (GCRGH).

Algorithm 2 GCRGH procedure

```
Initial random heuristic columns (arcs)
while stopping criteria not satisfied do
        Master Model (Arc-based)
        Fix the best arc to 1
        Pricing subproblem
end while
Post-Optimization (Sector-based)
   Re-optimize gantry speed & intensities
stop
```

4.3.4 Post-Optimization

The proposed column generation-based heuristic returns the final aperture shapes and the arc-dependent fluence rates, γ^k. To improve the treatment plan, we propose a post-optimization model with three features. First, the arc-dependent approach is replaced by sector-dependent fluence rates. Second, we consider all the voxels and restrict the rate of change in the fluence rate, Δ_γ, and the sector time, Δ_t, between adjacent sectors. Third, the MLC leaf positions at the intersection points of adjacent arcs must satisfy the maximum leaf-movement constraint. If necessary, a simple heuristic removes any inconsistency with as little change as possible.

Let the set of arcs found by the CG be K^*. The post-optimization model is as follows:

$$\textbf{Post-Opt}: \min_{\gamma,t} \quad F(\mathbf{z}) + w\,T \tag{4.13a}$$

s.t.

$$z_j = \sum\nolimits_{h\in H} D_j^h(A^{K^*})\,\gamma_h \qquad \forall j \in V \tag{4.13b}$$

$$\gamma_h \le R\,t_h \qquad \forall h \in H \tag{4.13c}$$

$$\tau_{h,h+1} \le t_h \le \overline{T} \qquad \forall h \in H \tag{4.13d}$$

$$t_{h+1} - t_h \le \Delta_t \qquad \forall h = 1, 2, \cdots, |H| - 1 \tag{4.13e}$$

$$\gamma_{h+1} - \gamma_h \le \Delta_\gamma \qquad \forall h = 1, 2, \cdots, |H| - 1 \tag{4.13f}$$

$$\sum\nolimits_{h\in H} t_h \le T \tag{4.13g}$$

$$t_h, \gamma_h \ge 0 \qquad \forall h \in H \tag{4.13h}$$

4.4 Experiments and results

We implemented the GCRGH algorithm in C++ and used IBM ILOG CPLEX 12.6.2 for the mathematical models. If not stated otherwise, the computational experiments were run on four threads of a 3.07 GHz Intel(R) Xeon(R) X5675 Linux workstation. The quadratic RRMP is solved at each iteration using the CPLEX Barrier Optimizer, which is based on an interior-point method. To evaluate the quality of the treatment plan, we use the dose volume histogram (DVH), the most common method in practice. These diagrams indicate the percentage of a volume that receives at least a certain dose. We export our plans to Computational Environment for Radiotherapy Research (CERR) to visualize the results and obtain DVHs [42].

4.4.1 Data and benchmark

To evaluate the efficiency of the proposed heuristic, we considered a challenging prostate case in the CORT dataset, with 180 sectors, 25,404 beamlets, and 699,864 voxels [40]. There are two tumors, PTV-56 and PTV-68, and seven healthy tissues including the bladder, rectum, left and right femoral heads, prostate bed, and penile bulb. The parameters are listed in Table 4.1. A pencil beam type algorithm referred as the Quadrant Infinite Beam (QIB) model is used for dose calculation in this case. To the best of our knowledge, CERR uses the CT information to do first-order heterogeneity corrections along the path of the pencil beam.

The fraction treatment is the standard 2 Gy per fraction, the prescribed radiation dose is 68 Gy for PTV-68, and the treatment plans were optimized for 34 fractions. Furthermore, the machine parameters of the VMAT problem, typically considered in the literature, are listed in Table 4.2 [40]. In proportion to the range of the gantry speed, ν_g, the delivery time is between 1 and 6 minutes.

Table 4.1 Prostate case parameters

Total # beamlets	25,404
Beamlet size (cm)	1×1
Voxel resolution (mm)	3, 3, 3
# Target voxels	9491
# Body voxels	690,373

Table 4.2 VMAT machine parameters

Maximum leaf speed, ν_l^U	3 cm/s
Gantry speed, ν_g	1–6°/s
Maximum dose rate, ρ^U	600 MU/min
Maximum fluence change, Δ_γ	2 MU
Maximum change of sector time, Δ_t	2 s

4.4.2 GCRGH heuristic treatment plan

In this section, we measure the performance of our GCRGH heuristic on the prostate case.

To find an acceptable treatment plan regarding DVH constraints, we dynamically adapt the structure underdose and overdose weights, $\underline{w}_s$ and $\overline{w}_s$, based on the coarse-adjusting stage proposed by Li et al. [75], during some iterations of the column-generation procedure and also during post-optimization. In this approach, we increase the weighting factors of the structures whose DVH measures are worse than the critical dosimetry references. The best delivery time found is 3.44 minutes (Plan-Opt). As shown in Figure 4.3 all the healthy tissues are far from the thresholds, and the tumor tissues are sufficiently irradiated.

A challenge in this case is *multi-organ voxels*: a voxel could be in more than one organ, especially at boundaries. This could introduce bias in the objective function and DVH diagrams. In these cases, if a voxel belongs to both tumor and healthy tissues, we penalize it twice in the objective function; if it is in two similar structures, we penalize the organ with higher priority. For example, if a voxel belongs to both PTV-68 and PTV-56, we choose PTV-68. Anyway the calculations for the treatment measures and DVH diagrams take all

the tissues into account. As shown in Figure 4.3, the tail of the rectum and the bladder have some overlapping parts and tumors. The more accuracy in the boundaries and the fewer the multi-organ voxels, the greater the accuracy in the DVHs and plans.

The computational time is about 4.34 minutes, which compares well with the literature, especially since we use only four threads. Note that this does not include the time required to read the data and plot the diagrams.

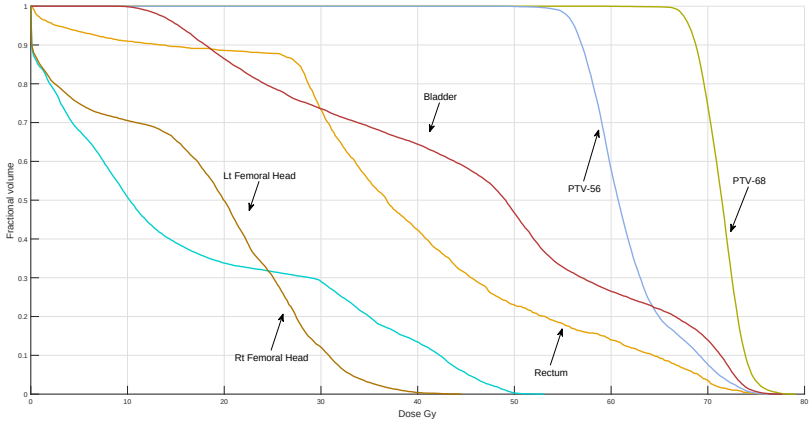

Figure 4.3 DVH plots for Plan-Opt for the prostate case using GCRGH.

4.4.3 Delivery time

In this section, we investigate the effect of delivery time on solution quality. To find the balance between these two objectives, we evaluate the heuristic with values of the penalty weight w of Equation (4.1a) ranging from 0 to infinity. Table 4.3 compares the delivery time and critical measures of 13 treatment plans. When $w = 0$, there is no constraint for delivery time, which results in a delivery time six minutes. For a very large penalty weight w, the gantry rotates at the maximum speed, one minute, with closed apertures. The results indicate a general trend of increasing the delivery time with increasing w, although it it is not completely monotone, due to the heuristic nature of the algorithm. Moreover, when the quality of the solution decreases when w increases, and the best value in terms of delivery time and plan quality is $w = 1$. For penalties between 0 and 1, the priority of delivery time becomes negligible and the plan quality is optimized, while the delivery time does not necessarily increases.

In Figure 4.4 we compare the DVH diagram for $w = 1$ (Plan-Opt) to that for $w = 10$ with delivery time about 3 minutes (Plan-3). In Plan-3, similar to Plan-Opt, the healthy tissues

Table 4.3 Delivery time vs. treatment plan dosimetry measures

	Delivery	PTV-56	PTV-68	Rectum			Bladder	
w	time (min)	V56 $\geq$ 95	V68 $\geq$ 95	V30 $\leq$ 80	V50 $\leq$ 50	V60 $\leq$ 25	V40 $\leq$ 70	V65 $\leq$ 50
0	5.98	**95.65**	**95.39**	**62.24**	**21.83**	**8.67**	**66.32**	**22.13**
1	3.44	**96.15**	**95.82**	**73.64**	**23.07**	**9.52**	**64.51**	**21.98**
5	3.34	**97.01**	93.09	86.73	**30.10**	**14.06**	**61.25**	**23.05**
10	3.32	84.50	92.11	81.35	**26.98**	**13.72**	**65.59**	**24.17**
20	3.10	79.94	89.14	85.15	**27.32**	**14.23**	**46.37**	**21.28**
30	2.74	82.58	88.54	87.07	**30.95**	**13.61**	**60.97**	**20.76**
50	3.01	76.32	78.58	**56.46**	**24.49**	**10.77**	**62.34**	**22.46**
100	2.37	90.70	87.70	82.20	**32.82**	**9.92**	**54.31**	**21.63**
150	1.91	87.10	90.69	89.23	50.68	**13.89**	90.76	**20.44**
250	1.84	94.94	86.12	90.42	76.08	**15.42**	99.84	**44.77**
500	1.74	86.55	88.63	90.53	74.94	**19.84**	99.84	**29.43**
1000	1.65	99.08	79.23	91.44	88.38	77.38	100.00	53.23
INF	1.10	0.00	0.00	0.00	0.00	0.00	0.00	0.00

Acceptable measures are printed in bold.

are protected, but the doses in the tumor tissues are substantially lower, especially for PTV-68. In addition, to assess the effect of increased treatment time on the solution quality, we restricted the total delivery time to 4, 5, and 6 minutes and compared Plans 4-6, respectively, to Plan-Opt in Figures 4.5 - 4.7. These treatment plans provide enough time for treatment delivery and could meet clinical needs, as expected. In comparison to Plan-Opt, the rectum is protected better but the bladder receives more dose in Plans 4-6. In general, Plan-Opt still has good enough quality and it is not dominated for all critical measures by other plans, while delivered in less time. The mean absolute difference between Plan-Opt and Plan-6, as the worst case, in the critical measures is about 2.34%. Therefore, the difference between plans with more delivery time and Plan-Opt is not meaningful and our algorithm finds a trade-off between the delivery time and the dose distribution.

4.4.4 Voxel aggregation

We now analyze the efficiency of the voxel aggregation algorithm and its effect in the prostate case. Its computational time (see Table 4.4) is about 11 seconds. The number of voxel transfers from one cluster to another has a decreasing trend. We run the algorithm for four iterations until the total average distance of the voxels from the cluster centroids is improved by less than one. The improvement in the solution after the first iteration is about 6.5%, and it seems that one iteration suffices.

Figure 4.8 shows the DVH curves for the full plan and the aggregated version. The latter

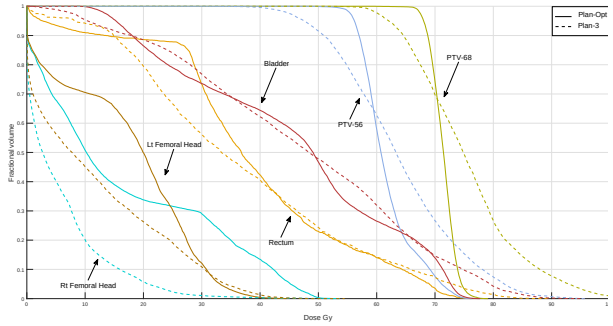

Figure 4.4 Plan-Opt (3.44 minutes) vs. Plan-3 (3 minutes)

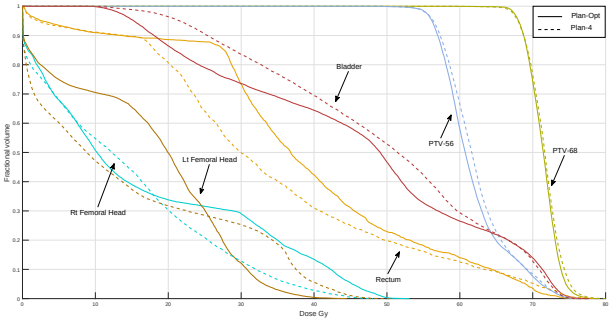

Figure 4.5 Plan-Opt (3.44 minutes) vs. Plan-4 (4 minutes)

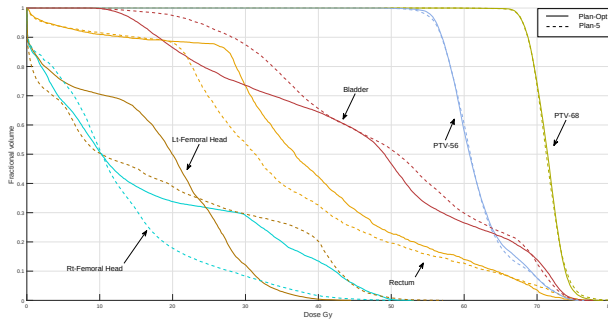

Figure 4.6 Plan-Opt (3.44 minutes) vs. Plan-5 (5 minutes)

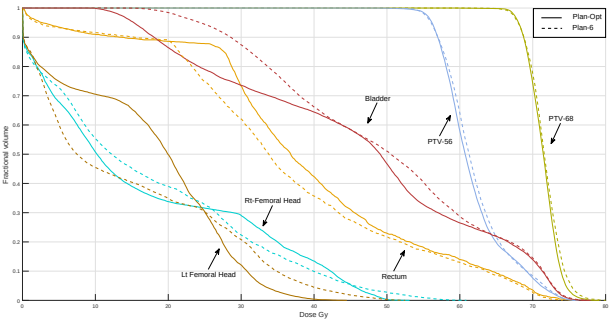

Figure 4.7 Plan-Opt (3.44 minutes) vs. Plan-6 (6 minutes)

Table 4.4 Voxel aggregation results

Iter.	# Transfer	CPU Time (s)	Avg. Dist.
0			176.99
1	37836	5.50	51.48
2	10454	1.99	42.17
3	3758	1.11	40.45
4	1755	0.86	39.94

has 5% of the normal voxels and 15% of the tumor voxels; it reduces the computational time from 28.90 to 4.34 minutes. The aggregated plan has similar target coverage for PTV-68 and PTV-56, even better in PTV-56, and the results for the normal tissues are adequate. Then, the aggregation has significantly reduced the computational time, and the quality of the resulting plan is acceptable.

4.4.5 Arc length

In the proposed approach, we assume that the arcs are of equal length. To evaluate the impact of this parameter, we tested four plans with very small (length 6°), small (length 8°), medium (length 12°), large (length 20°), and very large (length 30°) arcs. Table 4.5 gives the delivery times and critical dosimetry measures for these five arc lengths. As expected, using longer arcs reduces the delivery time, but also the treatment quality. Plans with the arcs of lengths 20° and 30° are not acceptable, because of the overdose in the normal tissues, especially in the rectum. In terms of computational time, plans with 6° and 8° arcs are more time-consuming due to more iterations of column generation. These plans take 10.83 and 7.78 minutes, respectively, while the plan with 12° arc takes 4.34 minutes. Figures 4.9 and 4.10 show the comparison of DVH curves of these two plans. Despite the higher computational time of the plans with 6° and 8° arcs, it resulted in more delivery time. Although both treatment plans provide acceptable quality in normal tissues, there was significant improvement in tumors quality in the 12°-arc plan. Finally, the critical dosimetry measures of the plan with 12° arcs are all in the preferred range and this plan offers better trade-off between computational time and solution quality.

Table 4.5 The effect of arc length on the delivery time and treatment plan dosimetry measures

	Delivery time	PTV-56	PTV-68	Rectum		Bladder		
l (°)	(min)	V56 $\geq$ 95	V68 $\geq$ 95	V30 $\leq$ 80	V50 $\leq$ 50	V60 $\leq$ 25	V40 $\leq$ 70	V65 $\leq$ 50
6	4.37	**95.36**	**98.21**	**73.58**	**22.73**	**10.71**	**69.13**	**23.35**
8	3.82	94.43	**95.72**	**77.21**	**22.62**	**10.26**	**64.73**	**20.83**
12	3.44	**96.15**	**95.82**	**73.64**	**23.07**	**9.52**	**64.51**	**21.98**
20	1.82	91.99	91.91	86.17	**31.80**	**12.02**	**63.39**	**20.39**
30	1.37	**98.99**	88.61	89.40	79.71	**14.85**	97.21	67.31

4.4.6 Leaf movement strategy

In this study, we assume that the MLC leaves movement are bidirectional, i.e., the leaves are free to move in any direction. However, some MLCs have only unidirectional leaf sequencing. In this technology, the leaves are aligned at one edge of the field at the beginning of the arc

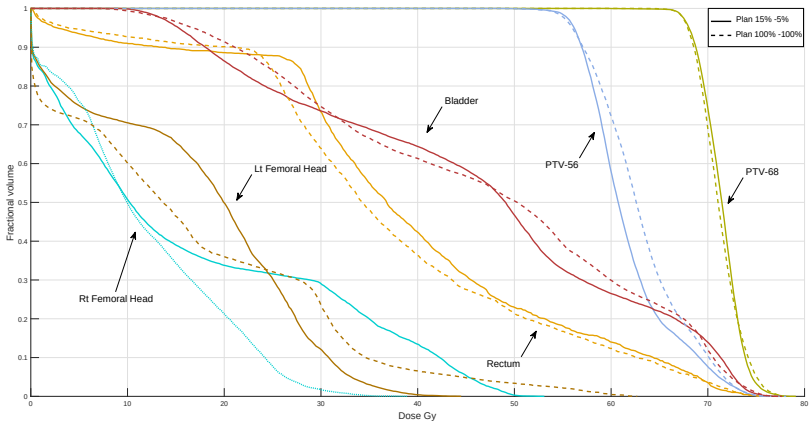

Figure 4.8 DVH curves for the aggregated plan (15%–5%; solid line) and full plan (100%–100%; dashed line) for the prostate case using GCRGH heuristic.

and at the opposite edge of the field at the end of the arc. In this section we compare these two approaches.

Table 4.6 presents the results for arc lengths of 12 ° and 20 ° to evaluate these two strategies for small and large arc lengths. The unidirectional approach has less leaf motion time; however, since the aperture opens and closes several times during the rotation, the treatment time is higher. With fewer arcs, the delivery time decreases. As the critical dosimetry measures indicate, both bidirectional and unidirectional strategies are acceptable for arc lengths of 12 °, but none is satisfactory for arc lengths of 20 °. Figure 4.11 shows the DVH diagrams for the 12 ° arcs. The diagrams are similar, showing that both strategies are acceptable. However, the bidirectional approach is somewhat better especially in terms of the over-dosage in tumors and rectum under-dosage, because of its flexibility in leaf motion.

Table 4.6 The effect of leaf motion strategy on the delivery time and treatment plan dosimetry measures

		Delivery time	PTV-56	PTV-68	Rectum		Bladder		
Strategy	l (°)	(min)	V56 $\geq$ 95	V68 $\geq$ 95	V30 $\leq$ 80	V50 $\leq$ 50	V60 $\leq$ 25	V40 $\leq$ 70	V65 $\leq$ 50
Bidirect	12	3.44	**96.15**	**95.82**	**73.64**	**23.07**	**9.52**	**64.51**	**21.98**
	20	1.82	91.99	91.91	86.17	**31.80**	**12.02**	**63.39**	**20.39**
Unidirect	12	5.11	**95.01**	**96.32**	**77.44**	**31.69**	**13.21**	**67.46**	**26.87**
	20	3.64	88.10	92.32	87.30	58.96	**8.90**	**53.42**	**18.22**

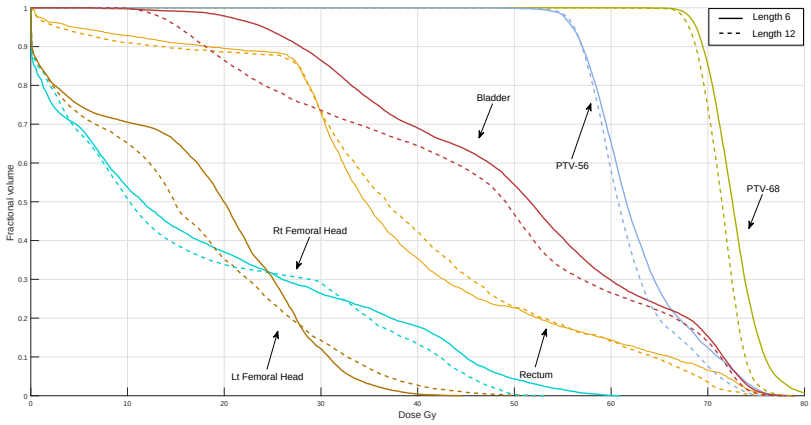

Figure 4.9 DVH curves for treatment plans with arc lengths 6° (solid line) and 12° (dashed line).

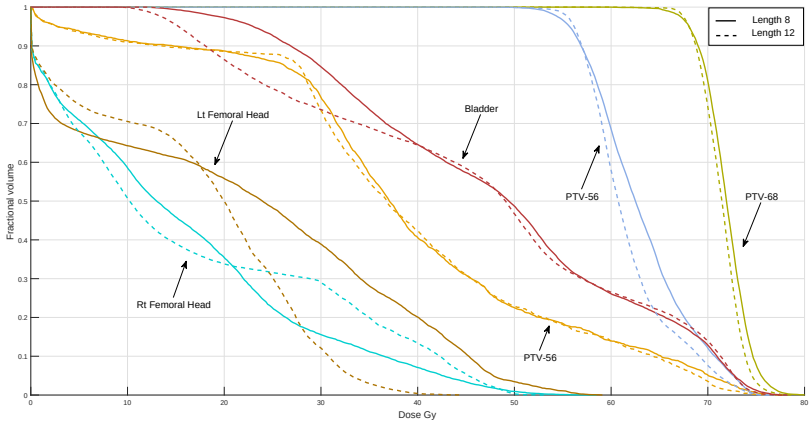

Figure 4.10 DVH curves for treatment plans with arc lengths 8° (solid line) and 12° (dashed line).

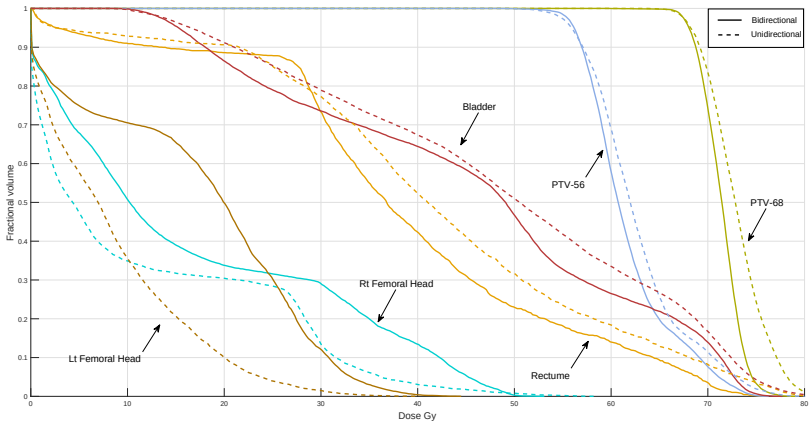

Figure 4.11 Comparison of unidirectional and free leaf-movement strategies for 12° arc lengths.

4.5 Discussion and conclusion

In this paper, we have developed a novel column-and-row generation algorithm embedded in a heuristic for VMAT treatment planning. The problem is decomposed into the PSP, which generates possible aperture shapes, and the RMP, which optimizes the dose rate and delivery time. The proposed RMP is a large-scale integer programming model that minimizes the quadratic dose deviation from the prescribed lower and upper bounds. In addition to voxel-based dose distribution constraints, the columns are also linked to delivery time constraints. The heuristic repeatedly solves the relaxed restricted master problem and fixes the best arcs. In the PSP, graph algorithms form the aperture shapes around the patient in polynomial time.

The proposed heuristic algorithm has the following advantages in comparison to the methods that can be found in the literature:

- Most of previous works in the literature take into account constant delivery time [96, 101] in VMAT treatment planning. Some recent methods minimize the delivery time after determining the fluence maps [39] or fixing the MLC shapes and dose rates at the final step [100]. In this paper, the delivery time is integrated into the column generation algorithm to simultaneously optimize the aperture shapes, dose rates, gantry speeds, and delivery time.

- Another contribution of the proposed approach when compared to papers such as Peng

et al. [100] is that we can consider most of the MLC leaf-movement constraints in the PSP rather than the RMP. Then, in this approach, it is not required to check the feasibility of all adjacent control-points and regenerate new columns in the master model, which makes the algorithm more efficient.

- This method can easily handle both bidirectional and unidirectional leaf motions according to the machine capabilities, which makes the model more flexible in practice.

In addition to the contributions in the model, we also propose an aggregation algorithm inspired by the K-means technique in clustering to reduce the number of voxel-based constraints. This aggregation takes about 11 seconds; it greatly reduces the number of constraints with a negligible effect on the treatment quality.

Finally, we have evaluated our algorithm on a prostate cancer benchmark to demonstrate the efficiency of our model. We solved this benchmark in about 4.34 minutes using only four threads, whereas some approaches in the literature require GPU computing. Moreover, we analyzed the effect of unidirectional and bidirectional leaf movement.

There are still many challenges which can be considered for the future works. First, the restricted master problem is the main bottleneck of the algorithm, requiring 60% of the computational time. To decrease this time and improve the voxel sampling, a dynamic voxel aggregation could be developed. The sampling would be more precise, fewer voxels would be required, and the computational time would decrease. Second, the columns generated at each iteration from different sectors are not disjoint and have similar effects; this could be investigated in future research. Another possibility would be to use GPU computing to accelerate the method.

Acknowledgements

This project was supported by the Vanier Canada Graduate Scholarship program and the Natural Sciences and Engineering Research Council of Canada (NSERC), No. DVC134707. The authors would like to thank Prof. David Craft, Harvard Medical School, and Dr. Martin Hinse, Medical Physicist at Laval Integrated Cancer Centre (CICL), who helped us by providing and evaluating, respectively, the case data. The authors also wish to thank two anonymous referees whose insightful comments have helped us to improve our paper.

CHAPTER 5 ARTICLE 2: INTEGRATING DVH CRITERIA INTO A COLUMN GENERATION ALGORITHM FOR VMAT TREATMENT PLANNING

Mehdi Mahnam

Department of Mathematics and Industrial Engineering, Polytechnique Montréal
Interuniversity Research Center on Enterprise Networks, Logistics and Transportation (CIRRELT),
Montreal, Canada

Michel Gendreau

Department of Mathematics and Industrial Engineering, Polytechnique Montréal
Interuniversity Research Center on Enterprise Networks, Logistics and Transportation (CIRRELT),
Montreal, Canada

Nadia Lahrichi

Department of Mathematics and Industrial Engineering, Polytechnique Montréal
Interuniversity Research Center on Enterprise Networks, Logistics and Transportation (CIRRELT),
Montreal, Canada

Louis-Martin Rousseau

Department of Mathematics and Industrial Engineering, Polytechnique Montréal
Interuniversity Research Center on Enterprise Networks, Logistics and Transportation (CIRRELT),
Montreal, Canada

Abstract. Volumetric-modulated arc therapy (VMAT) treatment planning is an efficient treatment technique with a high degree of flexibility in terms of dose rate, gantry speed, and aperture shapes during rotation around the patient. However, the dynamic nature of VMAT results in a large-scale nonconvex optimization problem. Determining the priority of the tissues and voxels to obtain clinically acceptable treatment plans poses additional challenges for VMAT optimization. The main purpose of this paper is to develop an automatic planning approach integrating dose-volume histogram (DVH) criteria in direct aperture optimization for VMAT, by adjusting the model parameters during the algorithm.

The proposed algorithm is based on column generation, an optimization technique that sequentially generates the apertures and optimizes the corresponding intensities. We take the advantage of iterative procedure in this method to modify the weight vector of the penalty function based on the DVH criteria and decrease the use of trial-and-error in the search for clinically acceptable plans.

We evaluate the efficiency of the algorithm and treatment quality using a clinical prostate case and a challenging head-and-neck case. In both cases, we generate 15 random initial weight vectors to assess the robustness of the algorithm. In the prostate case, our methodology obtained clinically

acceptable plans in all instances with only a 10% increase in the computational time, while simple VMAT optimization found just three acceptable plans. To have an idea with respect to the existing software, we compared the obtained DVH to a commercial software. The quality of the diagrams of the proposed method, especially for the healthy tissues, is significantly better while the computational time is less. In the head-and-neck case, the obtained treatment plans are clinically acceptable in 93.3% of instances while no plan was acceptable in simple VMAT. In sum, the results demonstrate the ability of the proposed optimization algorithm to obtain clinically acceptable plans without human intervention and also its robustness to weight parameters. Moreover, our proposed weight adjustment procedure proves to reduce the symmetry in the solution space and the time required for the post-optimization phase.

Keywords. Volumetric-modulated arc therapy, direct-aperture optimization, dose–volume criteria, column generation.

History. This article is published in *Physics in Medicine and Biology*, Vol. 64, No. 8, 1-14 , (2019).

5.1 Introduction

Volumetric-modulated arc therapy (VMAT) is an efficient form of external radiotherapy which has been widely used during the past decade. In this technology, the beam rotates around the patient's body while the dose rate, gantry speed, and beam shape change continuously [96]. The beams are formed by a multi-leaf collimator (MLC) that has a finite number of leaf pairs, each consisting of a leading and a trailing leaf.

Several optimization techniques have been developed for the treatment planning problem in VMAT [15, 17, 24, 26, 39, 89, 96, 99, 100]. In general, we categorize these methods into two main approaches: (1) two-stage and (2) direct aperture. In the former, at the first stage, each beam is discretized into beamlets, and fluence map optimization (FMO) is used to find the optimal intensity for each beamlet. At the second stage, the ideal fluence map is converted into a sequence of deliverable arcs, typically based on unidirectional leaf motion, maximizing the similarity of the dose distribution to the FMO plan [17, 39, 99, 113].

In the direct-aperture approach, the apertures around the patient and the corresponding intensities are optimized subject to the MLC constraints. In this approach, the column generation (CG) technique has been widely used. This algorithm sequentially generates new apertures and optimizes the corresponding intensities, ensuring to be compatible with adjacent apertures [89, 100, 101, 103]. Unkelbach et al. [123] provide a comprehensive review of optimization techniques for VMAT treatment planning.

Recent studies have extended VMAT optimization to take the treatment times and clinical criteria into account. Nguyen et al. [92] developed a non-greedy approach; it uses an L_2-norm fidelity term in the objective and a level set function to simultaneously optimize the fluence intensity and aperture shapes. Balvert and Craft [14] investigated the trade-off between delivery time and fluence map matching. They optimized the leaf trajectories and dose rates for a given delivery time and obtained the complete trade-off curve for delivery time and plan quality by solving the model heuristically with a range of delivery times. Recently, Mahnam et al. [82] have developed a CG-based heuristic for VMAT that optimizes the trade-off between delivery time and treatment quality.

One of the main technical challenges of treatment planning is to find the optimal model parameters for generating an acceptable plan within a reasonable time. In practice, the treatment planning system (TPS) technicians solve the problem several times for each patient, taking into account various model parameters, e.g., the overdose and underdose weights for target volumes and healthy organs. This manual procedure is time-consuming, especially for complex cases.

Several researchers have studied systematic techniques for the evaluation of treatment planning. The dose–volume histogram (DVH) is the most common method for evaluating the quality of the plan. It indicates the percentage of a volume that receives at least a certain dose. For example, in prostate cancer the planner may specify that "no more than 80% of the rectum is allowed to receive 30 Gy or more." Two approaches have been developed to handle DVH criteria. The first adds dose–volume constraints (DVCs) directly to the mathematical model, and the second automatically adjusts the penalty parameters in the objective function to reduce the violation of the predetermined thresholds.

In the first method, the nonconvex nature of the DVCs leads to a nonlinear model [41]. We can handle this nonlinearity by introducing binary variables, which results in a large mixed integer problem (MIP) [72, 102]. Despite many improvements to the MIP formulation Halabi et al. [58], the FMO problem with DVCs is nonconvex and NP-hard, i.e., the exact solution cannot be obtained in a polynomial computational time using current computing methods [122]. Romeijn et al. [106] proposed a linear approximation of the DVCs based on the Conditional Value-at-Risk (CVaR) in FMO. Then, Romeijn et al. [108] developed a column generation based algorithm for IMRT treatment planning and used the CVaR constraints in the model. However, this approach drastically increases the number of constraints and consequently the computational time.

The second method automatically adjusts the model parameters in the objective function to meet the predetermined DVH criteria [22, 23, 128]. Wu and Mohan [133] employed a gradient

optimization method for the FMO model and considered a simple algorithm adjusting voxel weights in the objective function based on dose-volume histogram. Li et al. [75] improved the previous work by a two-step approach for FMO problem: In the first step, the organ weights in the quadratic objective function are roughly adjusted; and in the second step, the voxel weighting factors are adjusted based on the DVH curves. In the same line of research, Zarepisheh et al. [137] have proposed an algorithm that automatically adjusts the FMO parameters to minimize the distance between the DVHs for the entire plan and the reference DVHs. They iteratively navigate the Pareto surface and project the plan corresponding to the reference DVHs onto that surface. Recently, fuzzy inference systems also have been used for the FMO problem [45].

To the best of our knowledge, most studies on DVH-based re-optimization have focused on FMO. The current work is on VMAT and such an approach could be effective because of the large scale of the VMAT problem. Moreover, in this paper, we take advantage of Direct Aperture Optimization (DAO) approach, incorporating the sequencing and intensity optimization using column generation [82, 86, 100]. To this end, we use the iterative procedure of column generation to automatically handle dose-volume criteria in VMAT treatment planning. Thus, the deliverability of the plan is considered at the same time of weight adjustment; Then, both the dosimetric-derived nonconvexity, i.e., the DVH criteria, and the hardware-derived nonconvexity, i.e., the MLC apertures, are taken into account, simultaneously. We test several strategies, in which the weight of the structures and voxels in the cost function are adjusted at the same time the apertures are generated.

5.2 Methods and materials

5.2.1 VMAT optimization model

In this section, we briefly describe our column generation-based heuristic algorithm for VMAT treatment planning [82]. In this technique, we decompose the complicated and nonlinear VMAT optimization model into two linear sub-problems, which iteratively generate and select apertures that are expected to improve the objective function. We focus on treatment plans with a single gantry rotation, which results in less total treatment time and required number of monitor units. However, this approach could easily be generalized to take into account multiple gantry rotations if required in practice.

Notation

We discretize each structure s of the patient into small cubic volume elements called *voxels*, $\mathcal{V}_s$, and denoted $\mathcal{V}_T$ and $\mathcal{V}_N$ for tumorous and normal tissues. Each beam is decomposed into a rectangular grid of *beamlets*, I. A beamlet is on if it is not blocked by either the leading or trailing MLC leaf, and the relative motion of the leaves controls the intensity. The estimated dose received by voxel j from beamlet i at unit intensity is given by the dose-influence matrix (D_{ij}), in Gy/MU.

The continuous dose delivery is discretized over a finite number of *sectors*, H, by changing the angle of the beam, with typically 2°-spaced beam angles. Each sector is associated with an aperture A specifying the position of the MLC trailing (left) and leading (right) leaves and the dose rate ρ (in MU/s). Another variable is the gantry speed in sector h, ν_h. Without loss of generality, we use its inverse as the sector time, t_h, to simplify the model. The absorbed dose in this problem is estimated by the product of dose intensity and sector time variables, which makes the model nonlinear. To avoid this nonlinearity, we replace $\rho_h\, t_h$ by a new variable called the *fluence rate*, γ_h. We assume that the dose absorbed by a given voxel can be determined by summing the dose from each of the beamlets comprising the aperture. Thus, the dose received at voxel j, z_j, is calculated as $z_j = \sum_{h\in H} D_j(A_h)\,\gamma_h$, where $D_j(A_h)$ denotes the total dose received by voxel j of aperture h, A_h. We measure the treatment quality via a convex objective function with a piecewise quadratic voxel-based penalty as follows [99, 100, 108]:

$$f(z) = \sum_{s\in S}\sum_{j\in\mathcal{V}_s} \underline{w}_j\,[\underline{d}_s - z_j]_+^2 + \overline{w}_j\,[z_j - \overline{d}_s]_+^2 \tag{5.1}$$

where $[\bullet]_+$ denotes $\max\{0, \bullet\}$ and $\underline{d}_s$ and $\overline{d}_s$ are prespecified lower and upper dose thresholds for structure s. Moreover, $\underline{w}_j$ and $\overline{w}_j$ are the weights for the underdose and overdose in voxel j, respectively. The weights could be equal for all voxels in the same structure or be independent. We adjust these parameters in Section 5.2.2 to obtain clinically acceptable treatment plans.

Column generation

In this model, each column k is a partial arc made up of the apertures, A_h^k, in a sequence of sectors from sector h_s^k to h_f^k, H^k. The procedure starts with a subset of initial columns completely surrounding the patient. The following two sub-problems are then solved repeatedly until no improving column is available:

- RMP: Given a set of columns ($K' \subseteq K$), we select the best subset that covers all the sectors, optimizing the intensities, gantry speed, and dose distribution.
- SP: Given the extra voxel information from the RMP and the effects of the beamlets on the dose distribution, we generate promising columns and add them to the RMP to improve its objective function.

Restricted master model: In the RMP, we determine the best combination of columns around the patient and optimize the corresponding fluence rates. We define the binary variable y: $y^k = 1$ if and only if column k is selected. The dose in each sector h is then $D_h(A_h^k)y^k\,\gamma_h$. To linearize the model, we assume a constant fluence rate through the covered sectors of column k, denoted γ^k, and we introduce a constraint to restrict it based on y^k. The formulation of the restricted master problem is described in Appendix B.

Although the fluence rate is fixed for the sectors in a given column, it can change between columns. Moreover, the gantry speed can change between sectors. To make CG more efficient in this phase, we use the voxel aggregation algorithm of Mahnam et al. [82] to cluster similar voxels and decrease the number of constraints.

After selecting the final apertures at the end of CG, we use a post-optimization (PO) model to determine the sector-based fluence rates. This model considers all the voxels and restricts changes in the fluence rate between adjacent sectors.

Subproblem(SP): In the subproblem, also called the pricing problem, we use the dose distribution z to compute the potential effect of each beamlet $i \in I$ in sector h for an increase of one unit of intensity:

$$\lambda_i^h = \sum\nolimits_{j\in\mathcal{V}} -\nabla f(z_j)\, D_{ij}^h, \tag{5.2}$$

where ∇f is the gradient of the objective function f. We then use a graph approach to determine the position of the leading and trailing leaves in the new arc. Each node defines a feasible arrangement of MLC leaves, and each edge determines the feasibility between two adjacent nodes. The cost of node n in sector h is based on the potential effects of the open beamlets, I_n^o, as follows:

$$c_n^h = \sum\nolimits_{i\in I_n^o} \lambda_i^h. \tag{5.3}$$

The network takes into account the MLC constraints by eliminating infeasible graph nodes and edges. These constraints avoid collisions of leaves with $\Delta^{\min} > 0$ and also ensure that the maximum tip difference is in the specified range $\Delta^{\max}$. Moreover, leaf movements between adjacent sectors are restricted based on the maximum leaf speed. Finally, we determine the

best MLC aperture for a given range of sectors by a polynomial-time shortest-path algorithm and add the new columns to the RMP if the objective value is negative.

Greedy Heuristic: As mentioned, the RMP is a MIP because of the binary variables y^k. At the beginning of the algorithm, we relax the binary requirement, and so the y^k variables are usually fractional. To find a feasible plan in a reasonable time, we fix the lower bound of the column with the largest fractional part to 1 at each CG iteration and remove the conflicting partial-arcs. Also, we keep other generated columns in the model for the next iterations.

More details about the CG-based heuristic and its efficiency can be found in our previous publication Mahnam et al. [82].

5.2.2 Adjustment approach

In this section, we formulate the adjustment model for the structure and voxel weight vectors, and also the adjustment procedure embedded in the column generation algorithm.

Weight adjustment

Let $\mathcal{F}$ be the feasible solution space of model RMP and f the voxel-based objective function. We formulate the treatment planning problem using the weighted-sum method to convert the multi-criteria DVH objectives into a single-objective optimization problem as follows:

$$\mathbf{P}: \min_{(y,\gamma,t)\in\mathcal{F}} w^\top f(z(y,\gamma,t)) \tag{5.4}$$

where w is a vector of non-negative weights representing the relative importance of the structures or voxels. For the l^{th} DV objective of structure s with dose value d_s^l, let $V_{d_s^l}$ and $v_{d_s^l}$ denote the desired and actual percentages of the structure volume, respectively.

To implement this general model in the course of column generation algorithm, we first find the treatment plan subject to the delivery constraints at each iteration. We then evaluate its DVH criteria, $\boldsymbol{v}$, and update the weight vector w based on the formulation. This process continues until we find an acceptable DVH or the stopping criteria are satisfied. The details of the algorithm are provided in subsequent sections.

In the structure-based weight vector, all voxels in a structure have the same weight in the objective function, while in the voxel-based adjustment, the weights are independent. The solution space of the model P is larger in the second approach, which makes the problem more complicated but also more flexible.

Structure-based weight vector: In this case, it suffices to find the underdose, w_s^-, and overdose, w_s^+, weighting factors of structure s. To adjust the weights during the CG, we use the formulations inspired by Li et al. [75], which increase the weight of structures corresponding to the violations from the prescribed thresholds. Let L_s^+ be the DVH criteria for the overdose in structure s. The total overdose is as follows:

$$\delta A_s^+ = \sum_{l \in L_s^+} \max(0, v_{d_s^l} - V_{d_s^l}). \tag{5.5}$$

Similarly, we can compute the total underdose of structure s, δA_s^-. We update the organ weights at each iteration of CG for the restricted master problem (RMP) based on the weights in the previous iteration and the ratio of the overdose (δA_s^+) or underdose (δA_s^-) in structure s to the total overdose and underdose in all structures. This formulation is shown for overdose weighting factor, w_s^+, in Equation (5.6) and the overdose weighting factors can be computed similarly.

$$w_{s,k+1}^+ = \alpha \, w_{s,k}^+ \, (1 + \frac{\delta A_s^+}{\sum_{s \in S} (\delta A_s^+ + \delta A_s^-)}) \tag{5.6}$$

where the parameter α controls the effectiveness of the weight adjustment. This adaptive parameter has a relatively small value in the initial iterations and increases at a constant rate as the algorithm proceeds. It helps to adjust the treatment plan, especially in the PO phase, where the values of the overdose and underdose are small.

Voxel-based weight vector: In this approach, the voxel weights are the same for each structure at the beginning of the algorithm but are adjusted independently during the CG according to the treatment plan. However, the DVH criteria are cumulative measures, in which there is no direct relationship between a certain voxel and a DVH goal. Let $\pi(z^s)$ be a permutation of the voxel doses in structure s, and let $\widetilde{\pi}(d^s)$ be the permutation that sorts z^s in nondecreasing order. Zarepisheh et al. [137] have shown that $\widetilde{\pi}(z^s)$ yields the best approximation to the DVH goals among all permutations of z. For the l^{th} DV objective in structure s, denoted $(d_s^l, V_{d_s^l})$, we obtain $\widetilde{\pi}(z^s)$ and for each voxel j we modify the weight at iteration $k+1$ as follows:

$$w_{j,s}^{k+1} = \begin{cases} \alpha\, w_{j,s}^{k} \frac{d_s^l}{z_{j,s}} & s \in T, V(\widetilde{\pi}(z_{j,s})) \leq V_{d_s^l}, z_{j,s} \leq d_s^l \\ \alpha\, w_{j,s}^{k} \frac{z_{j,s}}{d_s^l} & s \in N, V(\widetilde{\pi}(z_{j,s})) \geq V_{d_s^l}, z_{j,s} \geq d_s^l \\ w_{j,s}^{k} & \text{o.w.} \end{cases} \tag{5.7}$$

where $V(\widetilde{\pi}(d_j^s))$ is the percentage of the organ receiving dose z_j^s or more in the sorted version of the current solution. Figure 5.1 shows a sample of this criterion for $V30 \leq 80\%$ in a normal structure and the voxel weight adjustment area. If there is more than one goal point in the structure, we consider the penalty for voxel j based on the closest DVH reference point.

The difference between the actual and desired DVH criteria, especially in the final iterations of the algorithm, is usually insignificant. For example, $V30 = 80.01\%$ while the desired volume is 80%. In these cases, the weight of just few voxels will be modified during the weight adjustment, and the unsatisfied DVH goal will not be improved. Thus, in addition to α, which controls the intention of the weight adjustment, we need a parameter to increase the range of the affected voxels when the actual and desired criteria are very close. To affect an additional $\epsilon\%$ of the voxels, we adjust the desired dose d_s^l in the conditions of Equation (5.7) to $z_{j,s} \leq (1+\epsilon)\, d_s^l$ and $z_{j,s} \geq (1-\epsilon)\, d_s^l$ for tumorous and normal voxels, respectively. Figure 5.1 shows a DVH objective $(d_s^l, V_{d_s^l})$, the voxel weight adjustment area, and the $\epsilon\%$ extension in the range of affected voxels.

Proposed strategy

In the proposed CG, we dynamically update the weight vector. To this end, we must determine (1) the adjustment approach, (2) the best iteration for the adjustment, (3) a DVH evaluation heuristic, and (4) the post-optimization (PO). These strategies are explained in more detail below.

Adjustment approach: We first choose between structure-based adjustment (SA-CG) and voxel-based adjustment (VA-CG), explained in Section 5.2.2. The former has a smaller solution space and the latter has more flexibility.

Adjustment iteration: We perform the adjustment every p iterations. For small values of p, the objective function will change frequently, and our method approximates a greedy algorithm. On the contrary, when p is large, the weight adjustment will be less effective.

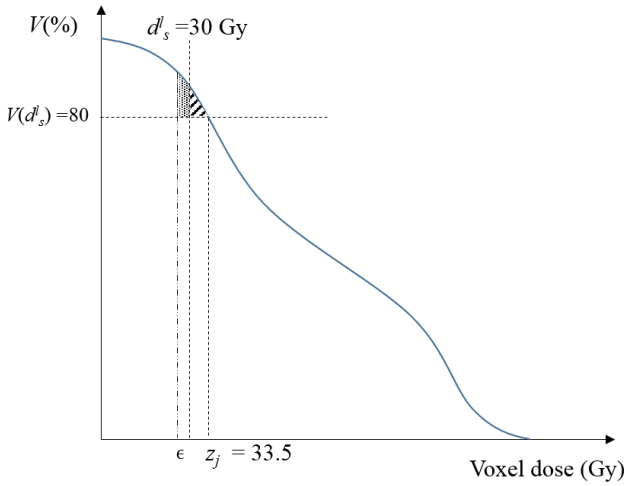

Figure 5.1 Voxel weight adjustment for $V30 \leq 80\%$ in a normal tissue. The voxel doses (z_j) are sorted in non-decreasing order on the horizontal axis, and the percentage of the organ is indicated on the vertical axis. The hatched area shows the penalized voxels. The $\epsilon\%$ extension in the range of affected voxels is shown in the dotted area.

DVH evaluation: As explained in Section 5.2.1, the variables associated with the columns, y^k, are fractional at the beginning of the CG procedure and are gradually fixed to 0 or 1. We developed two simple heuristics to evaluate the quality of the treatment plan during the algorithm: the partial relaxed plan (PRP) and the greedy plan (GP). In PRP, column variables in the solution may be fractional, and the doses at the voxels are based on the partial plan. Due to the fractional values, this estimation is usually optimistic. In GP, we fix the column with the largest value at each sector to 1 to make a complete feasible solution. We then solve the model again and evaluate the DVH criteria.

Post-optimization (*PO*): At the end of the column generation procedure, we can continue the re-optimization process. In the PO phase, the apertures are fixed, but the fluence rate is sector-dependent, i.e., the fluence rates in sectors are independent, but we restrict the changes between adjacent sectors. However, because it considers all the voxels, the PO model is large and time-consuming to solve. We perform a maximum of 20 iterations in the PO phase, updating the weights between the iterations. We terminate the algorithm when the DVH criteria are satisfied.

Figure 5.2 depicts a flowchart of our CG procedure with weight adjustment. To find the best strategy, we tested several approaches and parameter settings; see Section 5.3.

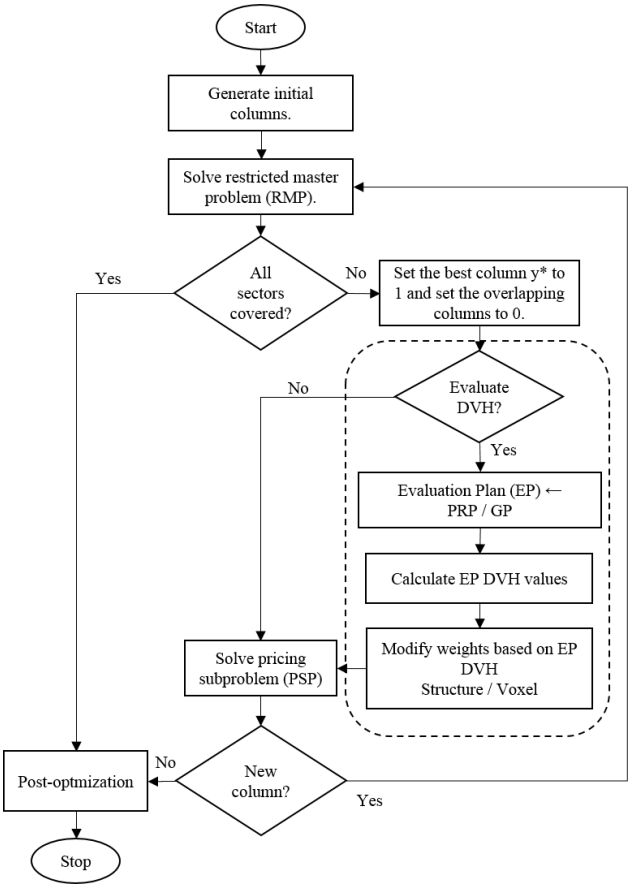

Figure 5.2 Flow chart of CG heuristic with weight adjustment. The adjustment process is determined by a dashed outline.

5.2.3 Materials

We evaluate the efficiency of the proposed algorithm on two clinical cases from the CORT data set [40]: a prostate (P) patient and a head-and-neck (H&N) patient. The prostate case has two target volumes with different prescription, PTV-56 and PTV-68, and six organs at risk: the bladder, rectum, left and right femoral heads, prostate bed, and penile bulb. The head-and-neck case has three target volumes, PTV-56, PTV-63, and PTV-70, and four organs at risk: the brainstem, spinal cord, and right and left parotids. Doses of 68 Gy in the prostate case and 70 Gy in the head-and-neck case were prescribed in 2 Gy per fraction. Then, the treatment plans were optimized for 34 and 35 fractions, respectively. The parameters for the two cases are listed in Table 5.1. As one can see, there are more voxels in the prostate case and more beamlets in the head-and-neck case. From the mathematical point of view, the former has more constraints, and the latter has more potential columns. Therefore, the algorithm is analyzed in terms of both aspects. Also, the machine parameters, typically considered in the literature [40], are listed in Table 5.2.

In both cases, the 360 degrees around the patient are covered by 180 equally spaced sectors. Based on the sensitivity analysis for the arc length in our previous work [82], we take into account 12° per arc, i.e., 30 arc segments.

We use standard DVH reference points based on those in the literature and the advice of a medical physicist; see Table 5.3. The goal is to ensure that 95% of the target volumes are covered by 100% of the prescribed dose while minimizing the dose to normal tissues. Moreover, to avoid pockets of high doses (hot spots) within the target, high dose values are restricted.

Table 5.1 Parameters of clinical cases

	Prostate (P)	Head & neck (H&N)
Total # beamlets	25,404	203,765
Beamlet size (cm)	1×1	0.5×0.5
Voxel resolution (mm)	3, 3, 3	3, 3, 5
# Target voxels	9,491	25,388
# Body voxels	690,373	251,893
Prescribed dose (Gy)	68	70
# Fractions	34	35

5.3 Results

We implemented the algorithms in C++ and used IBM ILOG CPLEX 12.6.2 for the mathematical models. The computational experiments were run on a 2.67 GHz Intel(R) Xeon(R)

Table 5.2 VMAT machine parameters

Maximum leaf speed, ν_l^U	3 cm/s
Gantry speed, ν_g	1–6°/s
Maximum dose rate, ρ^U	600 MU/min
Maximum fluence change, Δ_γ	2 MU
Maximum change in sector time, Δ_t	2 s

Table 5.3 Treatment plan dose-volume criteria

Prostate (P)		Head-and-neck (H&N)	
Structure	Measure	Structure	Measure
PTV-56	V56 $\geq$ 95%	PTV-56	V56 $\geq$ 95%
PTV-68	V68 $\geq$ 95%	PTV-63	V63 $\geq$ 95%
	V74.8 $\leq$ 1%	PTV-70	V70 $\geq$ 95%
Rectum	V30 $\leq$ 70%		V76.3 $\leq$ 1 %
	V50 $\leq$ 50%	Rt. Parotid	V50 $\leq$ 20%
	V65 $\leq$ 25%	Lt. Parotid	V50 $\leq$ 20%
Bladder	V40 $\leq$ 60%	Spinal cord	V48 $\leq$ 1%
	V65 $\leq$ 30%	Brainstem	V60 $\leq$ 1%
Femoral heads	V50 $\leq$ 1 %		

E7-8837 Linux workstation. To improve the efficiency of the algorithm for the subproblem, we used parallel programming techniques with a maximum of 10 threads. We solved the quadratic RMP at each iteration using the CPLEX Barrier Optimizer, which is based on an interior-point method.

To assess the effectiveness of the proposed algorithm in the prostate and head-and-neck cases, we randomly generated 15 scenarios for the initial weights of the structures in each case. For instance, the weight of bladder in the prostate case in one scenario is 0.2 while it is 0.4 in another scenario. This allows us to analyze the robustness of the algorithm to initial parameters and its adaptability to different cases and priorities. Then, we tested the generated scenarios on 15 strategies, where each strategy is a combination of an adjustment approach (`adjust. method`), the frequency of the weight adjustment ($\boldsymbol{p}$), and a DVH evaluation heuristic (`DVH eval.`).

The adjustment approach is structure- or voxel-based, and we adjust the weights every $p =$ 1, 5, or 10 iterations. Moreover, the DVH evaluation heuristic is Partial Relaxed Plan (PRP) or Greedy Plan (GP). In addition to weight adjustment during the column generation, we perform the DVH-based re-optimization for a maximum of 20 iterations in the PO phase.

5.3.1 Prostate case

The details of the strategies and the results are summarized in Table 5.4. In the first strategy, so-called *simple VMAT*, we test the column-generation based heuristic without weight adjustment neither during CG nor the PO phase [82]. Then, for each adjustment approach, we take into account one strategy, so-called *PO-Adjustment*, with adjustment only for the post-optimization iterations and six strategies with weight adjustment both during the CG and PO phases.

The cumulative number of instances with acceptable plans at the end of iterations 1, 5, 10, 15, and 20 in the PO phase are reported in the column `# plans during PO`. The `avg. iter.` column gives the average number of PO iterations, and the `avg. deliv. time` column gives the average delivery time (in minutes).

Table 5.4 The results of proposed strategies in the prostate case.

Strateg.	adjust. method	p	DVH eval.	# plans during PO					avg. iter.	avg. deliv. time (min)
				1	5	10	15	20		
S-P-1	Simple CG	N/P	N/P	3	-	-	-	-	-	3.02
S-P-2	SA-PO	N/P	N/P	3	7	10	11	13	8.40	3.07
S-P-3	SA-CG	1	PRP	8	11	14	14	14	3.73	3.14
S-P-4		5	PRP	4	10	13	13	14	5.73	3.13
S-P-5		10	PRP	4	10	13	13	14	5.40	3.07
S-P-6		1	GP	6	9	11	13	13	6.33	3.12
S-P-7		5	GP	6	9	12	13	13	6.40	3.16
S-P-8		10	GP	4	10	14	15	-	4.46	3.13
S-P-9	VA-PO	N/P	N/P	1	13	15	-	-	2.33	3.07
S-P-10	**VA-CG**	**1**	**PRP**	**13**	**15**	-	-	-	**1.27**	**3.20**
S-P-11		5	PRP	6	14	15	-	-	2.47	3.16
S-P-12		10	PRP	7	13	13	13	13	4.00	3.05
S-P-13		1	GP	2	13	15	-	-	3.27	3.06
S-P-14		5	GP	3	14	14	15	-	2.87	3.10
S-P-15		10	GP	7	15	-	-	-	1.60	3.09

The results indicate that the simple strategy S-P-1 finds just three clinically acceptable plans out of 15 and takes about 6.51 min. The main challenge is to cover PTV-56 and PTV-68 at their prescribed doses while satisfying the upper thresholds for the rectum and the target volumes. As a PO-Adjustment strategy, S-P-2 use CG to generate efficient apertures but adjust the structure weights in PO iterations. Strategies S-P-3 to S-P-8 use the structure-based adjustment also embedded in column generation (SA-CG) and find up to 13-15 plans gradually during the PO phase. Similar to S-P-2, strategy S-P-9 modifies the weight vector

only in PO iterations but based on voxel adjustment. Strategies S-P-10 to S-P-15 with voxel-based adjustment approach during the CG and PO procedures (VA-CG) find acceptable plans for 14-15 instances.

To compare the trends of the structure- and voxel-based strategies during PO phase, Figure 5.3 indicates the cumulative number of obtained acceptable plans at each iteration. It can be seen that the VA-CG strategies are closer to the top left side of the diagram, i.e., more plans in fewer iterations. It shows that the VA-CG approach finds 89 plans in at most three PO iterations; this value is only 55 for SA-CG. S-P-10 finds plans for all the instances in 7.18 minutes on average and at most two PO iterations (the average is 1.27). It requires about 10% more computational time than simple VMAT, which is negligible in comparison with the improvement. Also, the obtained average delivery time is about 3 minutes in different strategies.

Moreover, Figures 5.3a and 5.3b show that the results of Strategies S-P-2 and S-P-9, modifying the weight vectors only in the PO phase, are less efficient than strategies with adjustment during CG. These results gain a better insight into the value of the integration of DVH criteria in column generation. We conclude that adjusting the weight during the CG leads to more clinically acceptable plans within less computational time.

Figure 5.4 illustrates the DVHs for an instance solved by S-P-1 (simple VMAT) and S-P-10 (VA-CG) as the best found strategy. The plans for this instance, both are obtained in the first PO iteration of S-P-1 and S-P-10, respectively. It can be seen that the S-P-1 plan does not deliver the prescribed doses to the target volumes and the criteria associated to the femoral heads and target overdose are close to the pre-determined limits. However, the S-P-10 plan satisfies all the requirements for normal and target volumes.

5.3.2 Head-and-neck case

In the large and challenging head-and-neck case, the goal of the treatment plan is to cover all three targets while avoiding hot spots and sparing the parotid glands, spinal cord, and brainstem. Similarly to the prostate case, we compare the structure- and voxel-based weight adjustment approaches, PRP and GP evaluation heuristics, the frequency of the weight adjustment for $p = 1, 5$ and 10 in 15 randomly generated weight scenarios in the range of user experience. In total, we test 15 strategies; the results are summarized in Table 5.5.

The simple VMAT algorithm, S-HN-1, finds no acceptable treatment plan, but the proposed algorithm finds admissible plans for 14 out of 15 (93.33%) instances in three strategies. S-HN-3 to S-HN-8 strategies, using the SA-CG approach, find 11-14 acceptable plans during

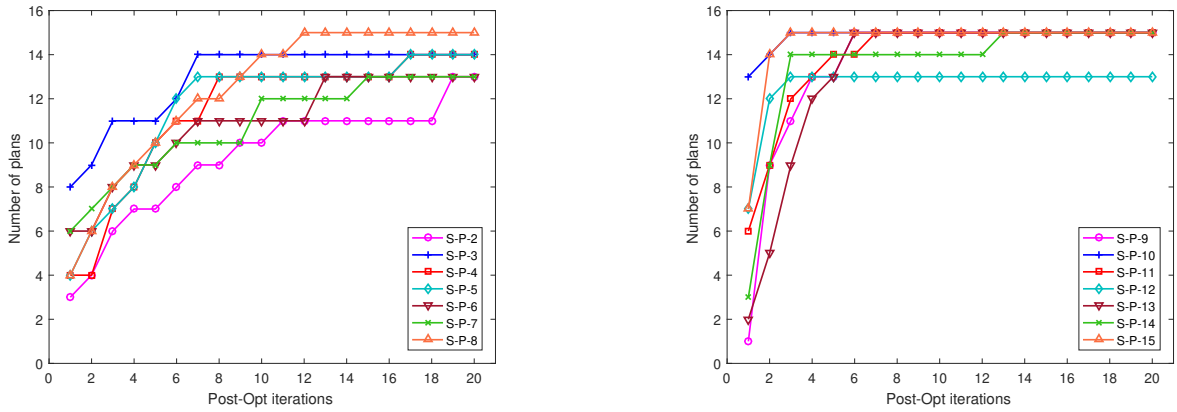

(a) Structure-based adjustment approach (b) Voxel-based adjustment approach

Figure 5.3 Number of clinically acceptable plans for the prostate case during the post-optimization iterations: (a) structure-based adjustment strategies, SA-PO and SA-CG, (b) voxel-based adjustment strategies, SA-PO and SA-CG.

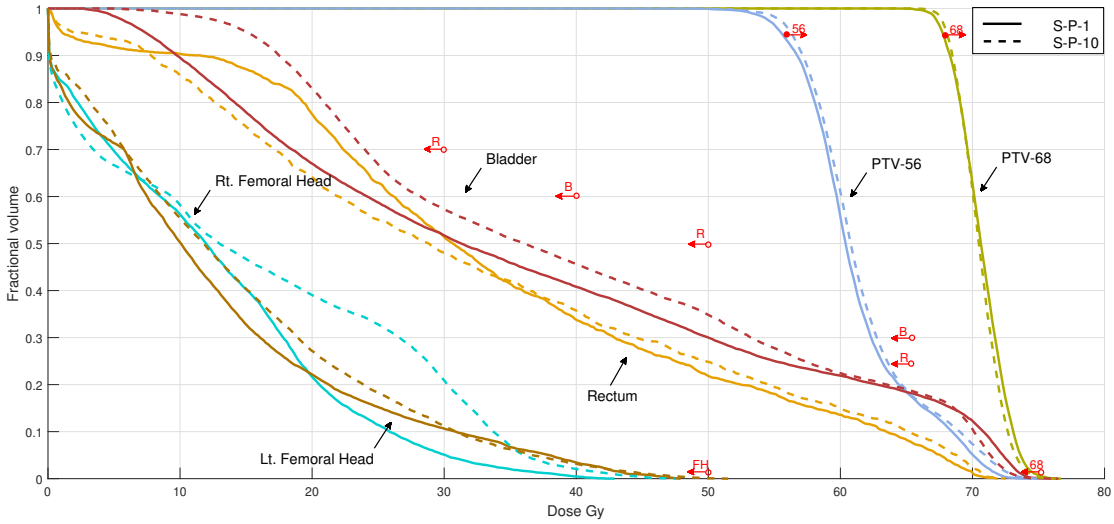

Figure 5.4 DVH of the prostate treatment plan for instance #1 in two strategies: S-P-1 (solid line) as simple VMAT and S-P-10 (dashed line) as the best found approach. Empty circles (○) indicate overdosage and solid circles (●) indicate underdosage DVH criteria. An arrow with a letter above indicates the direction of allowed curves for the specified structure. “B" is the bladder, “R" the rectum, “FM" the femoral heads; “56" indicates PTV-56 and “68" indicates PTV-68.

Table 5.5 The results of proposed strategies in the head & neck case

Strateg.	adjust. method	p	DVH eval.	# plans during PO					avg. iter.	avg. deliv. time (min)
				1	5	10	15	20		
S-HN-1	Simple CG	N/P	N/P	0	-	-	-	-	-	2.62
S-HN-2	SA-PO	N/P	N/P	0	0	5	7	10	14.47	2.62
S-HN-3	SA-CG	1	PRP	0	5	9	11	11	10.47	2.62
S-HN-4		5	PRP	0	1	8	12	14	12.20	2.62
S-HN-5		10	PRP	0	7	9	10	11	10.00	2.61
S-HN-6		1	GP	0	2	8	11	11	11.33	2.63
S-HN-7		5	GP	0	2	5	9	12	13.40	2.62
S-HN-8		10	GP	0	3	8	12	13	10.60	2.63
S-HN-9	VA-PO	N/P	N/P	0	9	11	11	11	8.27	2.62
S-HN-10	**VA-CG**	**1**	**PRP**	**0**	**12**	**12**	**14**	**14**	**5.07**	**2.62**
S-HN-11		5	PRP	0	9	12	14	14	6.07	2.63
S-HN-12		10	PRP	0	9	11	12	12	7.87	2.62
S-HN-13		1	GP	0	5	6	10	11	11.53	2.63
S-HN-14		5	GP	0	9	10	12	13	7.87	2.63
S-HN-15		10	GP	0	6	9	10	11	10.53	2.61

the PO iterations. This number is the same for the VA-CG approach, strategies S-HN-10 to S-HN-15. To differentiate between two approaches, we take into account the first 5 PO iterations which results in 20 and 50 acceptable plans for SA-CG and VA-CG, respectively. Figures 5.5a and 5.5b indicate the number of acceptable plans at each iteration for the SA-CG and VA-CG strategies. The comparison of two graphs shows clearly that VA-CG is significantly more efficient than SA-CG. S-HN-10 has the best performance: 14 acceptable plans found while the average computational time is 38.48 minutes. This strategy uses PRP heuristic in every CG iteration and solves the instances in an average of 5.07 PO iterations. The average delivery time is about 2.62 ± 0.01 minutes and robust for different strategies.

Furthermore, S-HN-2 and S-HN-9, which perform the adjustment only in the post-optimization phase, are among the least efficient strategies. Moreover, it can be seen that no acceptable plan was found in the first iteration of the PO phase because of high complexity of the case. However, the algorithm could adapt rapidly and reach an acceptable plan.

Figure 5.6 compares the DVHs for one of instances solved by S-HN-1 (simple VMAT) and S-HN-10 as a VA-CG approach. It can be seen that S-HN-1 fails to cover PTV-63 and also does not satisfy the tumor overdose criterion, $V76.3 \leq 1\%$. Also, the criteria associated to left and right parotids are close to their limit, $V50 \leq 20\%$. However, S-HN-10 finds an acceptable plan in the second PO iteration. The tail of PTV-63 and PTV-70 have some overlapping parts because of the multi-organ voxels and inaccuracy at the boundaries in both targets.

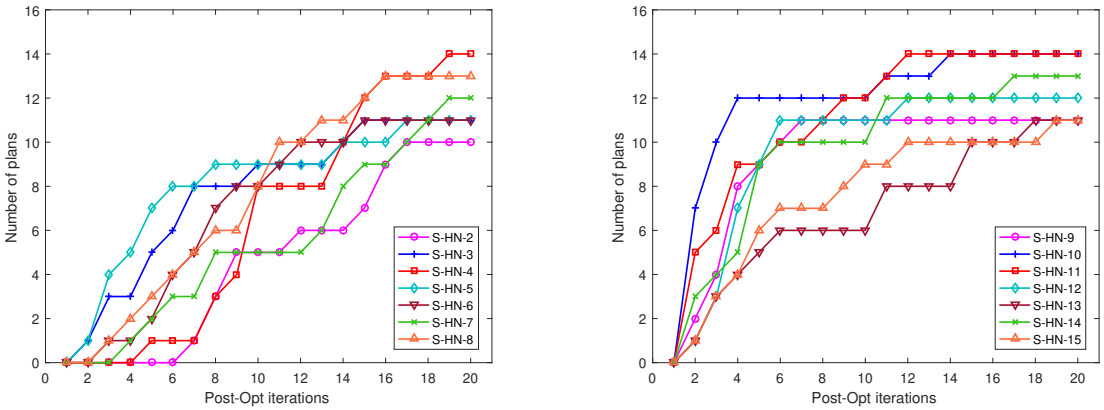

(a) Structure-based adjustment approach (b) Voxel-based adjustment approach

Figure 5.5 Number of clinically acceptable plans for the head-and-neck case during the PO iterations: (a) structure-based adjustment strategies, SA-PO and SA-CG, (b) voxel-based adjustment strategies, VA-PO and VA-CG.

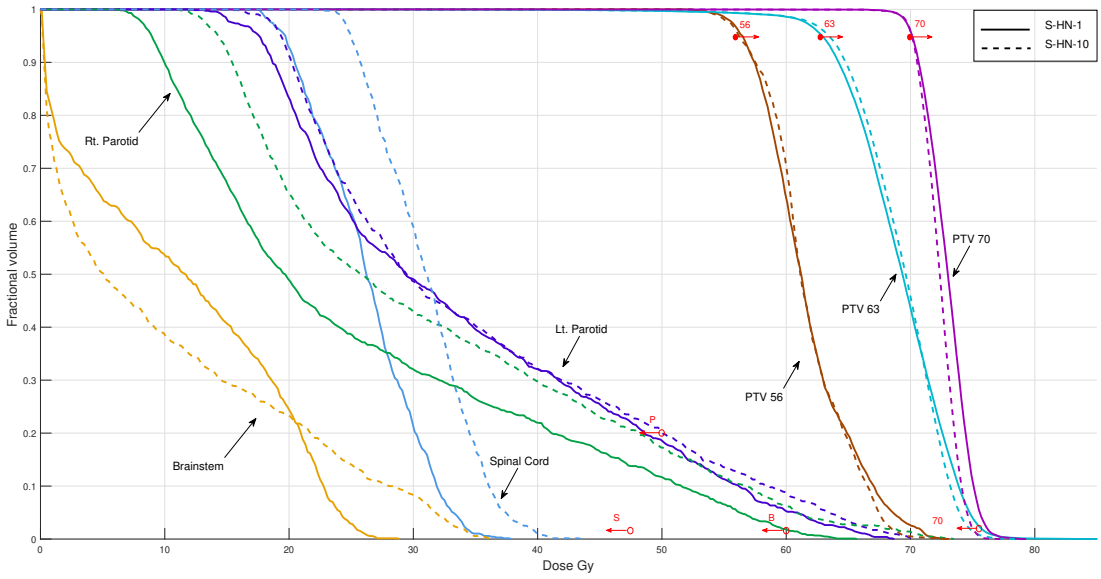

Figure 5.6 DVH of the head-and-neck treatment plan for instance #9 in two strategies: S-HN-1 as the simple VMAT (solid line) and S-HN-10 as the best obtained approach (dashed line). Empty circles (○) indicate overdosage and solid circles (●) indicate underdosage DVH criteria. The arrow with a letter above indicates the direction of allowed curves for the specified structure. “B" is the brainstem, “S" the spinal cord, and “P" the parotids; “56" indicates PTV-56, “63" indicates PTV-63, and “70" indicates PTV-70.

5.4 Discussion

The main difficulty in VMAT optimization is the large number of potential apertures and voxel-based constraints which does not allow additional DVH based constraints in the model. Therefore, to integrate the DVH criteria in the column generation technique, we need to find an efficient strategy that automatically obtains acceptable plans. To this end, we have implemented two adjustment approaches: structure-based and voxel-based. The former has a smaller solution space; the latter has more flexibility. We tested our approach on a prostate and a head-and-neck case. The simple VMAT optimization technique [82] found three plans in the prostate case (out of 15 scenarios with random initial weight vectors) and none in the head-and-neck case. The proposed algorithm could find the acceptable plans for most of instances in both cases which confirms its advantage over the simple VMAT optimization technique.

The voxel-based adjustment (VA-CG) was more successful even with a more complicated solution space. In the prostate case, S-P-10 found plans for all instances with an increase of just 10% in the computational time and 3 PO iterations. The results in the head-and-neck case confirm this conclusion. The best strategy was S-HN-10, finding acceptable plans for 93.3% of instances. The average of PO iterations to achieve an acceptable plan for all 15 instances is 5.07 iterations with an average computational time of 38.48 minutes.

The best strategies, S-P-10 and S-HN-10, had a high frequency of adjustment during the column generation process. This indicates that the integration is effective in improving the results and the adjustment is usefully employed. In both cases, PRP could find satisfying evaluations of DVH in less computational time than GP. The difference between the average PO iterations by S-P-9 (2.33) and the number found by S-P-10 (1.27) shows more efficiency in S-P-10, in which the DVH is evaluated inside CG frequently. In the larger head-and-neck case, there is an even greater difference between S-HN-9 and S-HN-10, such that the the number of acceptable plans found by S-HN-10 is 14 out of 15 and this number found by S-HN-9 is 10. These comparisons show the value of the integration of the weight adjustment procedure inside the CG algorithm rather than the PO-Adjustment approach.

From the dosimetry point of view (Figures 5.4 and 5.6), the target volumes are barely covered in both cases. This is likely due to the structure of column generation technique, which starts from no column, as the best plan for normal tissues, and gradually adds columns to cover the target volumes. The advantage of this approach is that it controls the dose to normal tissues.

In terms of computational time, the extra tasks of DVH evaluation and weight adjustment

increase the CPU time in automatic VMAT in comparison to simple VMAT. However, it is negligible as shown in the best obtained strategies, S-P-10 and S-HN-10. We believe that the symmetry of the model is one of the main causes of its complexity, and the weight adjustment breaks the symmetry and consequently decreases the computational time. Moreover, the number of PO iterations to find an acceptable plan decreases when we perform DVH evaluation during the CG. Therefore, we can find better treatment plans with minor additional computational time.

Finally, to have an idea of the efficiency of the proposed algorithm in comparison to a commercial software, a treatment plan is designed by an expert for the prostate case with Pinnacle. The DVH diagram of the plan is shown in Figure 5.7. This DVH is obtained from a treatment plan with double gantry rotation in about 20 minutes computational time. The other assumptions and parameters are the same as shown in Table 5.2. The computational time in our plan is less, 7.18 minutes, and at the same time, the quality of the diagrams, especially for the healthy tissues is significantly better. As shown, the DVH obtained from Pinnacle is not acceptable due to high dose to Rectum (V30 $>$ 70%), overdosage in PTV-68 (V74.8 $>$ 1 %) , and not enough coverage to PTV-56 (V56 $<$ 95 %). This single case does not allow us to draw any firm conclusion regarding the efficiency of the proposed algorithm in comparison to a commercial software. In addition, to fully assess the potential of this idea in the context of existing clinical software, we would need to have access to the core algorithm of these software, which is obviously not possible. However, we believe this shows, in a limited way, that our model and our algorithm can provide state-of-the-art results and they could possibly be used to improve existing software.

In sum, the advantages of the proposed algorithm in comparison to most studies in the literature and commercial software are as follows:

- To the best of our knowledge, most studies and software take into account DVH criteria as constraints in the mathematical model which makes the model non-linear or large and consequently more costly to solve.
- The DVH based models are mostly considered only in FMO while the current work is on VMAT and such an approach could be effective because of the large scale of the VMAT problem.
- The proposed algorithms integrating DVH constraints and direct aperture optimization are in large-scale [108] and non-applicable in practice for VMAT.
- In this paper, we incorporate the sequencing and intensity optimization using column generation. Thus, the deliverability of the plan is considered at the same time of weight

adjustment; Then, both the dosimetric-derived nonconvexity, i.e., the DVH criteria, and the hardware-derived nonconvexity, i.e., the MLC apertures, are taken into account, simultaneously.

- Less trial-and-error in the search for clinically acceptable plans increase the efficiency of the software and also the center.

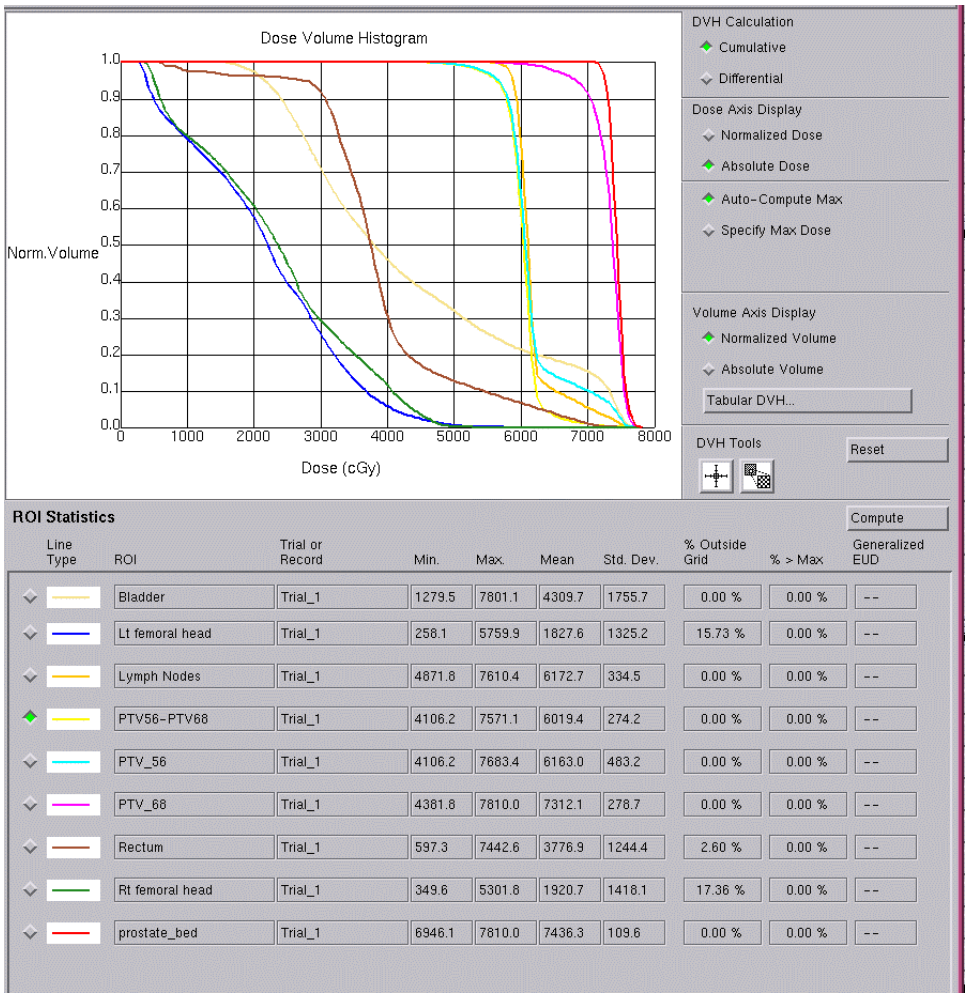

Figure 5.7 DVH of the prostate treatment plan with commercial software.

5.5 Conclusion

In this paper, we have taken into account both dosimetric and hardware constraints to produce deliverable plans for VMAT treatment planning and also dynamically adjusted the penalty weights of the objective function to automatically obtain clinically acceptable plans.

This approach increases the efficiency of the algorithm and consequently decreases the human interventions.

To this end, we integrated structure-based and voxel-based adjustment algorithms in the column generation technique to update the weight vectors based on DVH criteria in the objective function. This approach does not require additional dose-volume constraints in the master model, leading to minimal re-optimization in the PO phase and increasing the efficiency of the treatment planning. We evaluated our approach on a prostate and a head-and-neck case; the former has more voxels (constraints), and the latter has more beamlets (columns). The performance of the proposed voxel-based adjustment in column generation (VA-CG) is significantly better than simple VMAT, without weight adjustment, and also PO-Adjustment approach, considering weight adjustment only in the post-optimization phase.

Further work could be carried out with more analysis on a wide range of patients to analyze and improve the efficiency of the algorithm in practice in existing commercial software. Moreover, the proposed algorithm considers multiple DVH criteria in the treatment evaluation. It would also be possible to apply this methodology to the whole DVH curve. Future work will also consider the use of graphics processing unit (GPU) to accelerate the method.

Acknowledgements

The authors gratefully acknowledge financial support from the Natural Sciences and Engineering Research Council of Canada (NSERC) and the Vanier Canada Graduate Scholarship program (DVC134707). We also thank Prof. David Craft, Harvard Medical School, who helped us by providing the data, Dr. Marc-André Renaud, McGill University, for helpful comments, and Dr. Martin Hinse, Medical Physicist at Laval Integrated Cancer Centre (CICL), for comparison to commercial software. The authors also wish to thank the anonymous referees whose insightful comments have helped us to improve our paper.

CHAPTER 6 A MULTI-OBJECTIVE COLUMN GENERATION METHOD TO APPROXIMATE THE PARETO FRONT IN DIRECT APERTURE OPTIMIZATION

Abstract. Radiation therapy planning revolves around an inherent tradeoff between treating the tumor and sparing surrounding healthy tissues. The classic way to handle this problem is to solve a convex multi-objective programming model to obtain an ideal intensity profile and then decompose it into a set of feasible apertures with optimal dose intensities. In this paper, we address direct aperture optimization (DAO), which designs the apertures and their corresponding intensities, simultaneously, and propose a multi-objective column generation technique that efficiently approximates a non-dominated set of treatment plans. To this end, first, a novel first-order solution method, called Blended Conditional Gradients (BCG), is integrated into column generation to improve the computational performance for the single objective DAO. We then develop a Pareto-based column generation technique, to directly obtain apertures that approximate the Pareto frontier. We find an upper bound approximation of the Pareto front from a discrete set of points and their convex combinations and develop a lower bound for the Pareto frontier. In each iteration, the algorithm generates a column which reduces the maximum distance of two bounds of the Pareto front. We show the algorithm converges to the optimal Pareto frontier with a large enough number of iterations.

To evaluate the efficiency of the proposed algorithms, two clinical cases, a prostate and a head-and-neck, from CORT dataset benchmark are taken into account. For the BCG-based column generation algorithm, the results show this new method improves the plan quality, on average by 13.96% and 57.14% for the prostate and head-and-neck cases, respectively, in comparison to CPLEX, a commercial solver, in the same amount of time. Also, for the multi-objective column generation algorithm, the results in a two-dimensional objective space validate the algorithm can achieve an appropriate approximation of the Pareto frontier with a small number of columns and low computational effort.

Keywords. Radiation therapy treatment planning; column-generation; multi-criteria optimization; Pareto-optimality.

Collaboration. This chapter is the result of collaboration with Prof. Edwin Romeijn in Georgia Institute of Technology.

History. This chapter is prepared to be submitted to a peer-reviewed journal.

6.1 Introduction

Radiation therapy is an effective technique against cancer, from which approximately 50 percent of all cancer patients can benefit [63]. This method works by damaging the genetic material within cancerous cells and destroying their ability to reproduce. However, normal cells will also be damaged in this process and the treatment should be performed in such a way that it maximizes the dose of radiation to tumors, while minimizing the adverse effects of radiations to healthy tissues, simultaneously [52]. External radiation therapy is the most common type of radiotherapy in which the radiation beam is delivered from several directions by a linear accelerator (linac) mounted on a gantry.In Intensity Modulated Radiation Therapy (IMRT), a piece of equipment called multi-leaf collimator (MLC) is used to form the shape of the beam. This equipment has a finite number of leaves, leading and trailing, which move independently towards each other and shape the exposed field as an aperture. The treatment plan optimization is the process of automatically determining the beam directions, apertures, and intensities delivering the distribution of dose.

In the traditional approach to IMRT treatment planning, first, each beam is discretized into hundreds of small beamlets and the optimal amount of radiation intensity, or fluence, of each beamlet is determined by solving a problem, so-called fluence map optimization (FMO) [9, 94, 109]. FMO can not be directly delivered because of the uniformity of the source of radiation at any time. Then, in the second step, the obtained fluence map is decomposed into a number of apertures, and a deliverable MLC leaf-sequencing is planned [19, 54, 55]. However, this sequential approach may cause a potential loss in the treatment quality. Therefore, an integrated approach, so-called Direct Aperture Optimization (DAO), is proposed which directly models the aperture shapes and their intensities at the same time [118]. The number of aperture variables in DAO formulation is large, which requires significant computational time.

Column generation (CG) is a leading optimization technique to solve large-scale problems with decomposable structure [43]; which has successfully been used for several variants of DAO [82, 83, 87, 102, 108]. Despite decomposing the problem into a master model and pricing subproblems in column generation, the quadratic objective functions and large number of variables and constraints in real-life application result in large and complex models. In this paper, we first enhance the efficiency of the CG-based algorithms by integrating a new first-order optimization method, so-called Blended Conditional Gradients, in the master model. In this method, called CG-BCG, we manage to generate efficiently strong columns without solving the master model to optimality in each iteration. We then address the trade-off between contradictory normal and tumor structures, as one of the main technical challenges of

the treatment planning problem in practice, by developing a new multi-objective column generation method. Several multi-criteria optimization (MCO) techniques have been developed for IMRT problem. These techniques can be classified into several categories regarding the role of the decision maker [48]. In Lexicographic techniques, the decision maker prioritizes the objectives based on their importance a priori [22, 23, 78, 124].In interactive methods, the user guides the exploration during an interactive procedure [139]. In Pareto frontier (PF) optimization, we explore for a set of Pareto optimal solutions, in which we cannot improve any single objective without deteriorating at least one other objective [31, 34, 36, 37]. For a general review of MCO approaches in IMRT, we refer the reader to two comprehensive reviews by Küfer et al. [69] and Craft [33]. For the rest of the paper, we limit ourselves to approaches based on Pareto frontier optimization with convex objectives.

The purpose of this paper is to develop an efficient algorithm to find an approximation of a non-dominated set of solutions during the course of column generation avoiding a large number of columns. Unlike the classic PF optimization methods, we do not have an optimal point for a given priority of objectives in each iteration of column generation. However, the feasible points are deliverable to the patient, which is useful in practice. We provide lower bound and upper bounds for the Pareto front and generate columns that reduce the maximum gap of two bounds and improve the entire Pareto font. This extension to column generation, which we call Pareto-based column generation (PCG), is implemented for multi-criteria IMRT treatment planning also applicable to more classes of problems. We take into account feasible and deliverable apertures and deal with both dosimetric derived non-convexity, i.e., clinical objectives, and hardware derived non-convexity, i.e., MLC apertures, simultaneously. The main contributions of this study are:

- We develop a novel quadratic optimization method, based on BCG method integrated to column generation, as CG-BCG.
- We develop a lower bound for the single-objective problem at each iteration of the CG-BCG.
- The CG-BCG method is implemented for the DAO problem and is shown to be more efficient in comparison to the traditional Frank-Wolfe algorithm and also CPLEX software in the master model.
- We develop a new multi-objective column generation method, which improves the approximation of Pareto front rather than a single objective.
- We propose lower and upper bounds for the Pareto front and generate a column in each

iteration for the weight vector that reduces the maximum gap of two lower and upper bounds.

- We show that the proposed algorithm converges to the Pareto front after a large number of iterations.
- Finally, we test our algorithms on two benchmark clinical cases of IMRT in a bi-objective space. The results show that the proposed algorithms are able to find high-quality plans for clinical size problems efficiently.

The remainder of the paper is organized as follows. Section 6.2 surveys the multi-criteria approaches in radiation therapy. We summarize preliminary material in Section 6.3. Section 6.4 introduces the problem statement and the basic formulation. In Section 6.5, we propose our column-generation based quadratic optimization algorithm to enhance the efficiency of the single objective problem. In Section 6.6.1, we develop the Pareto-based Column Generation algorithm for Pareto frontier approximation. Section 6.7 presents the computational experiments and results for a prostate case and a head-and-neck case. Finally, Section 6.8 provides the conclusion and future potential area.

6.2 Literature review

There are a variety of methods to approximate the Pareto optimal set, which can be classified into inner approximation [114], outer approximation [16], and sandwich algorithms [66, 119]. In inner approximation, the bounding facets of the convex hull of the Pareto points contained in the set are used, while outer approximations find supporting tangential hyperplanes of the Pareto frontier and take their intersection to approximate the Pareto front. Sandwich methods combine these two techniques and we can have an upper bound on the approximation error. For more details on this topic, we refer the reader to a comprehensive review by [110].

In IMRT, Küfer et al. [67] have formulated the first multi-criteria model for FMO problem. Craft et al. [38] have introduced the sandwich method for higher dimensional problem. Later, they have shown that the number of required Pareto optimal solutions to represent the Pareto front of up to five dimensions is linearly dependent to the number of objectives [32]. Moreover, Craft and Richter [35] proposed a Pareto front navigation algorithm for the stop and shoot IMRT problem based on deliverable plans while the number of segments are restricted. In this work, the plans are already segmented to maximum 50 apertures, a priori, and two methods are developed to navigate by combining a limited number of plans. Shao and Ehrgott [116] also proposed a sandwich algorithm for the multiobjective linear

programming problem (MOLP) in FMO. In the same line of research, Ehrgott et al. [53] have proven that the Pareto front points lie on the boundary of a convex set if the objective functions are convex. They extended their algorithm for MOLP models to approximate the convex multi-objective nonlinear programming problems. Rennen et al. [104] enhanced the higher dimensional sandwich algorithms by introducing the concept of dummy points to the inner approximation and a new error measure. Bokrantz and Forsgren [18] proposed a sandwich algorithm for approximating Pareto fronts of MCO problems based on enumerating the vertices of an outer approximation of the Pareto front and dual techniques.

In most of these methods, the multi-criteria optimization has been formulated for the FMO problem. This model is easy to solve for multiple times, approximating the Pareto frontier. However, it is not deliverable in practice and a leaf sequencing algorithm is required to produce a deliverable plan.

6.2.1 Multi-objective column generation in IMRT treatment planning

Although the column generation technique has been widely used specially for DAO, few studies have addressed its implementation in MCO. Salari and Romeijn [111] proposed an exact bi-objective solution approach based on the special structure of DAO, optimizing the treatment quality and the beam-on time. The treatment quality is evaluated based on voxel-based least square penalty function and the beam-on time is expressed as the sum of all aperture intensities. First, they find the smallest beam-on time, beyond which the optimal solution is not to treat. Then, sequentially an optimal treatment plan for the obtained beam-on time is produced using the column-generation method; and the maximum range the solution remains optimal is determined. They decrease the beam-on time to the point the current solution is not valid and continue the procedure until no treatment plan is feasible for the new beam-on time. In another study, Salari and Unkelbach [112] proposed a multi-criteria column-generation for IMRT treatment planning. The idea to extend the standard CG to multi-criteria approach was to consider multiple weighted-sum restricted master models based on fixed weight vector scenarios, e.g., three in the case. For the multi-criteria pricing problem, they formulated a mixed-integer programming (MIP) model and three heuristics to obtain the aperture yielding the largest improvement in the entire Pareto front. However, the penalty weight scenarios are fixed during the column generation process and they can not guarantee that the non-dominated set is well-approximated. Recently, Lin et al. [77] developed a MOLP formulation for direct aperture optimization in IMRT treatment planning, so-called revised normal boundary intersection, and used the column generation algorithm to solve the linear models in its subproblems.

6.2.2 Multi-objective column generation in other applications

The integration of multi-objective techniques and column-generation has also rarely been studied in other applications. Moradi et al. [90] implemented column generation for the linear multi-commodity minimum cost flow problem based on a bi-objective simplex algorithm. In this method, two dual values, corresponding two objectives, are considered for each master model constraint. In the pricing subproblem, the column for the next iteration is generated such that the ratio of improvement of the second objective over deterioration of the first one is maximized. Moreover, Artigues et al. [11] developed a bi-criteria column generation for multi-vehicle covering tour problem with a min-max objective. In this special case, the route time is factual when the column is generated in the pricing subproblem. Then, instead of adding constraints in the master model, they easily remove the unsatisfied columns. This approach is not useful in problems such as IMRT planning, in which the effect of one particular column is in conjunction with other columns.

6.3 Preliminaries

For a set Y, we denote by $\text{conv}(Y)$ the convex hull of set Y; and for two sets Y_1 and Y_2, we denote by $Y_1 + Y_2$ the Minkowski sum, which is defined as $\{y_1 + y_2 \,|\, y_1 \in Y_1,\, y_2 \in Y_2\}$. Moreover, we define polyhedral $Y_+ = Y + \mathbb{R}^n_+$, where $\mathbb{R}^n_+$ is the non-negative cone.

We denote by e_i the i-th coordinate vector and and $\mathbf{1} = (1, 1, \cdots, 1) = e_1 + e_2 + \cdots$ denote the all-one vector. The probability simplex $\Delta^k = \text{conv}\,\{e_1, \cdots e_k\}$ is the convex hull of the coordinate vectors in dimension k. The shorthand $[\,.\,]_+$ denotes $\max\{0, .\}$ and $\|\,.\,\|$ denotes the Euclidean norm.

Let f be a differentiable convex function over a polytope $\mathcal{P}$. f is L-smooth such that

$$\| f'(x_1) - f'(x_2) \| \leq L \| x_1 - x_2 \|, \quad \forall x_1, x_2 \in \mathcal{P}, \tag{6.1}$$

Moreover, f is strongly convex if for some $\alpha > 0$ we have

$$f(x_2) - f(x_1) - \nabla f(x_1)(x_2 - x_1) \geq \alpha \| x_2 - x_1 \| /2, \quad \forall x_1, x_2 \in \mathcal{P}, \tag{6.2}$$

A hyperplane $\{z \in \mathbb{R}^n : w^\top z = w^\top b\}$ with non-zero normal w and offset b is denoted by $H(w, b)$. Moreover, the distance of a point a from hyperplane $H(w, b)$ is as follows:

$$\psi(w, a, b) = \|a - b\| / \|w\|. \tag{6.3}$$

6.4 Problem description

In this section, we briefly introduce the notation and basic formulation for the mathematical model of the direct aperture optimization in IMRT treatment planning.

Let S be the set of structures including the target volumes and organs at risk. Each structure $s \in S$ is discretized into small cubic volume elements called *voxels*, $\mathcal{V}_s$. There are also equi-spaced beam angles, $\mathcal{B}$, around the patient. Each beam is decomposed into a rectangular grid of *beamlets*.A beamlet (r, c), located in row r and column c of MLC, is open if it is not blocked by either the left and right leaves. The relative motion of the leaves controls the intensity. A two-dimensional $n_r \times n_c$ binary matrix A represents an *aperture* for an MLC with n_r rows and n_c columns. A sample of voxels and beamlets are shown in Figure (6.1).

The estimated dose received by voxel v from beamlet (r, c) at unit intensity is denoted D_{rcv}, in Gy/MU. $D = [D_{rcv}]$ is called the dose-influence matrix. We assume that the dose absorbed by a given voxel can be determined by adding the doses from each of the individual beamlets comprising the aperture.

6.4.1 The formulation

The dose irradiated from each aperture depends on its corresponding shape and intensity. Let K_b denote the set of allowed apertures from beam direction $b \in \mathcal{B}$, with respect to the MLC leaf positions. We also denote the set of all deliverable apertures by $K \equiv \cup_{b\in\mathcal{B}} K_b$. To form the shape of aperture k, we define a binary decision variable q^k_{rc} that is equal to 1 if beamlet (r, c) is open, between the left and right leaves of row r. We also define two integer variables τ^k_r and ν^k_r that represent the position of left and right leaves, respectively. The set of following constraints are used to form the aperture based on the consecutive open beamlets between left and right leaves in each row of MLC.

$$\tau^k_r \le \nu^k_r - 1 \qquad \forall k \in K, \forall r = 1, 2, \cdots, n_r \tag{6.4a}$$

$$1 \le \nu^k_r \le n_c + 1 \qquad \forall k \in K, \forall r = 1, 2, \cdots, n_r \tag{6.4b}$$

$$c\, q^k_{rc} \le \nu^k_r - 1 \qquad \forall k \in K, \forall r = 1, 2, \cdots, n_r, \forall c = 1, 2, \cdots, n_c \tag{6.4c}$$

$$(n_c + 1 - c)\, q^k_{rc} + \tau^k_r \le n_c \qquad \forall k \in K, \forall r = 1, 2, \cdots, n_r, \forall c = 1, 2, \cdots, n_c \tag{6.4d}$$

$$\sum_{c=1}^{n_c} q^k_{rc} = \nu^k_r - \tau^k_r - 1 \qquad \forall k \in K, \forall r = 1, 2, \cdots, n_r \tag{6.4e}$$

$$q^k_{rc} \in \{0, 1\} \qquad \forall k \in K, \forall r = 1, 2, \cdots, n_r, \forall c = 1, 2, \cdots, n_c \tag{6.4f}$$

$$\tau, \nu \in \mathbb{Z}_+^{n_r \times |K|}, \tag{6.4g}$$

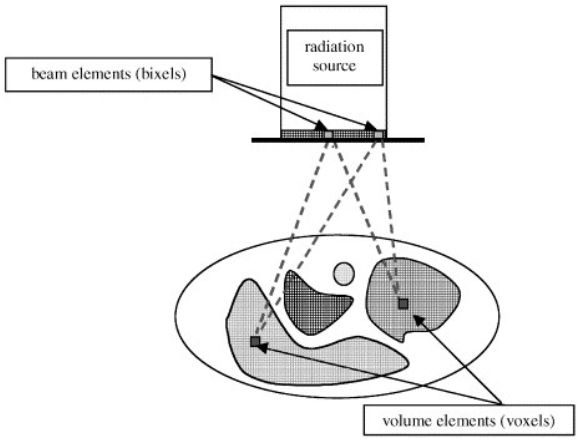

Figure 6.1 Voxels and beamlets in radiation therapy [59].

where constraints (6.4a)-(6.4b) are the MLC mechanical restrictions. Constraints (6.4a) ensure that left and right leaves in each pair have no overlap. The range of leaves are restricted in constraints (6.4b). In constraints (6.4c)-(6.4e), the model shapes the aperture based on the consecutive open beamlets between left and right leaves in each row of MLC. To simplify the model in the rest of the paper, we show this solution space as $\mathcal{Q}$.

The intensity of aperture k is denoted as variable x_k, which is dependent to the dose rate and also the amount of time it is irradiated from. In this model, the total intensity is restricted to Λ in practice. However, without loss of generality, we normalize the intensities and also assume a dummy aperture in K, which has no open beamlet and serves only as a placeholder. Thus, the total intensity is restricted to one as follows:

$$\sum\nolimits_{k\in K} x_k = 1 \tag{6.5}$$

Obviously, we can easily replace $\Lambda\, x_k$ to obtain the actual aperture intensity. The dose z_v absorbed by voxel v from all apertures is computed based on the dose-influence matrix D, the aperture shape q^k, and the aperture intensity x_k as follows:

$$z_v = \sum_{k\in K}\sum_{r=1}^{n_r}\sum_{c=1}^{n_c} \Lambda D^k_{rcv}\, q^k_{rc}\, x_k \qquad \forall v \in \mathcal{V} \tag{6.6}$$

To assess the treatment plan, several objective functions are developed in the literature. A well-known objective is the quadratic voxel-based least-square function penalizing the

underdose and overdose for involved voxels as follows [108]:

$$\sum_{s\in S}\sum_{v\in\mathcal{V}_s} \underline{\lambda}_s \left[d_v - z_v\right]_+^2 + \overline{\lambda}_s \left[z_v - d_v\right]_+^2 \tag{6.7}$$

where d_v is pre-specified dose for voxel v. Also, $\underline{\lambda}$ and $\overline{\lambda}$ are penalty weights obtained from the product of the weight of structure s, w_s, and the weight of the underdosage $\underline{\rho}$ and overdosage $\overline{\rho}$, respectively.

Finally, a simple presentation of the general model is as follows:

$$\begin{aligned}
\textbf{GP}: \quad \min \quad & \sum_{s\in S}\sum_{v\in\mathcal{V}_s} \underline{\lambda}_s \left[\underline{d}_v - z_v\right]_+^2 + \overline{\lambda}_s \left[z_v - \overline{d}_v\right]_+^2 && && (6.8a)\\
& z_v = \sum_{k\in K}\sum_{r=1}^{n_r}\sum_{c=1}^{n_c} D^k_{rcv}\, q^k_{rc}\, x_k && \forall v\in\mathcal{V} && (6.8b)\\
& \textstyle\sum_{k\in K} x_k = 1 && && (6.8c)\\
& q \in \mathcal{Q} && && (6.8d)\\
& x \in \mathbb{R}_+^{|K|} && && (6.8e)\\
& z \in \mathbb{R}^{|\mathcal{V}|}. && && (6.8f)
\end{aligned}$$

The non-linearity in equation (6.8b) and the binary variables q result in a large-scale mixed integer nonlinear programming model.

6.4.2 Column generation

To avoid the large number of columns and non-linearity in model GP, we decompose it into a master model and a pricing subproblem, and solve it by the column generation technique. Let A^k indicate the shape of aperture k and $D(A^k)$ denote the vector of dose deposition coefficients corresponding to aperture $k \in K$, i.e., $D_v(A^k) = \sum_{r=1}^{n_r}\sum_{c=1}^{n_c} D^k_{rcv} q^k_{rc}$. The problem reduces to the following master problem (MP):

$$\begin{aligned}
\textbf{MP}: \min \ & f(x) && && (6.9a)\\
& z_v = \sum_{k\in K} D_v(A_k)\, x_k && \forall v\in\mathcal{V} && (6.9b)\\
& \sum_{k\in K} x_k = 1 && && (6.9c)\\
& x_k \geq 0 && \forall k\in K, && (6.9d)
\end{aligned}$$

The feasibility space of the model is the probability simplex $\Delta^{|K|}$, where $|K|$ is the number of columns. However, set K is large and a restricted set of columns $K' \subseteq K$ is taken into account as RMP.

$$\textbf{RMP} : \min\ f(x) \tag{6.10a}$$

$$z_v = \sum_{k \in K'} D_v(A_k)\, x_k \qquad \forall v \in \mathcal{V} \tag{6.10b}$$

$$\sum_{k \in K'} x_k = 1 \tag{6.10c}$$

$$x_k \geq 0 \qquad \forall k \in K'. \tag{6.10d}$$

Given a small set of feasible apertures ($K' \subseteq K$) in RMP, the best subset optimizing the intensities and dose distribution, is selected. Therefore, each feasible solution to RMP provides a deliverable plan that can be feasible for GP.

The pricing subproblem (PSP) generates promising new apertures, expected to improve the RMP objective function. Let $(\overline{\boldsymbol{x}}, \overline{\boldsymbol{z}})$ be the optimal solution of RMP and D^b indicate the dose deposition matrix in direction b. The formulation of PSP to generate the column with the largest reduced cost is as follows:

$$\textbf{PSP} : \min_{q \in \mathcal{Q}} \sum_{b \in \mathcal{B}} \sum_{r=1}^{n_r} \sum_{c=1}^{n_c} \sum_{v \in V} \overline{\pi}_v D^b_{rcv} q_{rc}, \tag{6.11}$$

where $(\overline{\pi}_v : v \in \mathcal{V})^\top \equiv -\nabla f(\overline{\boldsymbol{z}})$ are the dual values of RMP. To find a new aperture that prices out (or determine that none exists at this stage), this model is solved for each beam $b \in \mathcal{B}$ by an efficient algorithm proposed by Romeijn et al. [108] in $O(n_r n_c)$ time per beam. If no new aperture with negative reduced cost is found, the model is tackled with the exact model.

In the RMP model, we require a large number of constraints in real cases to linearize the positive the $[\,.\,]_+$ operator for large number of voxels, which along with the quadratic objective function, make the model time-consuming. Moreover, this model is required to be solved several times during the column generation algorithm. To speed-up the algorithm, we propose a new first-order algorithm in Section 6.5.

6.5 Solution approach for the single-objective problem

In this section, we first present the standard Frank-Wolfe (FW) algorithm, a well-know method for quadratic problems, to solve the RMP and then integrate the blended conditional

gradients algorithm, as a novel first-order optimization method, into column generation.

6.5.1 CG-based Frank-Wolfe (CG-FW)

The Frank-Wolfe or conditional gradient algorithm is a classical first-order method for minimizing a smooth convex function $f : \mathcal{X} \to \mathbb{R}$ over a convex compact set $\mathcal{X} \subseteq \mathbb{R}^n$ [57]. The FW algorithm is an iterative method which minimizes a series of linear approximations of f over the feasible set $\mathcal{X}$. The candidate solution x_t in iteration t is updated through the following steps. Firstly, a first-order oracle computes $\nabla f(x_t)$. Secondly, the linear optimization oracle computes $p_t \in \arg\min_{x \in \mathcal{X}} < \nabla f(x_t), x_t >$, as the extreme point of $\mathcal{X}$. Finally, one sets $x_t = (1 - \alpha_t)x_{t-1} + \alpha_t p_t$ for some $\alpha_t \in [0, 1]$.

As explained earlier, the feasibility space $\mathcal{X}$ is the probability simplex $\Delta^{|K|}$ and the extreme points are the columns. The extreme point p_t is either already present among the existing columns, $K' \subseteq K$, or it has not been generated yet, and it belongs to $K'' = K \backslash K'$. The gradient of objective function f, defined in Equation (6.7), with respect to column k is

$$\nabla f(x_t)_k = 2\boldsymbol{D}(A^k)^\top(\overline{\boldsymbol{z}}_t - \underline{\boldsymbol{z}}_t), \tag{6.12}$$

where $\overline{z}_{vt} = \overline{\lambda}_v[z_{vt} - d_v]_+$ and $\underline{z}_{vt} = \underline{\lambda}_v[d_v - z_{vt}]_+$ for each voxel v. We can obtain the vertices with the lowest and highest gradients in the set of existing columns in RMP, K', as follows:

$$s_t = \arg\min_{k \in K'} \nabla f(x_t)_k, \tag{6.13}$$

$$a_t = \arg\max_{k \in K'} \nabla f(x_t)_k. \tag{6.14}$$

Moreover, the vertex with the lowest reduced cost, obtained by the pricing subproblem, is the extreme point with the minimum gradient in K'' as follows:

$$v_t = \arg\min_{k \in K \backslash K'} \nabla f(x_t)_k. \tag{6.15}$$

Thus, the extreme point p_t in the whole solution space $\Delta^{|K|}$ is e_{u_t}, where

$$u_t = \arg\min_{s \in \{s_t, v_t\}} \nabla f(x_t)_s. \tag{6.16}$$

Finally, the solution in each iteration t, is computed as follows:

$$x_{t+1} = (1 - \alpha_t)x_t + \alpha_t\, p_t, \tag{6.17}$$

where $\alpha_t = 2/(t+2)$ is the standard step-size for the FW algorithm. The pseudocode of the algorithm is shown in Algorithm 3. This method is interesting due to the low memory requirements and projection-free iterations.

Algorithm 3 Column generation-based Frank-Wolfe algorithm

1: $t \leftarrow 0$, x_0 be an initial point
2: $s_t \leftarrow \arg\min_{k \in K'} \nabla f(x_t)_k$
3: $v_t \leftarrow \arg\min_{k \in K \setminus K'} \nabla f(x_t)_k$ ▷ Based on pricing subproblem
4: $u_t \leftarrow \arg\min_{s \in \{s_t, v_t\}} \nabla f(x_t)_s$
5: $p_t \leftarrow e_{u_t}$
6: $\alpha_t \leftarrow 2/(t+2)$ or an alternative value
7: $x_{t+1} \leftarrow (1-\alpha_t)x_t + \alpha_t p_t$
8: $t \leftarrow t+1$ and go to step 2

6.5.2 CG-based Blended conditional gradients (CG-BCG)

The blended conditional gradients algorithm is a recent variant of FW method developed by [21]. This method is interesting in this problem because it uses less extreme points rather than the standard FW method, which results in less apertures in the IMRT problem and consequently less treatment time. In this algorithm, x_t in each iteration t is a convex combination of the active vertices of $\mathcal{X}$. At each iteration, the algorithm either searches for a better combination of active vertices or finds a new vertex, whichever promises the smaller objective value. In column generation, all vertices of the solution space are not in RMP; however, for this model that the feasibility space is a probability simplex, the vertex with the most negative reduced cost provided by the pricing subproblem is the extreme point required for BCG. The pseudocode of proposed CG-BCG algorithm is given in Algorithm 4.

In each iteration of CG-BCG, the algorithm determines the search direction either in the current RMP solution space or adding a new column. This is based on a value Φ_t, which is an estimation for the gap between the current function value $f(x_t)$ and the optimal function value. If the maximum possible progress with the existing columns, $\nabla f(x_t)_{a_t} - \nabla f(x_t)_{s_t}$, is greater than value Φ_t, the algorithm decides to search more deeply inside RMP feasibility space. Otherwise, PSP generates a new column for the model. We implement a line search method to find the local optimum on the line segment from the current solution x_t to the selected vertex of the simplex, p_t. The details of this procedure used in lines (14) and (24) of Algorithm (4) are described in Appendix C. The gradient function guarantees minimizing the objective over the line; however, the solution obtained is not optimal for the restricted master problem. Note that the line search between the vertices of the probability simplex keeps the

feasibility of constraint (6.10c). When the value of Φ_t is discovered to be an overestimate of the dual gap (in Line 20), it is halved.

Algorithm 4 Column generation based Blended Conditional Gradients

Input: smooth convex function f, $\kappa = 3$
Output: solution x^t for $t = 1, 2, \cdots, T$ and set of apertures K'

1: $x_0 \leftarrow e_1$, $S_0 \leftarrow \{0\}$, $K' \leftarrow \{A_0\}$, ▷ The first column is dummy.
2: $\Phi_0 \leftarrow \max_{x \in \mathcal{X}} (\nabla f(x_0)\, x_0 - \nabla f(x_0)\, x)/2$
3: **for** $t = 0$ **to** $T - 1$ **do**
4: $S_t \leftarrow \{k \in K' : x_k^t > 0\}$ ▷ Active columns
5: $a_t \leftarrow \arg\max_{k \in S_t} \nabla f(x_t)_k$
6: $s_t \leftarrow \arg\min_{k \in S_t} \nabla f(x_t)_k$
7: **if** $(\nabla f(x_t)_{a_t} - \nabla f(x_t)_{s_t} \geq \Phi_t)$ **then**
8: determine direction d based on $\nabla f(x_t)$
9: $\eta = \max\{\beta : x_t - \beta\, d \geq 0\}$
10: $\hat{x} = x_t - \eta\, d$
11: **if** $(f(\hat{x}) < f(x_t))$ **then**
12: $x_{t+1} \leftarrow \hat{x}$
13: **else**
14: $x_{t+1} \leftarrow \arg\min_{x \in [x_t, \hat{x}]} f(x)$ ▷ Line search between solution x_t and $\hat{x}$
15: $\Phi_{t+1} \leftarrow \Phi_t$
16: **else**
17: $v_t \leftarrow \arg\min_{k \in K \setminus K'} \nabla f(x_t)_k$ ▷ The best column obtained from PSP
18: **if** $|\nabla f(x_t)| < \epsilon$ and $v_t \geq 0$ **then**
19: **return** x_t
20: **if** $(\nabla f(x_t)\, x_t - \nabla f(x_t)_{v_t} \geq \Phi_t/\kappa)$ **then**
21: $\Phi_{t+1} \leftarrow \Phi_t$
22: **else**
23: $\Phi_{t+1} \leftarrow \Phi_t/2$
24: $x_{t+1} \leftarrow \arg\min_{x \in [x_t, e_{v_t}]} f(x)$ ▷ Line search between solution x_t and the new vertex e_{v_t}

Lower bound

The gap between the obtained feasible solution x_t of CG-BCG in each iteration t and the optimal value x^* consists of two parts: (1) a part between $f(x_t)$ and the optimal value of RMP, $f(x^*_{RMP})$, and (2), a part between $f(x^*_{RMP})$ and the optimal value of global problem, $f(x^*)$, due to missing columns. The following lemma obtains a lower bound of the problem in each iteration based on the indices s_t and v_t of columns with maximum possible progress obtained in RMP and PSP from Equations (6.13) and (6.15), respectively.

Lemma 1. *Let f be a smooth convex function, $S_t = \{k \in K' : x_k^t > 0\}$ set of active columns in iteration t. A lower bound on f in iteration t is as follows:*

$$\bar{l}_t = f(x_t) - \nabla f(x_t)\, x_t + \min\{\nabla f(x_t)_{s_t}, \nabla f(x_t)_{v_t}\}. \tag{6.18}$$

Proof. Provided by the convexity of f, for any $x \in \mathbb{R}_+^{|K'|}$ in each iteration t

$$f(x) \geq f(x_t) + \nabla f(x_t)\,(x - x_t) \tag{6.19}$$

and consequently

$$\min_{x\in\mathcal{X}} f(x) \geq f(x_t) + \min_{x\in\mathcal{X}} \nabla f(x_t)\,(x - x_t) \tag{6.20}$$

Thus, to find the lower bound, it is enough to solve the following model:

$$\bar{l}_t = f(x_t) + \min_{x\in\mathcal{X}} \nabla f(x_t)\,(x - x_t) \tag{6.21}$$

and

$$\bar{l}_t = f(x_t) - \nabla f(x_t)\, x_t + \min_{x\in\mathcal{X}} \nabla f(x_t)\, x \tag{6.22}$$

where $x \leq 1$ regarding Equation (6.10c) and the solution of the minimization in the last term is $\min\{\nabla f(x_t)_{s_t}, \nabla f(x_t)_{v_t}\}$ as discussed in Sections 6.5.1 and 6.5.2.

$$\bar{l}_t = f(x_t) - \nabla f(x_t)\, x_t + \min\{\nabla f(x_t)_{s_t}, \nabla f(x_t)_{v_t}\}. \tag{6.23}$$

■

Also, the lower bound of the problem would be updated as $\hat{l}_t = \max\{\hat{l}_{t-1}, \bar{l}_t\}$. This lower bound is valid only when the pricing-sub problem is solved, in line 18 of Algorithm 4, and we have information on both s_t and v_t.

Convergence of the algorithm

Braun et al. [21] have proven the convergence of the BCG algorithm for the probability simplex Δ^k as the feasibility space $\mathcal{X}$ and L-smooth function f; and also obtained the convergence rate as shown in the following lemma.

Lemma 2. *(Braun et al. 2018-Corollary 4.2) Let f be an α-strongly convex and L-smooth function over the probability simplex Δ^k with $k \geq 2$. Let x^* be a minimum point of f in Δ^k. Then, the algorithm converges with rate*

$$f(x_T) - f(x^*) \leq (1 - \frac{\alpha}{4Lk})^T.(f(x_0) - f(x^*)), \quad T = 1, 2, \cdots \tag{6.24}$$

If f is not strongly convex (i.e., $\alpha = 0$), we have

$$f(x_T) - f(x^*) \leq \frac{8L}{T}, \quad T = 1, 2, \cdots \tag{6.25}$$

In our problem, function f defined in Equation (6.7) is convex and also L-smooth. The Lipschitz constant L is provided in Appendix C. The procedure CG-BCG is similar to BCG. The difference is that we search for the vertex with minimum gradient among non-generated vertices using the pricing subproblem and add a new column rather than perform a Frank-Wolfe step. Therefore, we implicitly consider all extreme vertices in the feasibility space through RMP and PSP and the convergence rate of the algorithm is similarly $(1 - \alpha/(4L|K|))^T$.

6.6 Extension to multi-objective problem

In this section, we formulate the master model and pricing subproblem of column generation based on multiple objectives and present the detailed fundamentals and procedure of PCG algorithm to explore the Pareto frontier.

6.6.1 Multi-objective formulation

The general multi-objective model is formulated as follows:

$$\textbf{MOP}: \min_{x \in \mathcal{X}} f(x) = \{f_1(x), f_2(x), \cdots, f_n(x)\} \tag{6.26}$$

where $x = (x_1, x_2, \cdots, x_m)$ is the decision variable vector in the feasible set $\mathcal{X} \subseteq \mathbb{R}^m$, and $f : \mathbb{R}^m \to \mathbb{R}^n$ consists of n objectives in set $N = [1, 2, \cdots, n]$. Then, $\mathbb{R}^m$ is the decision space, and $\mathbb{R}^n$ is the objective space. We define the image of the feasible region under the objective function mapping $\mathcal{Y}$ as follows:

$$\mathcal{Y} = \{y \in \mathbb{R}^n : y_i = f_i(x),\, x \in \mathcal{X}\}. \tag{6.27}$$

Moreover, we define polyhedral $\mathcal{Y}_+$ as $\mathcal{Y} + \mathbb{R}^n_+$.

Definition 1. *For two vectors y^1 and y^2 in the objective space, we write $y^1 \leq y^2$ if and only if $y^1_i \leq y^2_i$ for all $i \in N$ and $y^1 \neq y^2$. Moreover, $y^1 < y^2$ if and only if $y^1_i < y^2_i$ for all $i \in N$.*

Definition 2 (Efficient set)**.** *A feasible solution $\hat{x}$ is called efficient if there does not exist any x such that $f(x) < f(\hat{x})$. The set of all efficient solutions is called the efficient set X_E in the decision space.*

Definition 3 (Pareto front)**.** *In the objective space, the image $\hat{y}$ of the efficient solution $\hat{x}$ is called a Pareto optimal or a non-dominated point (NDP). We refer to the set of all Pareto optimal objective vectors as the Pareto front Y^* in the objective space and the polyhedral corresponding to the epigraph of Y^* as Y_+^*.*

In addition to the efficient and Pareto sets, the ideal points are used as initial upper bounds in the Pareto front approximation.

Definition 4 (Ideal point)**.** *The ideal point $y^{ideal} \in \mathbb{R}^n$ with $y_i^{ideal} = \min_{x \in \mathcal{X}} f_i(x)$ is the point that corresponds to the optimal value for each objective function.*

To assess the treatment plan, several objective functions can be considered by the physician. We make the following mild assumptions on the feasibility set and the objective function f_i.

Assumption 1. *The feasible region is nonempty convex and compact subset of $\mathbb{R}^m$.*

Assumption 2. *Each function $f_i(x)$ is continuously differentiable and convex on the feasibility set.*

In this model, we consider the quadratic voxel-based least-square penalty function for n structures along the lines of equation (6.7). Romeijn et al. [107] have shown that the Pareto optimal set is a connected surface in the boundary of a convex set, and Ehrgott et al. [53] have shown that the polyhedral Y_+^* corresponding to the epigraph of the Pareto front is a convex set whenever multi-objective programming model is convex. The Pareto optimal solutions under these convexity assumptions can be found by the weighted-sum method, wherein each objective is associated with a weighting coefficient and the weighted sum of the objectives is minimized. We employ this method to transform the multi-criteria restricted master problem to a single objective model as follows:

$$\boldsymbol{MORMP(w):} \quad \min_{x \in \mathcal{X}} \sum_{i \in N} w_i \, f_i(x), \tag{6.28}$$

where $w \in \mathbb{R}_+^n$ is a non-negative weight vector for the objectives $i \in N$, and $\sum_{i \in N} w_i = 1$. Since the non-negative linear combinations preserve the convexity, this is a convex optimization problem. For any positive weight vector w, any optimal solution of MORMP(w) is an efficient solution for MOP. In other words, any x^* that is optimal for MORMP(w) for some weight vector w, defines a hyperplane $H(w, f(x^*))$ that supports the feasible objective space at $f(x^*)$. We compute the gradient of the multi-objective function $f(x)$ with respect to column k is a vector of gradients of functions $f_i(x)$, $\nabla \boldsymbol{f}(x)_k = (\nabla f_{ki} : i \in N)$, as computed in

Equation (6.12). Let $\hat{\boldsymbol{\pi}}$ be the dual multipliers of RMP, we solve the following PSP model with a polynomial-time algorithm developed by [108].

$$\min_{k \in K \setminus K'} \boldsymbol{w}^{\intercal} \nabla \boldsymbol{f}(\hat{x})_k - \boldsymbol{D}(A^k)\, \hat{\boldsymbol{\pi}}. \tag{6.29}$$

The general idea of the proposed Pareto-based column generation in this paper is to explore the Pareto front during the CG procedure rather than optimizing a single objective. To this end, we first develop lower and upper bounds for the Pareto front. These concepts are similar to outer and inner approximations in traditional MCO techniques; however, we do not have the optimal objective values for each weight vector w during CG. Then, in each iteration, we assess the gap between these two bounds and generate one column based on CG-BCG algorithm with a pre-assigned weight vector or a new weight that reduces the maximum gap. We continue this process until the maximum distance between the lower and upper bounds becomes less than some desired value $\varepsilon > 0$. In the remainder of this section, we first discuss some fundamental properties of the problem in Section 6.6.2, describe the details of the algorithm in Section 6.6.3, and discuss the convergence of the algorithm in Section 6.6.4.

6.6.2 Fundamental properties

In this section, we develop lower and upper bounds for the Pareto front and investigate their properties that provide the foundation of our solution method. We form the upper bound from a subset of obtained nondominated points and derive the lower bound from the hyperplanes supporting the Pareto front.

Upper Pareto front

In each iteration of column generation for MORMP(w), we have a feasible solution rather than an optimal solution. Let $Y^F \subseteq Y^*_+$ denote all obtained solutions in the criterion space; we define the upper bound of the Pareto front inspired by Ehrgott and Gandibleux [49] as follows.

Definition 5 (Upper bound of the Pareto front)**.** *For the set of obtained solutions, point $y \in Y^F$ in the objective space is an upper bound of the Pareto front if there does not exist any other obtained point $y' \in Y^F$ such that $y' < y$. The set of these obtained points are called upper nondominated points, denoted by Y^N.*

Although the epigraph of the optimal Pareto front, Y^*_+, for convex MOP is a convex set [53, 107], the similar set for the upper bounds Y^N is not necessarily convex. We define the extreme

supported upper nondominated points inspired by multi-objective integer programming [97] in definition 6. Examples for these points are shown in Figure 6.2.

Definition 6 (Extreme supported upper nondominated point)**.** *The point $\hat{y} \in Y^N$ is an extreme supported upper nondominated (ESN) if it is an upper nondominated point and an extreme point of $conv(Y^N)$. We denote the set of ESN points by $Y^U \subseteq Y^N$.*

Definition 7 (Upper Pareto front)**.** *Let $conv(Y^U)$ indicate the convex hull of the obtained ESN points. We define the lower envelope of $conv(Y^U)$ as the upper Pareto front (UPF) and each point in this set as an upper Pareto point.*

Remark 1. *The upper Pareto front is the closest approximation to the Pareto front Y^* in the set of obtained nondominated points, Y^N.*

Proof. We have $Y^U \subseteq Y^N$ from Definition 6 and consequently $conv(Y^U) \subseteq conv(Y^N)$. Moreover, there is no $y' \in conv(Y^N)$ and $y \in conv(Y^U)$, that $y' < y$, regarding the definition of extreme upper nondominated point. Thus, the lower envelop of $conv(Y^U)$ is equal to the lower envelop of $conv(Y^N)$.

Furthermore, for each extreme supported nondominated point $\hat{y} \in Y^U$, there is at least one point y^* on the Pareto front Y^* that $y^* \leq \hat{y}$, with respect to Definition 3. Thus, the corresponding epigraph of the convex hull $conv(Y^U)$ as $Y^U_+ = conv(Y^U) + \mathbb{R}^n_+ \subseteq Y^*_+$. We conclude that any facet of $conv(Y^U)$ is an approximation for Y^*. Finally, the lower envelop of Y^U, equal to the lower envelop of Y^N, is the closest approximation to Y^*. ■

The corollary of this remark is that the set of extreme supported nondominated points Y^U is enough to approximate the Pareto front rather than all upper nondominated points.

Lower Pareto front

In this section, we first define a lower-bound for the Pareto front inspired by Ehrgott and Gandibleux [49]. Then, we obtain two supporting hyperplanes for the Pareto front as lower-bounds. Finally, we consider the upper envelope of obtained hyperplanes as the closest lower-bound to the Pareto front, so-called lower Pareto front (LPF).

Definition 8 (Lower bound of Pareto front)**.** *A set Γ in the objective space is a lower bound for the Pareto front Y^* if the epigraph of the Pareto front is a subset of the epigraph of the lower bound, $Y^*_+ \subseteq \Gamma_+$.*

We develop two types of hyperplanes supporting the Pareto front based on existing ESN points and the facets between ESN points.

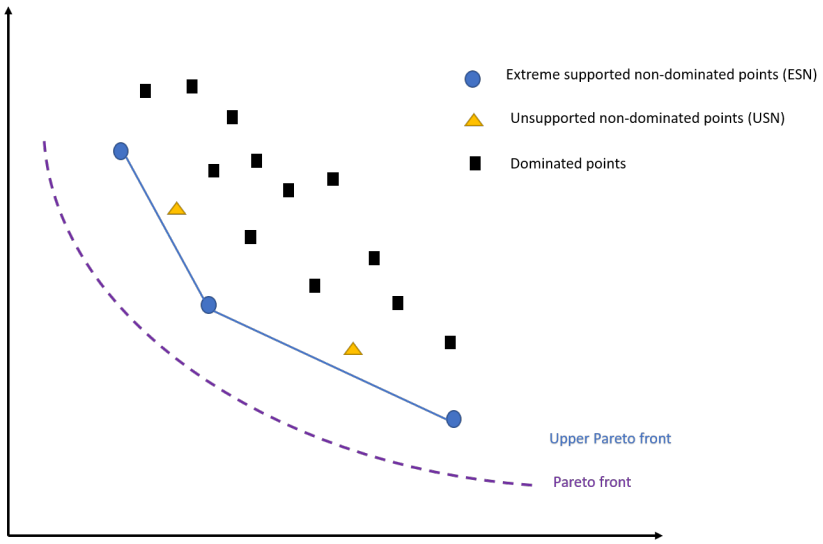

Figure 6.2 Pareto front and upper non-dominated points.

Lower bound based on existing ESN points: Each extreme supported nondominated point $\hat{y}_l \in Y^U$ is corresponding to a weighted-sum model (6.28) with a pre-assigned weight vector $\hat{w}_l$. Let $\hat{\gamma}_l$ indicate the lower bound of this model, as described in Section 6.5.2. A lower bound for the Pareto front Y^* based on point $\hat{\gamma}_l$ is obtained in lemma 3. This lower bound is schematically illustrated for the bi-objective space in Figure 6.3.

Lemma 3. *Let $\hat{y}_l$ be an ESN point in Y^U and $\hat{\gamma}_l$ be its lower bound based on normal vector $\hat{w}_l$. The hyperplane $H(\hat{w}_l, \hat{\gamma}_l)$ is a lower bound for the Pareto front denoted by Γ^l.*

Proof. It is shown by [107] that there is a point y_l^* on the Pareto front Y^* corresponding to the weight vector w_l. The hyperplane $H(\hat{w}_l, y_l^*)$ supports the feasible objective space at y_l^*, due to convexity of Y_+^*. Also, Lemma 1 provides that $\hat{\gamma}_l$ is a lower bound for function f corresponding to the normal vector $\hat{w}_l$, i.e., $\hat{w}_l^\top \hat{\gamma}_l \leq \hat{w}_l^\top y_l^*$. Thus, the hyperplane $H(\hat{w}_l, \hat{\gamma}_l)$, is parallel to tangent hyperplane to Y_+^* and include Y^*. Therefore this hyperplane is a lower bound for the Pareto front Y^*. ■

Lower bound based on the improvement estimation between ESN points: In addition to the existing ESN points and their corresponding weight vectors, we are also interested in the lower bound of PF based on non-assigned weight vectors between the ESN points in the criterion space. Let $\mathscr{P}$ indicate the lower envelope facets of the convex hull of Y^U. Each facet $\mathscr{P}_p \in \mathscr{P}$ includes n non-dominated points $\{\hat{y}_{p_1}, \cdots, \hat{y}_{p_n}\} \subseteq Y^U$; each point $\hat{y}_{p_l}$ has its corresponding weight vector $\hat{w}_{p_l}$ and lower bound $\hat{\gamma}_{p_l}$, respectively. We approximate

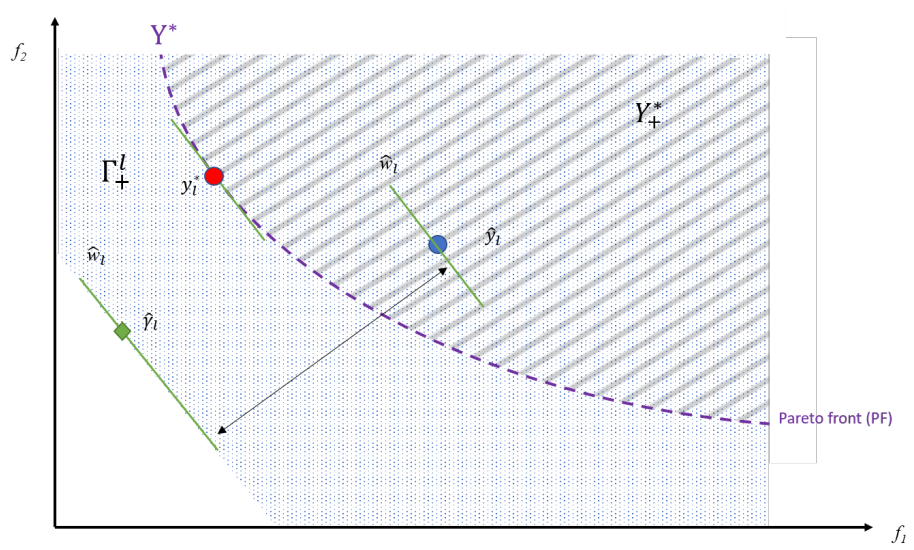

Figure 6.3 The lower bound of Pareto front based on existing ESN point $\hat{y}_l$ (Lemma 3).

a new lower bound for the Pareto front in Lemma 4. A sample of the this lower bound in a bi-objective model is shown in Figure 6.4.

Lemma 4. *Let $\overline{\gamma}_p$ indicate the intersection of hyperplanes $H(\hat{w}_{p_l}, \hat{\gamma}_{p_l})$ for all points $\hat{y}_{p_l} \in \mathscr{P}_p$ and $\overline{w}_p$ be any convex combination of weights vectors $\hat{w}_{p_l}$, $\Gamma^p = H(\overline{w}_p, \overline{\gamma}_p)$ is a lower bound for the Pareto front.*

Proof. As shown in Lemma 3, each lower bound hyperplane $H(\hat{w}_{p_l}, \hat{\gamma}_{p_l})$ is parallel to a supporting hyperplane for the Pareto front and $Y_+^* \subseteq \Gamma_+^l$. Any hyperplane passing through the intersection of these hyperplanes, $\overline{\gamma}_p$, with a convex combination of the pre-assigned weight vectors, $\overline{w}_p \in conv(\hat{w}_{p_1}, \cdots, \hat{w}_{p_n})$, is also supportive for $\Gamma_+^p = \cap_{l=p_1,\cdots,p_n} \Gamma_+^l$ and thus Y^*. Therefore, $H(\overline{w}_p, \overline{\gamma}_p)$ is a lower bound for the Pareto front. ■

The lower Pareto front: The upper envelope of hyperplanes $H(\hat{w}_l, \hat{\gamma}_l)$ for $\hat{y}_l \in Y^U$ and $H(\overline{w}_p, \overline{\gamma}_p)$ for $\mathscr{P}_p \in \mathscr{P}$, obtained from Lemmas 3 and 4, forms the lower Pareto front denoted by Γ^L as the closest lower bound to the Pareto front, see Figure 6.5. The upper envelope of a family of hyperplanes is a convex function. Thus, the LPF function is convex and its corresponding epigraph includes Y_+^*, i.e., $Y_+^* \subseteq \Gamma_+^L \equiv \{\cap_{l \in Y^U} \Gamma_+^l\} \cap \{\cap_{\mathscr{P}_p \in \mathscr{P}} \Gamma_+^p\}$.

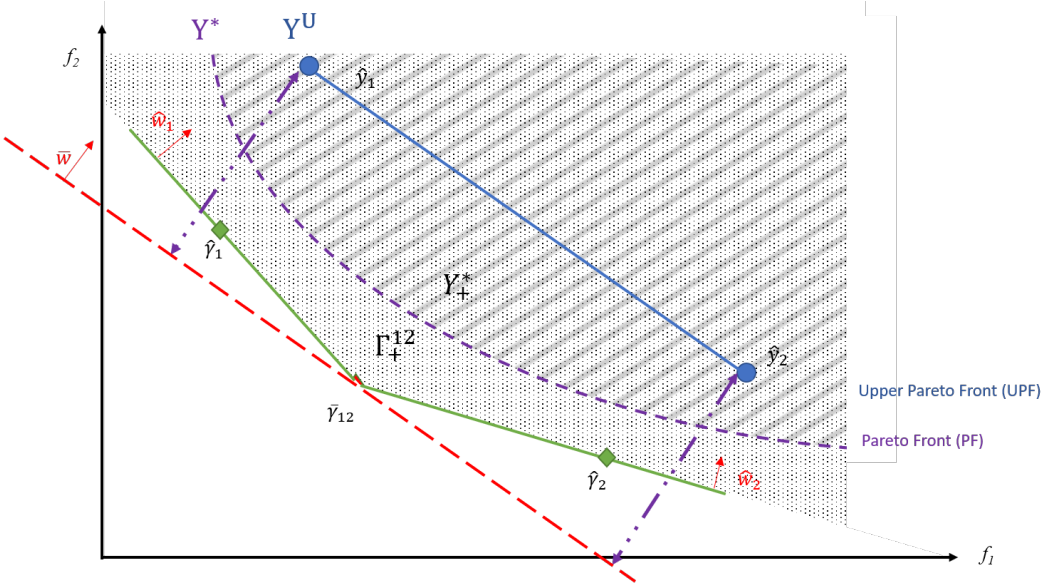

Figure 6.4 The lower bound of Pareto front based on new weight vector $\overline{w}$ between two ESN points (Lemma 4).

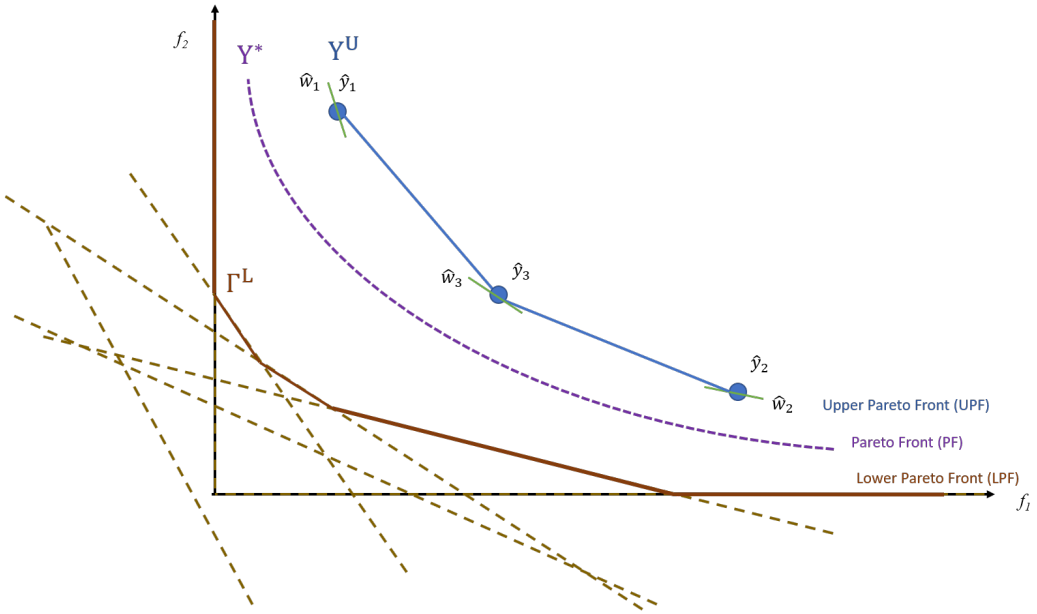

Figure 6.5 Lower Pareto front.

6.6.3 PCG algorithmic framework

In this section, we propose the details of PCG algorithm based on the bounds provided in Section 6.6.2. This is an iterative procedure, where during in each iteration, we approximate the Pareto front based on the UPF and assess an estimation of the potential improvement in UPF. We choose one of the existing points in UPF with its pre-assigned weight vector or consider a new weight vector for column generation and solve the proposed CG-BCG algorithm for the selected weight vector to generate one column and repeat the PCG procedure.

Step 1: Initialization

In the first step, PCG sequentially runs the CG-BCG algorithm, with a given number of iterations, for n extreme weight vectors corresponding to the objectives, i.e., $w = e^i$. This results in n initial nondominated points but do not necessarily lie on the Pareto front, because CG-BCG does not continue to optimality but provide efficient extreme points in the criterion space.

Step 2: Estimating the potential improvement of UPF

In each iteration, we assess the maximum potential improvement of obtained upper Pareto front based on the distance of UPF extreme points to lower bound hyperplanes proposed in Section 6.6.2.

$$\Delta d^1_{\hat{y}_l} = \psi(\hat{w}_l, \hat{y}_l, \hat{\gamma}_l). \tag{6.30}$$

This gap is due to non-optimal solution of CG in each iteration. The point with maximum potential improvement of set Y^U is as follows:

$$\tilde{y}_t = \arg\max_{\hat{y}_l \in Y^U_t} \Delta d^1_{\hat{y}_l}, \tag{6.31}$$

and the corresponding distance is denoted by $\Delta d^1_{\max} = \Delta d^1_{\tilde{y}_t}$.

Gap of UPF facets w.r.t. new weight vectors: For each $n-$subset facet $\mathscr{P}_p$ in the lower envelope of upper Pareto front, we can compute the maximum distance to the lower bound considering a non-assigned weight vector provided by Lemma 4. The set of lower envelope facets in 2-dimensional criterion space are adjacent pairs of UPF points, sorted in non-decreasing order of the first objective, i.e., $y^1_1 \leq y^1_2 \leq \cdots \leq y^1_l$. In higher dimensions, heuristic techniques are required to find efficient facets [38].

Based on Lemma 4, the new weight vector $\overline{w}_p$ is in the convex hull of the pre-assigned weight vectors of facet p as

$$\mathscr{W}_p = \{w \in \mathbb{R}^n | w = \sum_{i=1}^{n} \mu_i \hat{w}_{p_i},\ \sum_{i=1}^{n} \mu_i = 1,\ \mu_i \geq 0 \quad \forall i = 1, 2, \cdots, n\}. \tag{6.32}$$

Thus, the gap of facet p to the lower bound hyperplane Γ^p is

$$\Delta d_p^2 = \min_{i=1,\cdots,n} \psi(\overline{w}_p, \hat{y}_{p_i} \overline{\gamma}_p), \tag{6.33}$$

and the maximum improvement can be obtained with the following weight vector.

$$\overline{w}_p^{\max} = \arg\max_{w \in \mathscr{W}_p} \min_{\hat{y}_p \in p} \psi(w, \hat{y}_p, \overline{\gamma}_p). \tag{6.34}$$

This weight vector is optimal to minimize the gap of UPF to LPF in each iteration and decrease the maximum error of the algorithm. However, for more efficiency of the algorithm, specifically in initial iterations, we use two heuristics to find an efficient $\overline{w}_p$ instead of solving model (6.34). The first one is the normal vector of the facet p, if it is in set $\mathscr{W}_p$. The second heuristic is the mean vector $(1/n) \sum_{i=1}^{n} \hat{w}_{p_i}$.

The facet with maximum potential improvement of UPF is

$$\overline{p} = \arg\max_{p \in \mathscr{P}} \Delta d_p^2, \tag{6.35}$$

and its corresponding improvement is denoted by $\Delta d_{\max}^2 = \Delta d_{\overline{p}}^2$.

Step 3: Identifying the next weight vector for CG

Having the estimations of improvement for ESN points and UPF lower envelope facets, we identify the next weighted-sum problem for column generation. This choice depends on the maximum potential improvements in UPF and corresponds to the greedy strategy of maximizing the decrease and frequently used in multi-objective optimization [18].

$$\Delta d_{\max} = \max\{\Delta d_{\max}^1, \Delta d_{\max}^2\}. \tag{6.36}$$

If $\Delta d_{\max}^1 \geq \Delta d_{\max}^2$, it means the gap of existing point $\tilde{y}_t$ to LPF is greater than the similar gap for a new weight vector, and we set $y_t = \tilde{y}_t$ and $w_t = \tilde{w}_t$ for the next iteration of CG. Otherwise, the algorithm takes into account a new weight-vector $\overline{w}_{\overline{p}}$. In the latter, to have more efficiency, we use the set of columns in points of selected facet $\overline{p}$ as initial columns for the new point.

Step 4: column generation algorithm

In this step, we solve the CG-BCG algorithm proposed in Section 6.5 for the selected point y_t with the weight vector w_t and set K_t of columns. This algorithm continues until the obtained solution is optimal or a new extreme supported nondominated point in Y_t^U. The CG-BCG procedure does not necessarily generates a column in each iteration; thus, we continue the iterations to have at least one new column. This is required to update the lower bound as mentioned in Section 6.5.2.

Approximation error

We assess the approximation error based on the gap between UPF and LPF in each iteration of PCG as follows:

$$\mathscr{S}_t = \max_{y \in Y_t^U} \min_{\gamma \in \Gamma_t^L} \|y - \gamma\|. \tag{6.37}$$

If $\mathscr{S}_t$ becomes less than an acceptable error ε, we stop the PCG algorithm. In such a case, we say that the upper Pareto front is ε-closed to Pareto front Y^*. The obtained lower and upper Pareto fronts are finite number of hyperplanes, e.g., two piece-wise linear functions in 2D objective space, and we can easily find the maximum distance. It should be noted that $\Delta d_{\max}$ in Equation (6.36) considers the maximum potential improvement in the upper Pareto front while $\mathscr{S}$ evaluate the error of actual approximation of Pareto front based on UPF.

Pseudocode

The detailed pseudocode of the proposed algorithm for the Pareto-based column generation algorithm is shown in Algorithm 5.

6.6.4 Convergence of the PCG algorithm

In this section, we investigate the behaviour of PCG algorithm. We first show the convergence of a weighted-sum function and then analyze the convergence of PCG.

As discussed in Section 6.5.2, the single-objective function of the DAO problem converges to optimality. Let L_i denote the Lipschitz constant of function f_i and $\rho(L_i)$ be its corresponding convergence rate. The worst-case convergence rate of the weighted-sum function of n objectives is shown in Lemma 5.

Lemma 5. *Let $\overline{\rho}$ indicate the convergence rate of weighted function with a weight vector $\overline{w}$. We have $\overline{\rho} \leq \rho(L_{\max})$, where $L_{\max} = \max_{i=1,\cdots,n} L_i$.*

Algorithm 5 Pareto-based Column Generation (PCG)

Set $t \leftarrow 0$, $Y_t^U \leftarrow \emptyset$
for (i = 1 to n) **do** ▷ Initial extreme points
  $w_i \leftarrow e_i$, $K_i \leftarrow \{k_1\}$
  function $\hat{y}_i = \text{GCG}(K_i, w_i)$
  $Y_t^U = Y_t^U \cup \{\hat{y}_i\}$
  Update $\mathscr{S}_t$
while (no stop criteria and $\mathscr{S}_t > \varepsilon$) **do**
  Update the UPF set Y_t^U ▷ List of extreme supported points
  Update the lower envelope facets of UPF, $\mathscr{P}$
  $\Delta d^1_{\max} \leftarrow \max_{\hat{y}_l \in Y_t^U} \Delta d^1_{\hat{y}_l} \in Y_t^U$ ▷ The existing point with max LB gap
  $\Delta d^2_{\max} \leftarrow \max_{p \in \mathscr{P}} \Delta d^2_p$
  if $\Delta d^1_{\max} \geq \Delta d^2_{\max}$ **then**
    $\tilde{y}_t \leftarrow \arg\max_{\hat{y}_l \in Y_t^U} \Delta d^1_{\hat{y}_l} \in Y_t^U$ ▷ The existing point with max LB gap
    $y_t \leftarrow \tilde{y}_t, w_t \leftarrow \tilde{w}_t, K_t \leftarrow \tilde{K}_t$
  else
    $\overline{P} \leftarrow \arg\max_{p \in \mathscr{P}} \Delta d^2_p$
    $\overline{y}_t \leftarrow \arg\min_{\hat{y}_l \in Y_t^U} \psi(\overline{w}_{\overline{P}}, \hat{y}_l, \overline{y}_{\overline{P}})$ ▷ The closest existing point for the new weight with max LB gap
    $y_t \leftarrow \overline{y}_t, w_t \leftarrow \overline{w}_t, K_t \leftarrow \overline{K}_{\overline{y}_t}$
  function $\hat{y}_t = \text{GG-BCG}(K_t, w_t)$
  $Y_t^U = Y_t^U \cup \{\hat{y}_t\}$
  Update $\mathscr{S}_t$
Return Y^U

Proof. By corollary 1 of Appendix C, the Lipschitz constant of weighted-sum function f is $\overline{L} = \sum_{i=1}^{n} w_i L_i$. We have also $\sum_{i=1}^{n} \overline{w}_i = 1$, thus $\overline{L} \leq L_{\max}$ and consequently $\rho(\overline{L}) \leq \rho(L_{\max})$. ■

Therefore, each point $\hat{y}$ on UPF with weight-vector $\hat{w}$ individually converges to its optimal value using CG-BCG. The optimal vector $\hat{y}^* = f(\hat{x}^*)$ is a Pareto point on the Pareto front Y^* based on Karush-Kahn-Tucker (KKT) conditions as:

$$\sum_{i=1}^{n} \hat{w}_i \nabla f_i(\hat{x}^*) = 0. \tag{6.38}$$

In the next step, we define the ε-closeness of UPF and LPF, based on the gap $\mathscr{S}$ as follows.

Definition 9. *Y_t^U is called ε-closed to Pareto front Y^* if $\mathscr{S}_t < \varepsilon$.*

As the PCG algorithm proceeds from iteration t to $t+1$, if an extreme supported nondominated point $\hat{y}$ is chosen as the the point with maximum distance to LPF, it becomes closer to its optimal value, and consequently to the Pareto front, by convergence rate $\rho(\hat{L})$ which is less than or equal to $\rho(L_{\max})$. If a new point $\overline{y}_t$ with a new weight vector in the criterion space is selected by solving model (6.34), its convergence rate to PF is $\overline{\rho} \leq \rho(L_{\max})$. Thus, the gap $\mathscr{S}_t$ between LPF and UPF is non-increasing due to the way it is defined and it is guaranteed that we have a new ESN point and a strict improvement, even by a little, in UPF at each iteration as explained in Section 6.6.3. Therefore, the algorithm converges ε-closed to PF by large number of iterations as it is numerically shown in Section 6.7.3. If we do not solve model (6.34) to optimality and employ heuristics to find the maximum potential improvement in lower envelope facets of UPF, the algorithm may go through a sequence of degenerate steps. In this case, using an appropriate anti-cycling rule, avoiding repetitive weight vectors will prevent the algorithm from cycling.

6.7 Computational results

We implemented the algorithms in C++ and the computational experiments were run on a 2.1 GHz Intel E5-2683 v4 Broadwell Linux workstation. To compare the proposed methods to a commercial solver, we used IBM ILOG CPLEX 12.6.2 for the mathematical models.

6.7.1 Data and benchmark

We evaluate the efficiency of the proposed algorithms on two clinical cases from the CORT dataset [40]: a prostate (PR) patient and a head-and-neck (H&N) patient. The prostate case

has two target volumes, PTV-56 and PTV-68, and five organs at risk: the bladder, rectum, left and right femoral heads, and body. The head-and-neck case has three target volumes, PTV-56, PTV-63, and PTV-70, and nine organs at risk: the brainstem, spinal cord, right and left parotids, cerrebelum, lips, larynx,chiasma, and external. The doses of 68 Gy in the prostate case and 70 Gy in the head-and-neck case were prescribed in 2 Gy per fraction. The parameters for the two cases are listed in Table 6.1. As one can see, there are more voxels in the prostate case and more beamlets in the head-and-neck case. From the mathematical point of view, the former has more constraints, and the latter has more potential columns. Therefore, the algorithm is analyzed in terms of both aspects. Besides, the number of voxels at each structure and the percentage of each structure in the model are reported in Table 6.2.

Table 6.1 Parameters of the CORT prostate and Head-and-neck cases

	P	H&N
Total # beamlets	25,404	203,765
Beamlet size (cm)	1×1	0.5×0.5
Voxel resolution (mm)	3, 3, 3	3, 3, 5
# Target voxels	9,491	25,388
# Body voxels	690,373	251,893
Prescribed dose (Gy)	68	70
# Fractions	34	35

Table 6.2 Number of voxels in the model

P			H&N		
structure	# voxels	(%) voxels in the model	structure	# voxels	(%) voxels in the model
PTV-56	9,491	100	PTV-56	2,104	100
PTV-68	6,770	100	PTV-63	22,682	100
Rectum	1,764	50	PTV-70	5,768	100
Bladder	11,596	50	Spinal cord	380	100
Rt. Femoral head	5,974	20	Brain stem	423	100
Lt. Femoral head	5,957	20	Lt. Parotid	434	100
Body	690,373	1.1	Rt. Parotid	612	100
			Cerebellum	2,631	100
			Lips	140	100
			Larynx	139	100
			Chiasma	37	100
			External	251,893	1

6.7.2 CG-BCG vs. CG-FW and CPLEX

In this section, we compare the efficiency of CG-based blended conditional Gradient and CG-based Frank-Wolfe with CPLEX solver. We consider three weight vectors for each case to evaluate the algorithms. The details of weights are reported in Table 6.3. In these scenarios, w_1 is more biased to target volumes and w_2 and w_3 are more biased to the Bladder and Rectum, respectively. The results for weight vectors w_1, w_2, and w_3 of PR and H&N cases are summarized in Tables 6.4 - 6.9. In each row, we compare the objective values, number of generated columns, and number of non-zero columns, in the same levels of computational time, 3, 10, 30, 60, 120, and 180 seconds. The computational time for PSP and RMP subproblems are also reported in each method.

As mentioned earlier, in the standard column generation, we solve the restricted master problem to optimality in each iteration. In CG with Frank-Wolfe, FW does not solve RMP to optimality but still generates one column per iteration. Finally, CG-BCG neither solves RMP to optimality nor necessarily generates a new column in each iteration, only if required to improve the solution. In all instances, we observe that CPLEX takes much more time for RMP, while the final objective value is greater than CG-BCG. In FW, as expected, the computational time of the search algorithm was less specifically in initial iterations. However, PSP was solved in every iteration and a new column was added to the model. This significantly increases the dimension of the solution space and results in high computational time. CG-BCG presents better results in terms of both the computational time and objective value in all instances for both cases. The gap after three minutes of computational time between the objective value of CG-BCG and the lower bound in the prostate case is about 8%, while this value is about 15% for CG-FW and 23% for CPLEX, respectively. Therefore, CG-BCG is, on average, 13.96% more efficient than CPLEX. In the head-and-neck case, the objective value within the same amount of time in CG-BCG is, on average, 6.56% and 57.15% better than CG-FW and CPLEX, respectively. The gap in H&N is significantly more because the beam is larger and there are much more potential apertures.

Table 6.3 The balanced scenarios for the weight-vector

P				H&N			
structure	w_1	w_2	w_3	structure	w_1	w_2	w_3
PTV-56	0.2	0.1	0.1	PTV-56	0.06	0.1	0.04
PTV-68	0.49	0.49	0.49	PTV-63	0.12	0.2	0.08
Rectum	0.1	0.01	0.37	PTV-70	0.23	0.3	0.2
Bladder	0.1	0.37	0.01	Spinal cord	0.1	0.08	0.13
Rt. Femoral head	0.05	0.01	0.01	Brain stem	0.1	0.08	0.14
Lt. Femoral head	0.05	0.01	0.01	Lt. Parotid	0.07	0.04	0.03
Body	0.01	0.01	0.01	Rt. Parotid	0.07	0.04	0.09
				Cerebellum	0.05	0.03	0.07
				Lips	0.07	0.04	0.1
				Larynx	0.07	0.04	0.1
				Chiasma	0.05	0.04	0.07
				External	0.01	0.01	0.01

Table 6.4 Results of CPLEX, CG-FW, and CG-BCG for the weight vector w_1 in the Prostate case

No.	CPLEX						CG-FW						CG-BCG						
	Pricing Time (sec)	RMP Time (sec)	Total Time (sec)	Obj. value	# total col.	# non-zero col.	Pricing Time (sec)	RMP Time (sec)	Total Time (sec)	Obj. value	# total col.	# non-zero col.	Pricing Time (sec)	RMP Time (sec)	Total Time (sec)	Obj. value	# total col.	# non-zero col.	LB
1	0.07	3.53	3.60	1007.69	4	4	1.63	1.38	3.01	379.25	118	118	1.17	3.84	5.01	266.84	78	56	0.00
2	0.16	11.33	11.49	683.53	8	8	4.12	5.92	10.04	307.49	302	302	1.71	8.29	10.00	249.18	110	70	109.73
3	0.31	30.47	30.78	467.02	17	17	8.62	21.38	30.00	276.73	629	629	2.29	27.72	30.01	240.33	157	93	171.36
4	0.51	60.89	61.40	360.84	28	27	13.12	46.93	60.05	265.55	954	954	2.88	57.14	60.02	236.28	158	115	200.44
5	0.78	120.21	120.99	299.78	45	27	19.50	100.59	120.09	257.47	1414	1414	3.40	116.65	120.05	234.46	232	128	206.67
6	0.97	180.45	181.42	279.67	58	43	24.68	155.41	180.09	253.69	1776	1776	3.88	176.14	180.02	233.45	263	141	215.36

Table 6.5 Results of CPLEX, CG-FW, and CG-BCG for the weight vector w_2 in the Prostate case

No.	CPLEX						CG-FW						CG-BCG						
	Pricing Time (sec)	RMP Time (sec)	Total Time (sec)	Obj. value	# total col.	# non-zero col.	Pricing Time (sec)	RMP Time (sec)	Total Time (sec)	Obj. value	# total col.	# non-zero col.	Pricing Time (sec)	RMP Time (sec)	Total Time (sec)	Obj. value	# total col.	# non-zero col.	LB
1	0.09	3.75	3.84	1681.34	4	4	1.51	1.5	3.01	642.63	115	115	0.78	2.24	3.02	505.10	47	42	0
2	0.17	10.88	11.05	860.22	8	7	3.82	6.19	10.01	531.73	296	296	1.41	8.60	10.01	457.19	89	66	269.11
3	0.33	30.23	30.56	629.69	18	16	8.10	21.96	30.06	491.16	632	632	2.01	27.99	30.00	445.39	130	85	359.45
4	0.47	60.36	60.88	531.86	29	26	12.63	47.41	60.04	476.39	977	977	2.47	57.53	60.00	442.55	160	103	389.86
5	1.04	120.47	121.51	494.24	44	38	18.84	101.26	120.10	466.10	1459	1459	3.10	116.90	120.00	439.76	200	130	407.451
6	0.94	183.17	184.11	478.86	56	44	23.72	156.36	180.08	461.31	1838	1838	3.25	176.77	180.02	439.04	207	1.22	407.451

Table 6.6 Results of CPLEX, CG-FW, and CG-BCG for the weight vector w_3 in the Prostate case

No.	CPLEX						CG-FW						CG-BCG						
	Pricing Time (sec)	RMP Time (sec)	Total Time (sec)	Obj. value	# total col.	# non-zero col.	Pricing Time (sec)	RMP Time (sec)	Total Time (sec)	Obj. value	# total col.	# non-zero col.	Pricing Time (sec)	RMP Time (sec)	Total Time (sec)	Obj. value	# total col.	# non-zero col.	LB
1	0.06	3.44	3.50	1361.08	4	4	1.6	1.41	3.01	428.38	119	119	0.74	2.26	3.00	305.96	66	51	55.81
2	0.11	9.95	10.06	902.71	8	7	4.08	5.92	10.02	341.85	305	305	1.38	8.62	10.00	285.31	127	89	220.51
3	0.22	31.34	31.56	481.43	17	15	8.61	21.45	30.06	313.64	631	631	1.91	28.10	30.01	279.15	176	112	241.74
4	0.33	60.66	60.99	377.29	28	25	14.17	45.89	60.06	303.09	961	961	2.24	57.76	60.00	277.08	205	118	248.63
5	0.51	121.67	122.18	327.54	45	36	19.61	100.42	120.03	295.54	1429	1429	2.74	117.27	120.01	275.47	247	137	259.60
6	0.64	182.91	183.55	310.86	58	45	24.65	155.37	180.02	292.03	1795	1795	2.98	177.03	180.01	275.08	261	137	259.60

Table 6.7 Results of CPLEX, CG-FW, and CG-BCG for the weight vector w_1 in the H&N case

No.	CPLEX						CG-FW						CG-BCG						
	Pricing Time (sec)	RMP Time (sec)	Total Time (sec)	Obj. value	# total col.	# non-zero col.	Pricing Time (sec)	RMP Time (sec)	Total Time (sec)	Obj. value	# total col.	# non-zero col.	Pricing Time (sec)	RMP Time (sec)	Total Time (sec)	Obj. value	# total col.	# non-zero col.	LB
1	0.27	2.75	3.03	3015.90	2	2	2.65	0.38	3.03	1431.86	29	29	2.66	0.46	3.12	1044.18	17	17	0
2	0.59	13.53	14.12	1919.88	4	4	8.27	1.84	10.11	791.78	94	94	7.01	3.07	10.08	652.52	40	36	0
3	0.96	31.75	32.71	1539.10	6	6	21.92	8.12	30.04	639.24	255	255	15.71	14.32	30.03	586.58	107	89	0
4	1.48	65.33	66.81	1135.27	9	9	38.24	21.89	60.13	615.94	449	449	23.63	36.37	60.00	572.26	168	141	239.20
5	2.13	131.49	133.62	920.81	13	12	63.63	56.55	120.08	602.91	750	750	36.15	84.02	120.17	564.58	273	225	391.25
6	2.45	177.13	179.58	875.21	15	14	14.16	96.07	180.23	597.09	994	994	38.66	141.42	180.08	562.64	294	234	397.41

Table 6.8 Results of CPLEX, CG-FW, and CG-BCG for the weight vector w_2 in the H&N case

No.	CPLEX						CG-FW						CG-BCG						
	Pricing Time (sec)	RMP Time (sec)	Total Time (sec)	Obj. value	# total col.	# non-zero col.	Pricing Time (sec)	RMP Time (sec)	Total Time (sec)	Obj. value	# total col.	# non-zero col.	Pricing Time (sec)	RMP Time (sec)	Total Time (sec)	Obj. value	# total col.	# non-zero col.	LB
1	0.22	2.83	3.06	2587.73	2	2	2.73	0.40	3.13	1243.63	30	30	2.80	0.28	3.08	1199.66	12	12	0
2	0.46	12.99	13.45	1573.62	4	4	8.21	1.80	10.02	769.62	93	93	8.10	2.07	10.16	687.15	36	34	0
3	0.83	42.46	43.29	1274.68	7	7	21.86	8.26	30.12	629.95	253	253	18.76	11.36	30.12	578.50	82	71	0
4	1.06	69.39	70.45	1142.77	9	9	38.10	22.01	60.10	601.96	445	445	32.66	27.39	60.06	553.35	143	122	53.86
5	1.42	123.12	124.54	939.55	12	12	63.50	56.92	120.42	586.35	746	746	48.82	71.32	120.14	541.80	228	189	258.22
6	1.78	180.97	182.75	840.24	15	14	83.92	96.09	180.00	579.46	988	988	55.33	124.74	180.07	538.63	261	210	312.61

Table 6.9 Results of CPLEX, CG-FW, and CG-BCG for the weight vector w_3 in the H&N case

No.	CPLEX						CG-FW						CG-BCG						
	Pricing Time (sec)	RMP Time (sec)	Total Time (sec)	Obj. value	# total col.	# non-zero col.	Pricing Time (sec)	RMP Time (sec)	Total Time (sec)	Obj. value	# total col.	# non-zero col.	Pricing Time (sec)	RMP Time (sec)	Total Time (sec)	Obj. value	# total col.	# non-zero col.	LB
1	0.33	2.53	2.86	2716.20	2	2	2.71	0.35	3.06	1306.46	26	26	2.61	0.45	3.06	872.77	17	17	0.00
2	0.62	11.79	12.41	1763.86	4	4	8.34	1.72	10.06	756.33	86	86	7.13	2.96	10.10	612.04	48	42	0.00
3	1.00	28.32	29.32	1428.38	6	6	22.33	7.72	30.04	608.60	234	234	15.39	14.63	30.03	556.53	109	93	0.00
4	1.44	68.29	69.72	1166.59	9	9	39.60	20.41	60.01	583.29	422	422	24.05	35.96	60.02	541.78	173	139	195.99
5	2.02	122.65	124.67	971.81	12	11	67.19	52.84	120.03	569.71	705	705	30.46	89.57	120.03	535.19	228	177	278.22
6	2.59	190.03	192.62	850.54	15	14	90.19	89.93	180.12	563.73	933	933	37.54	142.47	180.01	531.95	292	227	362.16

6.7.3 Pareto approximation results

We implemented the PCG algorithm for the Prostate case with two objectives, the penalty function for the bladder and PTV-68. The results for 1000 iterations are shown in Table 6.10. In this table, column `# total apertures` lists the total number of apertures generated during the algorithm, `# ESN` shows the total number of extreme upper non-dominated points on the approximated Pareto front, `# non-extreme non-dominated points` indicates the total number of upper non-dominated points, `comp. time (min)` shows the cumulative computational time in minutes, and `gap` shows the approximation error of upper Pareto front to the lower Pareto front as explained in Section 6.6.3. Although the non-extreme points do not lie on the upper Pareto front; this number shows the flexibility of the technician to evaluate similar treatment plans to extreme points with respect to other clinical features. Moreover, the lower and upper Pareto fronts for the Prostate case obtained after 100, 250, 500, and 1000 iterations are shown in Figure 6.6.

As expected, the approximation error has a decreasing trend and the Pareto front is well-approximated by upper Pareto front. In this case, it seems 500 iterations is enough to achieve acceptable Pareto frontier with reasonable computational time. This validates the efficiency of the algorithm with large number of non-dominated points, despite relatively small number of generated columns. In practice, each point is a deliverable treatment plan with assigned apertures and useful for the technician.

For the head-and-neck case, the target PTV-70 is close to the spinal cord, and thus, we chose these two critical structures. The results for 1000 iterations are shown in Table 6.11. Also, the comparison for 100, 250, 500, and 1000 iterations of the obtained upper Pareto fronts in the head-and-neck case are shown in Figure 6.7. In this case, the objective values are close to zero and the obtained lower bounds are negative, while a lower bound of the problem is zero, due to non-negative dose intensities and the quadratic formulation of the objective function. Therefore, the lower Pareto front is the horizontal and vertical axes of the bi-objective space. We observe less number of non-dominated points in this case but the UPF is close enough to LPF after 500 iterations.

6.8 Conclusion

In this paper, we first improved the efficiency of the column generation-based method for direct aperture optimization, by integrating the blended conditional gradient algorithm, as a new first-order optimization technique, to solve the restricted master model. This algorithm does not find the optimal solution of RMP in each iteration of CG, but balances between

Table 6.10 Results of PCG for the prostate case with two objectives of PTV-68 and bladder

Iter.	# total apertures	# ESN	# non-extreme non-dominated	comp. time (min)	gap
1	31	3	1	0.97	2178.1
10	40	6	2	1.36	1269.97
25	55	7	4	1.93	1095.64
50	80	7	2	3.13	1004.72
100	130	8	7	5.79	779.14
250	280	13	18	11.50	373.19
500	530	22	61	34.84	204.55
800	830	31	112	62.14	147.07
1000	1030	33	160	90.42	107.89

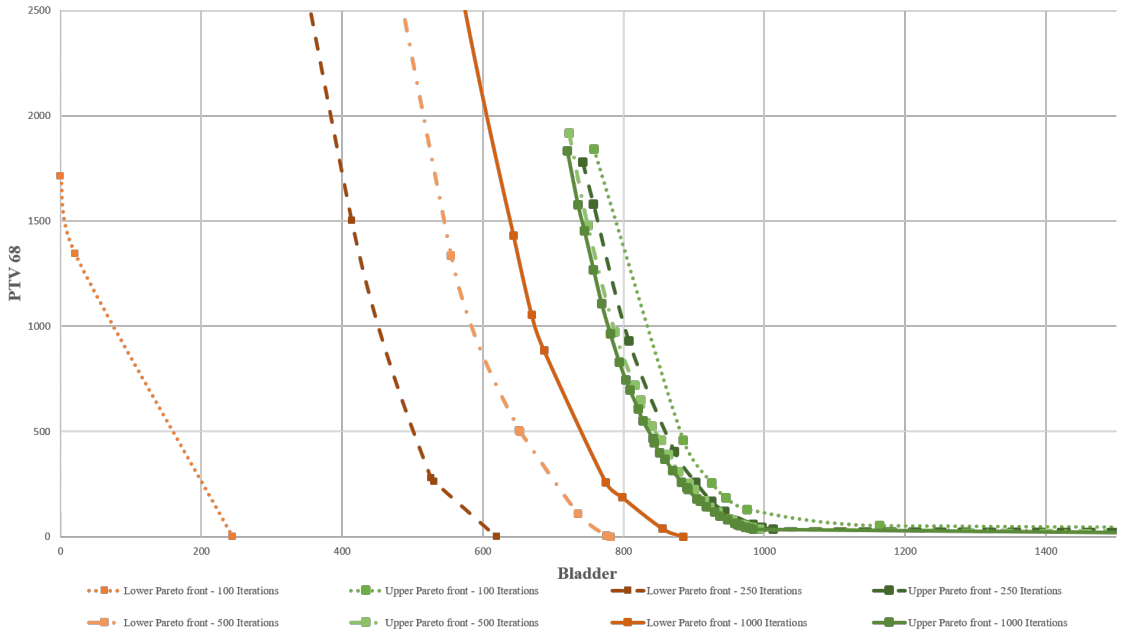

Figure 6.6 The comparison of obtained upper Pareto fronts of PCG for the prostate case after 100, 250, 500 and 1000 iterations.

Table 6.11 Results of PCG for the head-and-neck case with two objectives of PTV-70 and spinal cord

Iter.	# total apertures	# ESN	# non-extreme non-dominated	comp. time (min)	gap
1	31	3	1	0.97	2178.1
10	40	6	2	1.36	1269.97
25	55	7	4	1.93	1095.64
50	80	7	2	3.13	1004.72
100	130	8	7	5.79	779.14
250	280	13	18	11.50	373.19
500	530	22	61	34.84	204.55
800	830	31	112	62.14	147.07
1000	1030	33	160	90.42	107.89

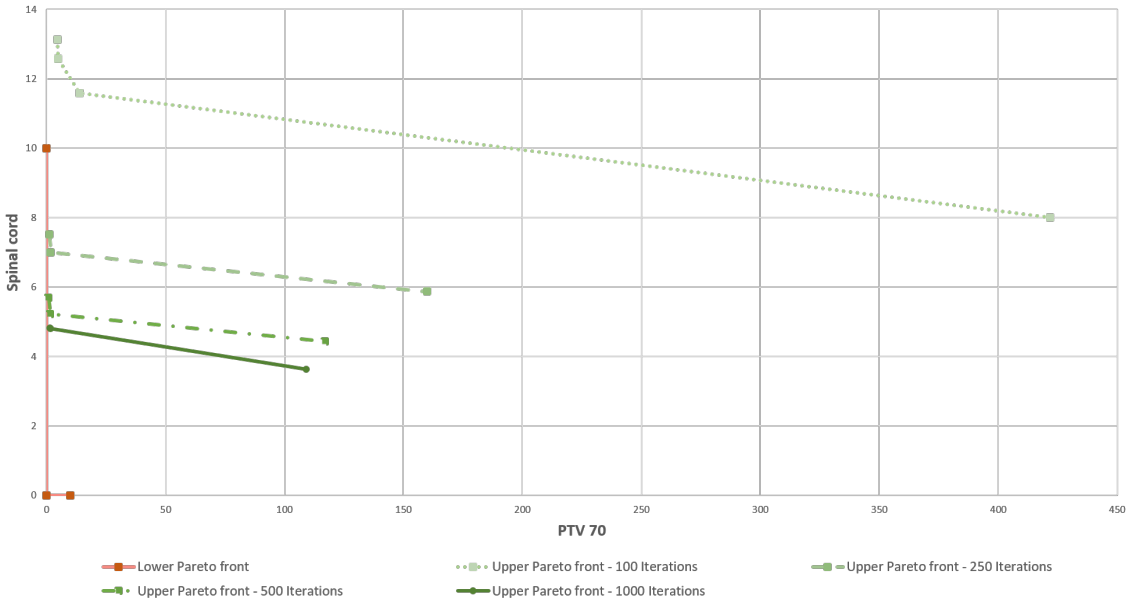

Figure 6.7 The comparison of obtained upper Pareto fronts of PCG for the head-and-neck case after 100, 250, 500 and 1000 iterations.

searching in the solution space of RMP and generating new columns. As a result, a smaller number of inner iterations is usually needed to solve each RMP and the running times per outer iteration is reduced. Another advantage of CG-BCG is that the solutions are close-to-optimality, but at the same time not far from the central trajectory in the dual feasible set. Therefore, a more stable column generation strategy is likely to be obtained. This method outperforms CPLEX in terms of both solution quality and time efficiency.

We then extended the column generation algorithm to approximate the Pareto frontier for contradictory objectives in DAO treatment planning. To this end, we developed lower and upper bounds for the Pareto front and assess the potential improvement of the upper bound with the pre-assigned and new weight vectors. In each iteration, the algorithm generates a column which is most beneficial to reduce the maximum gap of two bounds and improves the entire Pareto front. This technique dynamically adds the required weight vectors during the algorithm.

For two prostate and head-and-neck cases with contradictory objectives between target coverage and normal tissue sparing, the results demonstrate numerically the decreasing trend of the approximation error between lower and upper bounds of the Pareto front and achieving acceptable plans in reasonable time. This method is also useful for the technician to analyze the details of obtained deliverable plans at each iteration in terms of other clinical criteria and choose the most appropriate plan. In addition, the user can interactively work with the points that the physician prefers and navigate between specific weight vectors with respect to user experience or observation during the procedure.

For the future work, there are still many challenges to be considered. We can evaluate other clinical objectives and also in higher dimensions. Also, this technique is useful for other classes of problems requiring both column generation and multi-objective optimization to provide acceptable solutions in practice.

CHAPTER 7 GENERAL DISCUSSION

In radiation therapy, IMRT is the most widely used technique around the world and VMAT is an advanced rotational format of IMRT. Minimizing the treatment time to reduce the patient discomfort and uncertainty of the treatment, obtaining clinically admissible plans, and finding the trade-off between contradictory structures are among the main challenges of treatment planning in these technologies.

In this dissertation, we studied the applications of column generation in IMRT and VMAT treatment planning to improve the efficiency of the algorithms in terms of computational time, treatment time, and quality of the plans. In Chapter 4, we proposed a column-and-row generation method to optimize the solution quality and the treatment time in VMAT, simultaneously; while, in Chapter 5, we take advantage of the iterative procedure of column generation to adjust the objective function of the proposed mathematical model based on nonlinear clinical criteria. From a practical point of view, the model proposed in the first article is beneficial to decrease delivery time and consequently discomfort of the patient; while the technique employed in the second article makes the VMAT treatment planning more robust to initial parameters and decreases the trial-and-errors to find clinically acceptable plans. The method in Chapter 5 is also compared to commercial treatment planning system, and the results validated the efficiency of of the proposed algorithm. However, our approach in Chapter 6 is more focused on developing new methodologies in column generation, based on their application for DAO problem in IMRT. First, a new solution method is proposed to solve the master model, generating strong columns without solving to optimality in each generation. In Chapters 4 and 5, we use CPLEX to solve the master model, and we show that the proposed algorithm in Chapter 6 outperforms CPLEX. Second, we propose a multi-objective column generation method, which finds a set of nondominated solutions, approximating the Pareto frontier. To the best of our knowledge, this is the first algorithm which dynamically navigates the entire Pareto front during the column generation iterations. We designed these two algorithms for the multi-criteria IMRT treatment planning problem; however, both methods can be effective for general large-scale convex optimization problems with similar structure.

CHAPTER 8 CONCLUSION AND RECOMMENDATION

In this dissertation, we studied the application of column generation technique in IMRT and VMAT treatment planning problems. In the following, we first present a summary of the contributions achieved by this dissertation. Then we highlight its limitations and possible future research directions.

8.1 Contributions

In the first essay of this dissertation, we addressed the simultaneous delivery time and aperture shape optimization for the VMAT treatment planning. Most of previous works in the literature take into account constant delivery time or minimize the delivery time after fixing the MLC shapes at the final step. In this study, the delivery time is integrated into the column generation algorithm to simultaneously optimize the aperture shapes, dose rates, gantry speeds, and delivery time. To this end, we developed a column-and-row generation algorithm embedded in a greedy heuristic. In the master model, in addition to voxel-based dose distribution constraints, the columns are also linked to delivery time constraints. Another contribution of the proposed approach when compared to papers is that we can consider most of the MLC leaf-movement constraints in the PSP rather than the RMP. Then, in this approach, it is not required to check the feasibility of all adjacent control-points and regenerate new columns in the master model, which makes the algorithm more efficient. Moreover, this method can easily handle both bidirectional and unidirectional leaf motions according to the machine capabilities, which makes the model more flexible in practice. In addition to the contributions in the model, we also proposed an aggregation algorithm inspired by the K-means technique in clustering to reduce the number of voxel-based constraints. This aggregation takes about 11 seconds; but greatly reduces the number of constraints with a negligible effect on the treatment quality. The results on a prostate cancer benchmark demonstrate the efficiency of our model to decrease the delivery time of the plan to the patient even though its priority is considered much less in comparison to the the clinical objectives.

As the second essay of this dissertation, we take advantage of iterative procedure of column generation to automatically handle dose-volume criteria in VMAT treatment planning. To this end, we adjust the weight of structures and voxels based on DVH criteria during iterations of column generation. This approach increases the efficiency of the algorithm and consequently decreases the human interventions. The results on a prostate and a head-and-neck case shows significant improvement to achieve clinically acceptable plans. In the prostate

case, the proposed algorithm found 100% admissible plans for instances with randomly-generated weights. The results in the head-and-neck case confirm this conclusion. In this case, it finds acceptable plans for 93.3% of instances. Moreover, to have an idea of the efficiency of the proposed algorithm in comparison to a commercial software, a treatment plan is designed by an expert for the prostate case with Pinnacle software. The computational time in the commercial software was about 20 minutes, while the process of the proposed algorithm in this project is less, 7.18 minutes. The quality of the DVH diagrams, especially for the healthy tissues is significantly better in the proposed method.

In the third essay, we addressed the DAO treatment planning and improved the efficiency of the algorithm integrating a new first-order gradient algorithm, BCG, to column generation. Also, we developed a lower-bound for the single-objective problem at each iteration of the algorithm. The proposed method outperformed the classic Frank-Wolfe method and also CPLEX solver, significantly. For two prostate and head-and-neck cases in several weight sets, in average, the gap of the final solution in CG-BCG to the lower bound of the problem was three times better in comparison to CPLEX. Another contribution of this was on extending the column generation technique to the multi-objective framework which approximate the Pareto frontier for contradictory objectives. In this method, a column is generated to improve the entire Pareto set rather than a single-objective solution. To this end, we developed lower and upper bounds for the Pareto front and assessed the existing and also potential improvements of the weight vectors in each iteration, and then generate a column that reduces the maximum gap of two bounds. Our technique has an advantage over other algorithms that dynamically adds weight vectors and obtains deliverable treatment plans. It is shown that the proposed algorithm converges to the Pareto front for large number of iterations. The results demonstrate numerically the decreasing trend of the maximum distance between lower and upper bounds of the Pareto frontier in reasonable time.

8.2 Limitations and future research directions

For the future works, we believe there are still many challenges which can be considered in the first essay. To decrease the computational time in the master model and improve the voxel sampling, a dynamic voxel aggregation could be developed. In this extension, the clusters dynamically update during the column generation iterations and fewer voxels would be required in the master model to achieve acceptable plans. In addition, we have noted that the columns generated at each iteration from different sectors are not disjoint and have similar effects; this could be investigated in future research. For another future research, we recommend to consider a wide range of lengths instead of fixed and equal arc segments in the model.

In integrating DVH criteria in VMAT treatment planning studied in the second essay, more analysis on a wide range of patients is required to validate the efficiency of the algorithm in practice in comparison to the existing commercial software. Moreover, we considered a finite number and pre-determined DVH criteria in the treatment evaluation. Considering the whole DVH curve is interesting and can be the subject of future research.

The proposed multi-objective column generation approach in the third essay was evaluated in the bi-objective space. Although the fundamentals of the algorithm are the same for the cases with more than two objectives, the algorithm would be more complicated in terms of computational aspects especially to find the lower bound for the Pareto frontier. Moreover, this technique is useful for other classes of problems requiring both column generation and multi-objective optimization to provide acceptable solutions in practice.

REFERENCES

[1] Varian linear accelerator. `https://www.varian.com/ch/about-varian/newsroom/image-gallery/inside-varian-linear-accelerator`. Accessed: 2019-06-20.

[2] Benefits of third generation VMAT radiation technology for IGRT, IMRT, SRS, SRT and SBRT with arc, 2013. URL `http://www.dhrc.in/16-Feb-2011.html`.

[3] Warren P Adams and Hanif D Sherali. Linearization strategies for a class of zero-one mixed integer programming problems. *Operations Research*, 38(2):217–226, 1990.

[4] Ravindra K. Ahuja, Thomas L Magnanti, and James B Orlin. *Network flows: theory, algorithms, and applications*. Prentice hall, 1993.

[5] Kerem Akartunalı, Vicky Mak-Hau, and Thu Tran. A unified mixed-integer programming model for simultaneous fluence weight and aperture optimization in VMAT, tomotherapy, and cyberknife. *Computers and Operations Research*, 56:134–150, 2015.

[6] Markus Alber and Rembert Reemtsen. Intensity modulated radiotherapy treatment planning by use of a barrier-penalty multiplier method. *Optimization Methods and Software*, 22(3):391–411, 2007.

[7] Dionne M. Aleman, Arvind Kumar, Ravindra K. Ahuja, H. Edwin Romeijn, and James F. Dempsey. Neighborhood search approaches to beam orientation optimization in intensity modulated radiation therapy treatment planning. *Journal of Global Optimization*, 42(4):587–607, 2008.

[8] Dionne M. Aleman, H. Edwin Romeijn, and James F. Dempsey. A response surface approach to beam orientation optimization in intensity-modulated radiation therapy treatment planning. *INFORMS Journal on Computing*, 21(1):62–76, 2009.

[9] Dionne M. Aleman, Daniel Glaser, H. Edwin Romeijn, and James F. Dempsey. Interior point algorithms: guaranteed optimality for fluence map optimization in IMRT. *Physics in Medicine and Biology*, 55(18):5467–82, 2010.

[10] American Cancer Society. Treatment Types, 2013. URL `http://www.cancer.org/treatment/treatmentsandsideeffects/treatmenttypes/`.

[11] Christian Artigues, Nicolas Jozefowiez, and Boadu M Sarpong. Column generation algorithms for bi-objective combinatorial optimization problems with a min–max objective. *EURO Journal on Computational Optimization*, 6(2):117–142, 2018.

[12] Davaatseren Baatar, Horst W. Hamacher, Matthias Ehrgott, and Gerhard J. Woeginger. Decomposition of integer matrices and multileaf collimator sequencing. *Discrete Applied Mathematics*, 152(1-3):6–34, 2005.

[13] Gladys Bahr, James G. Kereiakes, Howard Jaye Horwitz, Pearl J. Compaan, John A. G. Holt, and K. A. Goode. The method of linear programming applied to radiation treatment planning. *Radiology*, 91:686–693, 1968.

[14] Marleen Balvert and David Craft. Fast approximate delivery of fluence maps for IMRT and VMAT. *Physics in Medicine and Biology*, 62(4):1225–1247, 2017.

[15] James L Bedford. Treatment planning for volumetric modulated arc therapy. *Medical Physics*, 36(11): 5128–5138, 2009.

[16] Harold P Benson. An outer approximation algorithm for generating all efficient extreme points in the outcome set of a multiple objective linear programming problem. *Journal of Global Optimization*, 13 (1):1–24, 1998.

[17] Rasmus Bokrantz. Multicriteria optimization for volumetric-modulated arc therapy by decomposition into a fluence-based relaxation and a segment weight-based restriction. *Medical Physics*, 39(11):6712–6725, 2012.

[18] Rasmus Bokrantz and Anders Forsgren. An algorithm for approximating convex pareto surfaces based on dual techniques. *INFORMS Journal on Computing*, 25(2):377–393, 2013.

[19] Natashia Boland, Horst W. Hamacher, and Frank Lenzen. Minimizing beam-on time in cancer radiation treatment using multileaf collimators. *Networks*, 43(4):226–240, 2004.

[20] Thomas R. Bortfeld, Josef Burkelbach, Robert Boesecke, and Wolfgang Schlegel. Methods of image reconstruction from projections applied to conformation radiotherapy. *Physics in Medicine and Biology*, 35:1423–1434, 1990.

[21] Gábor Braun, Sebastian Pokutta, Dan Tu, and Stephen Wright. Blended conditonal gradients. In Kamalika Chaudhuri and Ruslan Salakhutdinov, editors, *Proceedings of the 36th International Conference on Machine Learning*, volume 97 of *Proceedings of Machine Learning Research*, pages 735–743, Long Beach, California, USA, 09–15 Jun 2019. PMLR.

[22] Sebastiaan Breedveld, Pascal RM Storchi, Marleen Keijzer, Arnold W Heemink, and Ben JM Heijmen. A novel approach to multi-criteria inverse planning for IMRT. *Physics in Medicine and Biology*, 52 (20):6339–6353, 2007.

[23] Sebastiaan Breedveld, Pascal RM Storchi, and Ben JM Heijmen. The equivalence of multi-criteria methods for radiotherapy plan optimization. *Physics in Medicine and Biology*, 54(23):7199–7209, 2009.

[24] Karl Bzdusek, Henrik Friberger, Kjell Eriksson, Björn Hårdemark, David Robinson, and Michael Kaus. Development and evaluation of an efficient approach to volumetric arc therapy planning. *Medical Physics*, 36(6):2328–2339, 2009.

[25] Milton E. Ixquiac Cabrera, Erick O. Montenegro, Juan Francisco Vélez Lucero, Luis Alejandro Izquierdo Linares, and J. M. Ixquiac Cabrera. Comparative analysis of volumetric modulated arc radiotherapy (VMAT) versus intensity modulated radiotherapy (IMRT) using the tg119 tests, 2012.

[26] Daliang Cao, Muhammad KN Afghan, Jinsong Ye, Fan Chen, and David M Shepard. A generalized inverse planning tool for volumetric-modulated arc therapy. *Physics in Medicine and Biology*, 54(21): 6725, 2009.

[27] Fredrik Carlsson, Anders Forsgren, Henrik Rehbinder, and Kjell Eriksson. Using eigenstructure of the hessian to reduce the dimension of the intensity modulated radiation therapy optimization problem. *Annals of Operations Research*, 148(1):81–94, 2006.

[28] Mark P Carol. Peacock$^{\text{TM}}$: A system for planning and rotational delivery of intensity-modulated fields. *International Journal of Imaging Systems and Technology*, 6(1):56–61, 1995.

[29] Paul S. Cho, Seungsoo Lee, Robert J. Marks, Seungjong Oh, Steve Sutlief, and Mark H. Phillips. Optimization of intensity modulated beams with volume constraints using two methods: cost function minimization and projections onto convex sets. *Medical Physics*, 25(435–443), 1998.

[30] Cristian Cotrutz and Lei Xing. Segment-based dose optimisation using a genetic algorithm. *Physics in Medicine and Biology*, 48:2987–2998., 2003.

[31] Cristian Cotrutz, Michael Lahanas, C Kappas, and Dimos Baltas. A multiobjective gradient-based dose optimization algorithm for external beam conformal radiotherapy. *Physics in Medicine and Biology*, 46(8):2161, 2001.

[32] David Craft. Calculating and controlling the error of discrete representations of pareto surfaces in convex multi-criteria optimization. *Physica Medica: European Journal of Medical Physics*, 26(4):184–191, 2010.

[33] David Craft. Multi-criteria optimization methods in radiation therapy planning: a review of technologies and directions. *arXiv preprint arXiv:1305.1546*, 2013.

[34] David Craft and Michael Monz. Simultaneous navigation of multiple pareto surfaces, with an application to multicriteria imrt planning with multiple beam angle configurations. *Medical Physics*, 37(2): 736–741, 2010.

[35] David Craft and Christian Richter. Deliverable navigation for multicriteria step and shoot imrt treatment planning. *Physics in Medicine and Biology*, 58(1):87, 2012.

[36] David Craft and Christian Richter. Deliverable navigation for multicriteria step and shoot imrt treatment planning. *Physics in Medicine and Biology*, 58(1):87–103, 2013.

[37] David Craft, Tarek Halabi, and Thomas R. Bortfeld. Exploration of tradeoffs in intensity-modulated radiotherapy. *Physics in Medicine and Biology*, 50(24):5857, 2005.

[38] David Craft, Tarek F Halabi, Helen A Shih, and Thomas R. Bortfeld. Approximating convex pareto surfaces in multiobjective radiotherapy planning. *Medical physics*, 33(9):3399–3407, 2006.

[39] David Craft, Dualta McQuaid, Jeremiah Wala, Wei Chen Ehsan Salari, and Thomas R. Bortfeld. Multicriteria VMAT optimization. *Medical Physics*, 39(2):686–696, 2012.

[40] David Craft, Mark Bangert, Troy Long, Dávid Papp, and Jan Unkelbach. Shared data for intensity modulated radiation therapy (IMRT) optimization research: The CORT dataset. *GigaScience*, 3:37–48, 2014.

[41] Joseph O. Deasy. Multiple local minima in radiotherapy optimization problems with dose–volume constraints. *Medical Physics*, 24(7):1157–1161, 1997.

[42] Joseph O Deasy, Angel I Blanco, and Vanessa H Clark. CERR: A computational environment for radiotherapy research. *Medical Physics*, 30(5):979–985, 2003.

[43] Guy Desaulniers, Jacques Desrosiers, and Marius M. Solomon. *Column Generation*. Springer, 2005.

[44] Martin Desrochers and Francois Soumis. A column generation approach to urban transit crew scheduling. *Transportation Science*, 23:1–13, 1989.

[45] Joana Dias, Humberto Rocha, Tiago Ventura, Brígida Ferreira, and Maria do Carmo Lopes. Automated fluence map optimization based on fuzzy inference systems. *Medical Physics*, 43(3):1083–1095, 2016.

[46] Pınar Dursun, Z. Caner Taşkın, and İ. Kuban Altınel. Using branch-and-price to determine optimal treatment plans for volumetric modulated arc therapy (VMAT). *Computers and Operations Research*, 110:1 – 17, 2019.

[47] Matthew A. Earl, David M. Shepard, S. Habibddin Naqvi, X. Allen Li, and Cedric X. Yu. Inverse planning for intensity-modulated arc therapy using direct aperture optimization. *Physics in Medicine and Biology*, 48:1075–1089, 2003.

[48] Matthias Ehrgott. *Multicriteria Optimization*. Springer, Berlin, 2005.

[49] Matthias Ehrgott and Xavier Gandibleux. Bound sets for biobjective combinatorial optimization problems. *Computers and Operations Research*, 34(9):2674–2694, 2007.

[50] Matthias Ehrgott and Rick Johnston. Optimisation of beam directions in intensity modulated radiation therapy planning. *OR Spectrum*, 25(2):251–264, 2003.

[51] Matthias Ehrgott, Çiğdem Güler, Horst W. Hamacher, and Lizhen Shao. Mathematical optimization in intensity modulated radiation therapy. *4OR*, 6:199–262, 2008.

[52] Matthias Ehrgott, Çiğdem Güler, Horst W. Hamacher, and Lizhen Shao. Mathematical optimization in intensity modulated radiation therapy. *Annals of Operations Research*, 175(1):309–365, 2010.

[53] Matthias Ehrgott, Lizhen Shao, and Anita Schöbel. An approximation algorithm for convex multi-objective programming problems. *Journal of Global Optimization*, 50(3):397–416, 2011.

[54] Konrad Engel. A new algorithm for optimal multileaf collimator field segmentation. *Discrete Applied Mathematics*, 152(1-3):35–51, 2005.

[55] Konrad Engel and Antje Kiesel. Approximated matrix decomposition for imrt planning with multileaf collimators. *OR Spectrum*, pages 1–24, 2009.

[56] Dominique Feillet, Pierre Dejax, Michel Gendreau, and Crille Gueguen. An exact algorithm for the elementary shortest path problem with resource constraints: Application to some vehicle routing problems. *Networks*, 44(3):216–229, 2004.

[57] Marguerite Frank and Philip Wolfe. An algorithm for quadratic programming. *Naval Research Logistics Quarterly*, 3(1-2):95–110, 1956.

[58] Tarek Halabi, David Craft, and Thomas R. Bortfeld. Dose–volume objectives in multi-criteria optimization. *Physics in Medicine and Biology*, 51(15):3809–3818, 2006.

[59] Horst W. Hamacher and Karl-Heinz Küfer. Inverse radiation therapy planning - a multiple objective optimization approach. *Discrete Applied Mathematics*, 118(1-2):145–161, 2002.

[60] Haitham Hindi. A tutorial on optimization methods for cancer radiation treatment planning. In *American Control Conference (ACC), 2013*, pages 6804–6816. IEEE, 2013.

[61] Allen Holder. Designing radiotherapy plans with elastic constraints and interior point methods. *Health Care Management Science*, 6(1):5–16, 2003.

[62] Allen Holder and Bill Salter. *A Tutorial on Radiation Oncology and Optimization*, volume 76 of *International Series in Operations Research and Management Science*, pages 4–1–4–47. Springer New York, 2005.

[63] Gospodarowicz MK Jaffray DA. Radiation therapy for cancer. In Susan Horton Rengaswamy Sankaranarayanan, Hellen Gelband and Prabhat Jha, editors, *Disease Control Priorities, Cancer*, chapter 14. The World Bank, third edition, 2015. doi: 10.1596/978-1-4648-0349-9. URL `https://elibrary.worldbank.org/doi/abs/10.1596/978-1-4648-0349-9`.

[64] Thomas Kalinowski. The complexity of minimizing the number of shape matrices subject to minimal beam-on time in multileaf collimator field decomposition with bounded fluence. *Discrete Applied Mathematics*, 157(9):2089–2104, 2009.

[65] Alina Kiessling. An introduction to parallel programming with OpenMP. Technical report, The University of Edinburgh, 2009.

[66] Kathrin Klamroth, Jørgen Tind, and Margaret M. Wiecek. Unbiased approximation in multicriteria optimization. *Mathematical Methods of Operations Research*, 56(3):413–437, 2003.

[67] Karl-Heinz Küfer, Horst W. Hamacher, editor="Schlegel Wolfgang Bortfeld, Thomas R.", and Thomas R. Bortfeld. A multicriteria optimization approach for inverse radiotherapy planning. In *The Use of Computers in Radiation Therapy*, pages 26–28, Berlin, Heidelberg, 2000. Springer Berlin Heidelberg.

[68] Karl-Heinz Küfer, Alexander Scherrer, Michael Monz, Fernando Alonso, Hans Trinkaus, Thomas R. Bortfeld, and Christian Thieke. Intensity-modulated radiotherapy–a large scale multi-criteria programming problem. *OR Spectrum*, 25(2):223–249, 2003.

[69] Karl-Heinz Küfer, M. Monz, A. Scherrer, P. Suss, F. Alonso, A. S. Azizi Sultan, Thomas R. Bortfeld, and C. Thieke. *Multicriteria Optimization in Intensity Modulated Radiotherapy Planning*, volume 26 of *Optimization and Its Applications*. Springer Science and Business Media LLC, 2009.

[70] Marc Langer. Optimization of beam weights under dose-volume restrictions. *International Journal of Radiation Oncology Biology Physics*, 13:1255–1260, 1987.

[71] Marc Langer, Sue Morrill, Robert R. Brown, Oliver Lee, and Rania Elnaggar Lane. A comparison of mixed integer programming and fast simulated annealing for optimized beam weights in radiation therapy. *Medical Physics*, 23:957–964, 1996.

[72] Eva K. Lee, Tim Fox, and Ian Crocker. Integer programming applied to intensity-modulated radiation therapy treatment planning. *Annals of Operations Research*, 119(1):165–181, 2003.

[73] Eva. K. Lee, Tim Fox, and Ian Crocker. Simultaneous beam geometry and intensity map optimization in intensity-modulated radiation therapy. *International Journal of Radiation Oncology Biology Physics*, 64(1):301–20, 2006.

[74] Wilfrid Levin, Hanne Marginus Kooy, Jay Steven Loeffler, and Thomas F. Delaney. Proton beam therapy. *British Journal of Cancer*, 93(8):849–54, 2005.

[75] Nan Li, Masoud Zarepisheh, Andres Uribe-Sanchez, Kevin Moore, Zhen Tian, Xin Zhen, Yan Jiang Graves, Quentin Gautier, Loren Mell, Linghong Zhou, et al. Automatic treatment plan re-optimization for adaptive radiotherapy guided with the initial plan DVHs. *Physics in Medicine and Biology*, 58(24): 8725, 2013.

[76] Gino J. Lim and Wenhua Cao. A two-phase method for selecting IMRT treatment beam angles: Branch-and-prune and local neighborhood search. *European Journal of Operational Research*, 217: 609–618, 2012.

[77] Kuan-Min Lin, Matthias Ehrgott, and Andrea Raith. Integrating column generation in a method to compute a discrete representation of the non-dominated set of multi-objective linear programmes. *4OR*, 15(4):331–357, 2017.

[78] Troy Long, Michal Matuszak, Mary Feng, Benedick A. Fraass, Randall Ten Haken, and H. Edwin Romeijn. Sensitivity analysis for lexicographic ordering in radiation therapy treatment planning. *Medical physics*, 39(6Part1):3445–3455, 2012.

[79] Shuang Luan, Chao Wang, Daliang Cao, Danny Z. Chen, David M. Shepard, and Cedric X. Yu. Leaf-sequencing for intensity-modulated arc therapy using graph algorithms. *Medical Physics*, 35(1):61–69, 2008.

[80] James B. MacQueen. Some methods for classification and analysis of multivariate observations. In *Proceedings of the Fifth Berkeley Symposium on Mathematical Statistics and Probability, Volume 1: Statistics*, pages 281–297, Berkeley, Calif., 1967. University of California Press.

[81] Gikas Steven Mageras and Radhe Mohan. Application of fast simulated annealing to optimization of conformal radiation treatments. *Medical Physics*, 20(3), 1993.

[82] Mehdi Mahnam, Michel Gendreau, Nadia Lahrichi, and Louis-Martin Rousseau. Simultaneous delivery time and aperture shape optimization for the volumetric-modulated arc therapy (VMAT) treatment planning problem. *Physics in Medicine and Biology*, 62(14):5589–5611, 2017.

[83] Mehdi Mahnam, Michel Gendreau, Nadia Lahrichi, and Louis-Martin Rousseau. Integrating DVH criteria into a column generation algorithm for VMAT treatment planning. *Physics in Medicine and Biology*, 64(8), 2019.

[84] Andrew R. Martin and Antoni Gaya. Stereotactic body radiotherapy: a review. *Clin Oncol (R Coll Radiol)*, 22(3):157–72, 2010.

[85] Richard L. Maughan. *Neutron Beam Therapy.* John Wiley & Sons, Inc., 2006.

[86] Chunhua Men, H. Edwin Romeijn, Z Caner Taşkın, and James F. Dempsey. An exact approach to direct aperture optimization in IMRT treatment planning. *Physics in Medicine and Biology*, 52(24): 7333–7352, 2007.

[87] Chunhua Men, Xuejun Gu, Dongju Choi, Amitava Majumdar, Ziyi Zheng, Klaus Mueller, and Steve B. Jiang. GPU-based ultrafast IMRT plan optimization. *Physics in Medicine and Biology*, 54(21):6565–6573, 2009.

[88] Chunhua Men, Xun Jia, and Steve B. Jiang. GPU-based ultra-fast direct aperture optimization for online adaptive radiation therapy. *Physics in Medicine and Biology*, 55(15):4309–4319, 2010.

[89] Chunhua Men, H. Edwin Romeijn, Xun Jia, and Steve B. Jiang. Ultrafast treatment plan optimization for volumetric modulated arc therapy (VMAT). *Medical Physics*, 37(11):5787–5791, 2010.

[90] Siamak Moradi, Andrea Raith, and Matthias Ehrgott. A bi-objective column generation algorithm for the multi-commodity minimum cost flow problem. *European Journal of Operational Research*, 244(2): 369–378, 2015.

[91] Ibrahim Muter, Ş İlker Birbil, and Kerem Bülbül. Simultaneous column-and-row generation for large-scale linear programs with column-dependent-rows. *Mathematical Programming*, 142(1–2):47–82, 2013.

[92] Dan Nguyen, Qihui Lyu, Dan Ruan, Daniel O'Connor, Daniel A Low, and Ke Sheng. A comprehensive formulation for volumetric modulated arc therapy planning. *Medical Physics*, 43(7):4263–4272, 2016.

[93] Andrzej Niemierko. Reporting and analyzing dose distributions: a concept of equivalent uniform dose. *Medical Physics*, 24:103–110, 1997.

[94] Arinbjörn Ólafsson and Stephen J Wright. Linear programing formulations and algorithms for radiotherapy treatment planning. *Optimization Methods and Software*, 21(2):201–231, 2006.

[95] Sheelagh O'Rourke, Helen McAneney, and Thomas Hillen. Linear quadratic and tumour control probability modelling in external beam radiotherapy. *Journal of Mathematical of Biology*, 58(4-5):799–817, 2009.

[96] Karl Otto. Volumetric modulated arc therapy: IMRT in a single gantry arc. *Medical Physics*, 35(1): 310–317, 2008.

[97] Özgür Özpeynirci and Murat Köksalan. An exact algorithm for finding extreme supported nondominated points of multiobjective mixed integer programs. *Management Science*, 56(12):2302–2315, 2010.

[98] David A. Palma, Wilko F A R Verbakel, Karl b. Otto, and Suresh Senan. New developments in arc radiation therapy: a review. *Cancer Treatment Reviews*, 36(5):393–399, 2010.

[99] Dávid Papp and Jan Unkelbach. Direct leaf trajectory optimization for volumetric modulated arc therapy planning with sliding window delivery. *Medical Physics*, 41(1):011701–01–011701–10, 2014.

[100] Fei Peng, Xun Jia, H. Edwin Romeijn Xuejun Gu, Marina A Epelman, and Steve B Jiang. A new column-generation-based algorithm for VMAT treatment plan optimization. *Physics in Medicine and Biology*, 57(14):4569–88, 2012.

[101] Fei Peng, Steve B Jiang, H. Edwin Romeijn, and Marina A Epelman. VMATc: VMAT with constant gantry speed and dose rate. *Physics in Medicine and Biology*, 60(7):2955, 2015.

[102] Felisa Preciado-Walters, Ronald Rardin, Marc Langer, and Van Thai. A coupled column generation, mixed integer approach to optimal planning of intensity modulated radiation therapy for cancer. *Mathematical Programming*, 101(2), 2004.

[103] Marc-André Renaud, Monica Serban, and Jan Seuntjens. On mixed electron-photon radiation therapy optimisation using the column generation approach. *Medical Physics*, 44:4287–4298, 2017.

[104] Gijs Rennen, Edwin R van Dam, and Dick den Hertog. Enhancement of sandwich algorithms for approximating higher-dimensional convex pareto sets. *INFORMS Journal on Computing*, 23(4):493–517, 2011.

[105] H. Edwin Romeijn and James F. Dempsey. Intensity modulated radiation therapy treatment plan optimization. *TOP*, 16(2):215–243, 2008.

[106] H. Edwin Romeijn, Ravindra K. Ahuja, James F. Dempsey, Arvind Kumar, and Jonathan G. Li. A novel linear programming approach to fluence map optimization for intensity modulated radiation therapy treatment planning. *Physics in Medicine and Biology*, 48(21):3521–3542, 2003.

[107] H. Edwin Romeijn, James F. Dempsey, and Jonathan G. Li. A unifying framework for multi-criteria fluence map optimization models. *Physics in Medicine and Biology*, 49(10):1991–2013, 2004.

[108] H. Edwin Romeijn, Ravindra K. Ahuja, James F. Dempsey, and Arvind Kumar. A column generation approach to radiation therapy treatment planning using aperture modulation. *SIAM Journal on Optimization*, 15(3):838–862, 2005.

[109] H. Edwin Romeijn, Ravindra K. Ahuja, James F. Dempsey, and Arvind Kumar. A new linear programming approach to radiation therapy treatment planning problems. *Operations Research*, 54(2): 201–216, 2006.

[110] Stefan Ruzika and Margaret M. Wiecek. Approximation methods in multiobjective programming. *Journal of Optimization Theory and Applications*, 126(3):473–501, 2005.

[111] Ehsan Salari and H. Edwin Romeijn. Quantifying the trade-off between imrt treatment plan quality and delivery efficiency using direct aperture optimization. *INFORMS Journal on Computing*, 24(4): 518–533, 2012.

[112] Ehsan Salari and Jan Unkelbach. A column-generation-based method for multi-criteria direct aperture optimization. *Physics in Medicine and Biology*, 58(3):621, 2013.

[113] Ehsan Salari, Jeremiah Wala, and David Craft. Exploring trade-offs between VMAT dose quality and delivery efficiency using a network optimization approach. *Physics in Medicine and Biology*, 57(17): 5587–5600, 2012.

[114] Bernd Schandl, Kathrin Klamroth, and Margaret M. Wiecek. Norm-based approximation in multicriteria programming. *Computers and Mathematics with Applications*, 44(7):925–942, 2002.

[115] Alexander Scherrer, Karl-Heinz Küfer, Thomas R. Bortfeld, Michael Monz, and Fernando Alonso. IMRT planning on adaptive volume structures—a decisive reduction in computational complexity. *Physics in Medicine and Biology*, 50(9):20–33, 2005.

[116] Lizhen Shao and Matthias Ehrgott. Approximately solving multiobjective linear programmes in objective space and an application in radiotherapy treatment planning. *Mathematical Methods of Operations Research*, 68(2):257–276, 2008.

[117] David M. Shepard, Michael C. Ferris, Gustavo H. Olivera, and T. Rockwell Mackie. Optimizing the delivery of radiation therapy to cancer patients. *Siam Review*, 41(4):721–744, 1999. Times Cited: 80.

[118] David M. Shepard, Matthew A. Earl, X. Allen Li, S. Habibddin Naqvi, and Cedric X. Yu. Direct aperture optimization: A turnkey solution for step-and-shoot IMRT. *Medical physics*, 29(6):1007–1018, 2002.

[119] Rajendra S Solanki, Perry A Appino, and Jared L Cohon. Approximating the noninferior set in multiobjective linear programming problems. *European Journal of Operational Research*, 68(3):356–373, 1993.

[120] Spiridon V. Spirou and Chen-Shou Chui. A gradient inverse planning algorithm with dose-volume constraints. *Medical Physics*, 25(3):321–333, 1998.

[121] Canadian Cancer Society's Advisory Committee on Cancer Statistics. Canadian cancer statistics. Technical report, Canadian Cancer Society, 2018.

[122] Ali T. Tuncel, Felisa Preciado, Ronald L. Rardin, Marc Langer, and Jean-Philippe P. Richard. Strong valid inequalities for fluence map optimization problem under dose-volume restrictions. *Annals of Operations Research*, 196(1):819–840, 2012.

[123] Jan Unkelbach, Thomas R. Bortfeld, David Craft, Markus Alber, Mark Bangert, Rasmus Bokrantz, Danny Chen, Ruijiang Li, Lei Xing, Chunhua Men, Simeon Nill, Dávid Papp, Edwin Romeijn, and Ehsan Salari. Optimization approaches to volumetric modulated arc therapy planning. *Medical Physics*, 42(3):1367–1377, 2015.

[124] Rens van Haveren, Sebastiaan Breedveld, Marleen Keijzer, Peter Voet, Ben Heijmen, and Włodzimierz Ogryczak. Lexicographic extension of the reference point method applied in radiation therapy treatment planning. *European Journal of Operational Research*, 2017.

[125] François Vanderbeck. Computational study of a column generation algorithm for bin packing and cutting stock problems. *Mathematical Programming*, 86(3):565–594, 1999.

[126] Varian Medical Systems. Varian's 120-leaf multileaf collimator, 2013. URL `http://filecache.drivetheweb.com/mr5mr_varian/154577/MLC+-+gold.jpg`.

[127] Lynn J. Verhey. Comparison of three-dimensional conformal radiation therapy and intensity-modulated radiation therapy systems. *Seminars in Radiation Oncology*, 9(1):78–98, 1999.

[128] Peter WJ Voet, Maarten LP Dirkx, Sebastiaan Breedveld, Dennie Fransen, Peter C Levendag, and Ben JM Heijmen. Toward fully automated multicriterial plan generation: A prospective clinical study. *International Journal of Radiation Oncology Biology Physics*, 85(3):866–872, 2013.

[129] Jeremiah Wala, Ehsan Salari, Wei Chen, and David Craft. Optimal partial-arcs in VMAT treatment planning. *Physics in Medicine and Biology*, 57(18):5861–5874, 2012.

[130] WCRFI. Worldwide cancer statistics. Technical report, World Cancer Research Fund International, 2012.

[131] Steve Webb. Optimisation of conformal radiotherapy dose distribution by simulated annealing. *Physics in Medicine and Biology*, 34:1349–1370, 1989.

[132] Steve Webb and Alan Effraim Nahum. A model for calculating tumor control probability in radiotherapy including the effects of inhomogeneous distributions of dose and clonogenic cell density. *Physics in Medicine and Biology*, 38:653–666, 1993.

[133] Qiuwen Wu and Radhe Mohan. Algorithms and functionality of an intensity modulated radiotherapy optimization system. *Medical physics*, 27(4):701–711, 2000.

[134] Cedric X. Yu. Intensity-modulated arc therapy with dynamic multileaf collimation: An alternative to tomotherapy. *Physics in Medicine and Biology*, 40:1435–1449, 1995.

[135] Cedric X. Yu and Grace Tang. Intensity-modulated arc therapy: principles, technologies and clinical implementation. *Physics in Medicine and Biology*, 56(5):R31–54, 2011.

[136] Marco Zaider and Gerald N. Minerbo. Tumor control probability: A formulation applicable to any temporal protocol of dose delivery. *Physics in Medicine and Biology*, 45:279–293, 2000.

[137] Masoud Zarepisheh, Troy Long, Nan Li, Zhen Tian, H. Edwin Romeijn, Xun Jia, and Steve B Jiang. A DVH-guided IMRT optimization algorithm for automatic treatment planning and adaptive radiotherapy replanning. *Medical Physics*, 41(6):061711, 2014.

[138] Yin Zhang and Michael Merritt. Dose-volume-based imrt fluence optimization: A fast least-squares approach with differentiability. *Linear Algebra and its Applications*, 428(5-6):1365–1387, 2008.

[139] Peter Ziegenhein, Cornelis Ph Kamerling, and Uwe Oelfke. Interactive dose shaping part 1: a new paradigm for IMRT treatment planning. *Physics in Medicine and Biology*, 61(6):2457–2470, mar 2016.

APPENDIX A SUPPLEMENTS OF CHAPTER 4

A.1 Equivalent RRMP′ model

In this appendix, we show the RRMP′ is an equivalent model for the RRMP with a single column γ. We use this model to provide a simultaneous reduced cost as the objective function of the PSP.

As mentioned in Section 4.3.1, there are two columns y and γ in the RRMP. Any optimal solution $(\widetilde{y}, \widetilde{\gamma}, \widetilde{t})$ of the RRMP in which $\widetilde{\gamma}^k < \widetilde{y}^k\, R\,\overline{T}$ for at least one index k can be transformed into an equivalent optimal solution via

$$y^k = (R\,\overline{T})^{-1}\gamma^k \qquad\qquad \forall k \in K'. \tag{A.1}$$

Therefore, we can consider the equivalent problem RRMP′ in which Constraint (4.8g) is removed and y^k is replaced by $\gamma^k/(R\,\overline{T})$ in (4.8c) and (4.8d):

$$\sum\nolimits_{k\in K'} a_h^k\,\gamma^k = R\,\overline{T} \qquad\qquad \forall\, h \in H \tag{A.2}$$

$$\sum\nolimits_{k\in K'} \tau_{h,h+1}^k\,\gamma^k \le R\,\overline{T}\,t_h \qquad\qquad \forall\, h \in H \tag{A.3}$$

Constraint (A.2) is dominated by Equations (4.8c) and (4.8h). This leads to a model based only on column γ:

$$\textbf{RRMP}'\textbf{:}\ \min_{\gamma,t} \qquad \mathbf{F}(z) + w\,T \tag{A.4}$$

$$z_j = \sum\nolimits_{k\in K'} D_{jh}(A_h^k)\,\gamma^k \qquad\qquad \forall\, j \in V_s \tag{A.5}$$

$$\sum\nolimits_{k\in K'} \tau_{h,h+1}^k\,\gamma^k \le R\,\overline{T}\,t_h \qquad\qquad \forall\, h \in H \tag{A.6}$$

$$\sum\nolimits_{k\in K'} a_h^k\,\gamma^k = R\,t_h \qquad\qquad \forall\, h \in H \tag{A.7}$$

$$\sum\nolimits_{h\in H} t_h \le T \tag{A.8}$$

$$\underline{T} \le t_h \le \overline{T} \qquad\qquad \forall\, h \in H \tag{A.9}$$

$$\gamma^k \ge 0 \qquad\qquad \forall\, k \in K' \tag{A.10}$$

APPENDIX B SUPPLEMENTS OF CHAPTER 5

B.1 Formulation of the master model

The formulation of the restricted master problem is as follows:

$$\textbf{RMP}: \min\ f(z) \tag{B.1a}$$

s.t.

$$z_j = \sum\nolimits_{k\in K'} \sum\nolimits_{h\in H_k} D_{jh}(A_h^k)\,\gamma^k \qquad \forall j \in \mathcal{V} \tag{B.1b}$$

$$\sum\nolimits_{k\in K'} b_h^k\, y^k \le 1 \qquad \forall h \in H \tag{B.1c}$$

$$\gamma^k \le \Gamma^k\, y^k \qquad \forall k \in K' \tag{B.1d}$$

$$\sum\nolimits_{k\in K'} b_h^k\, \gamma^k \le \overline{\rho}\, t_h \qquad \forall\, h \in H \tag{B.1e}$$

$$\sum\nolimits_{k\in K'} \tau_{h,h+1}^k\, y^k \le t_h \qquad \forall\, h \in H \tag{B.1f}$$

$$\underline{T} \le t_h \le \overline{T} \qquad \forall\, h \in H \tag{B.1g}$$

$$y^k \in \{0,1\},\ \gamma^k \ge 0 \qquad \forall k \in K' \tag{B.1h}$$

where z_j, the dose absorbed by voxel j, is computed in Constraint B.1b based on the sectors covered by column k, H_k; the aperture shape, A_h^k; and the column fluence rate, γ^k. In Constraint B.1c b_h^k indicates the coverage of sector h by column k, and the constraint ensures that each sector h is covered by at most one column. Constraints B.1d and B.1e enforce the upper bound on the fluence rate. In constraints B.1d, the fluence rate of each column is restricted to the maximum fluence rate of column k, Γ^k, if selected, based on the maximum dose rate and the minimum gantry speed. In constraints B.1e, the fluence rate at each sector is bounded by the maximum dose rate $\overline{\rho}$ and the sector time. Also, Constraints B.1f ensure that the time spent at sector h is sufficient to allow the leaf movements to reach the next aperture A_{h+1}^k. Finally, Constraints B.1g enforce the lower and upper bounds on the sector time.

APPENDIX C SUPPLEMENTS OF CHAPTER 6

C.1 Line search algorithm in CG-BCG

The line search algorithm in lines (15) and (25) of Algorithm 4 is easily implemented based on the bisection algorithm. In this algorithm, two solutions x^1 and x^2 are given and the output is solution $\overline{x} = \mu\, x_1 + (1-\mu)\, x_2$ where $\mu \in [0,1]$. To implement this method with less computational time, we formulated the gradient $\nabla f(x)$ according to μ as follows and tried to find the root of this function.

$$\nabla f(\mu_) = \sum_{s\in S}\sum_{v\in V_s} 2\,(z_v^1 - z_v^2)\,(\overline{\lambda}_v\,[\mu\, z_v^1 + (1-\mu) z_v^2 - \overline{d}_v]_+ - \underline{\lambda}_v\,[\underline{d}_v - \mu\, z_v^1 - (1-\mu) z_v^2]_+) \tag{C.1}$$

The pseudo-code of this algorithm is shown in Algorithm (6). This algorithm is recursive and we consider $\overline{\mu}_0 = 1$ and $\underline{\mu}_0 = 0$ for the first iteration.

Algorithm 6 Bisection (x_1, x_2, μ_t, $\overline{\mu}_t$, $\underline{\mu}_t$)

Input: $\underline{\mu}_0 \leftarrow 0, \overline{\mu}_0 \leftarrow 1$

Output: μ^* and solution x^*

$\overline{x}_t \leftarrow \mu_t\,(x_1 + x_2)\mu_t\, x_1 + (1-\mu)\, x_2$

compute $\nabla f(\mu_t)$

if $(|\nabla f(\mu_t)| < \epsilon)$ **then**

    return μ_t and $\overline{x}_t$

if $(\nabla f(1)\, \nabla f(\mu_t) < 0)$ **then**

    $\mu_{t+1} \leftarrow 0.5\,(\mu_t + \overline{\mu}_t)$

    $\underline{\mu}_{t+1} \leftarrow \mu_t$, $\overline{\mu}_{t+1} \leftarrow \overline{\mu}_t$

else

    $\mu_{t+1} \leftarrow 0.5\,(\underline{\mu}_t + \mu_t)$

    $\underline{\mu}_{t+1} \leftarrow \underline{\mu}_t$, $\overline{\mu}_{t+1} \leftarrow \mu_t$

Bisection (x_1, x_2, μ_{t+1}, $\overline{\mu}_{t+1}$, $\underline{\mu}_{t+1}$)

C.2 L-smoothness of function f

To use the mathematical properties of the model specifically in the convergence of the CG-FW and CG-BCG algorithms, we need to show that the objective function f in Equation (6.7) is L-smooth and obtain the Lipschitz constant L.

First, we define L-smooth function as follows:

Definition 10. *Function f is L-smooth over a polytope $\mathcal{P}$, if for any $x_1, x_2 \in \mathcal{P}$, there is a Lipschitz scalar L for which*

$$\|f'(x_1) - f'(x_2)\| \le L\|x_1 - x_2\|, \quad \forall x_1, x_2 \in \mathcal{P} \tag{C.2}$$

We have also the following basic lemma for definition of the L-smooth function.

Lemma 6. *If $f : \mathcal{X} \to \mathbb{R}$ and $\frac{\partial f}{\partial x_k}$ exists, it is continuous and there is a constant $L \geq 0$ such that*

$$|\frac{\partial f}{\partial x_k}| \leq L \quad \forall k \in K \tag{C.3}$$

where L is the Lipschitz constant of the function.

We use the above lemma to find the Lipschitz constant of our function.

Lemma 7. *Function f in model RMP is Lipschitz continuous and the Lipschitz constant L is*

$$\sum_{s\in S}\sum_{v\in\mathcal{V}_s}\sum_{k\in K} 2\,\overline{\lambda}_v\, D_v^{k'}\, D_v^k. \tag{C.4}$$

Proof. In model RMP, $f : \mathbb{R}^m \to \mathbb{R}$ and $x_k \in [0, 1]$ for all columns k. We have

$$\frac{\partial f}{\partial x_{k'}} = \sum_{s\in S}\sum_{v\in\mathcal{V}_s} 2\, D_v^{k'}(\overline{\lambda}_v[z_v - \overline{d}_v]_+ - \underline{\lambda}_v[\underline{d}_v - z_v]_+). \tag{C.5}$$

Since $z_v \geq z_v - \overline{\lambda}_v$, $\underline{d}_v\,[\underline{d}_v - z_v]_+ \geq 0$, and $z_v \geq 0$, we have

$$\frac{\partial f}{\partial x_{k'}} \leq \sum_{s\in S}\sum_{v\in\mathcal{V}_s} 2\, D_v^{k'}\overline{\lambda}_v z_v, \tag{C.6}$$

and $z_v = \sum_{k\in K} D_v^k\, y_k$, thus

$$\begin{aligned}\frac{\partial f}{\partial x_{k'}} &\leq \sum_{s\in S}\sum_{v\in\mathcal{V}_s} 2\, D_v^{k'}\overline{\lambda}_v \sum_{k\in K} D_v^k\, x_k,\\ &\leq \sum_{s\in S}\sum_{v\in\mathcal{V}_s}\sum_{k\in K} 2\,\overline{\lambda}_v\, D_v^{k'}\, D_v^k\, x_k,\\ &\leq \sum_{s\in S}\sum_{v\in\mathcal{V}_s}\sum_{k\in K} 2\,\overline{\lambda}_v\, D_v^{k'}\, D_v^k.\end{aligned} \tag{C.7}$$

Finally, considering $\overline{D}_v = \max_{k\in K} D_v^k$, we have the Lipschitz constant as follows:

$$L = \sum_{s\in S}\sum_{v\in\mathcal{V}_s}\sum_{k\in K} 2\,\overline{\lambda}_v\,\overline{D}_v\, D_v^k. \tag{C.8}$$

■

Corollary 1. *Let L_i indicate the Lipschitz constant of f_i and w_i be the weight of objective i. The Lipschitz constant of weighted sum function is*

$$L(w) = \sum_{i=1}^{n} w_i L_i. \tag{C.9}$$

Proof. We can easily decompose function f and also obtained Lipschitz in Equation (C.8) based on the set of structures, S, and obtain the weighted Lipschitz constant. ■